ISSN 1023-9855

Thoracic Medicine

Volume 39 • Number 2 • June 2024

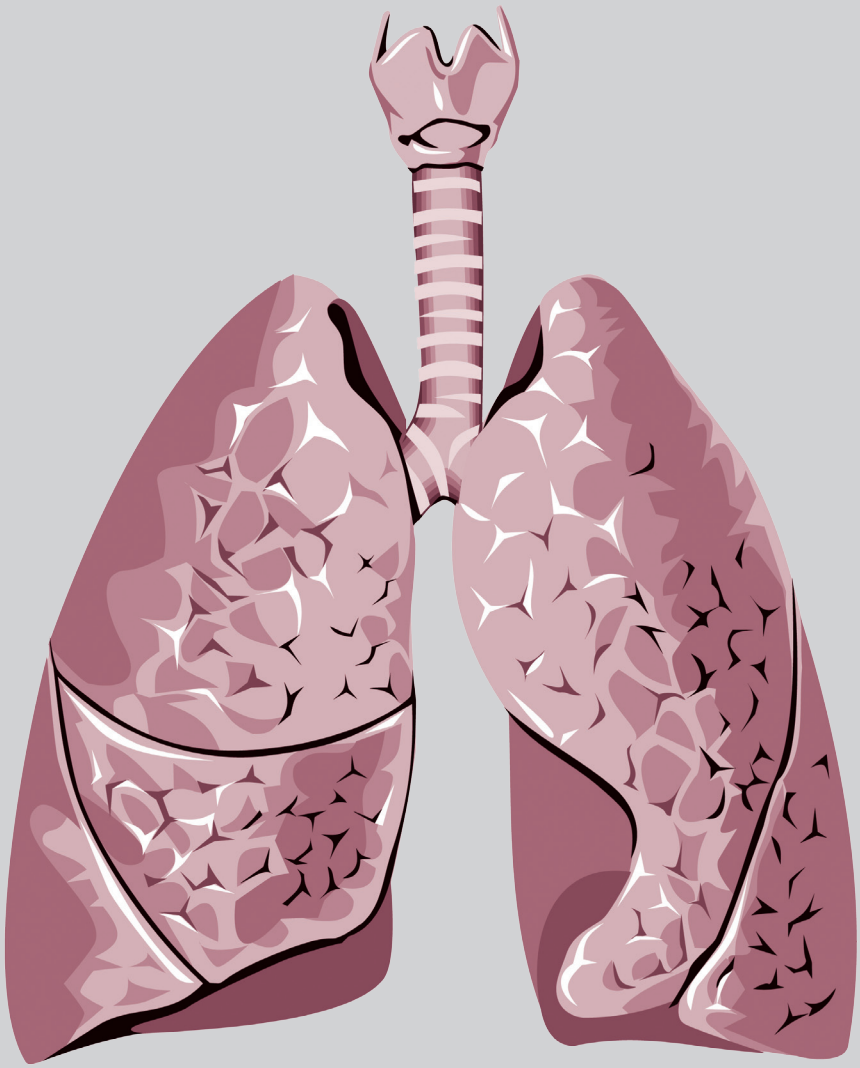

The Official Journal of

Taiwan Society of Pulmonary and Critical Care Medicine

Taiwan Society of Sleep Medicine

Taiwan Society for Respiratory Therapy

Taiwan Society of Tuberculosis and Lung Diseases

Thoracic Medicine

The Official Journal of
Taiwan Society of Pulmonary and Critical Care Medicine
Taiwan Society for Respiratory Therapy
Taiwan Society of Sleep Medicine
Taiwan Society of Tuberculosis and Lung Diseases

Thoracic Medicine

The Official Journal of
Taiwan Society of Pulmonary and Critical Care Medicine
Taiwan Society for Respiratory Therapy
Taiwan Society of Sleep Medicine
Taiwan Society of Tuberculosis and Lung Diseases

Volume 39
Number 2
June 2024

CONTENTS

Orginial Articles

Case Reports

Safety and Feasibility of Radial Endobronchial Ultrasound-guided Transbronchial Cryobiopsy without Fluoroscopy in the Diagnosis of Lung Diseases

Yu-Chu Kuo[1], Biing-Ru Wu[1,2], Meng-Fang Shen[1], Wei-Chih Liao[1,5,6], Chih-Yu Chen[1,2,5], Wei-Chun Chen[1,6], Chia-Hung Chen[1,2,4,5], Wen-Chien Cheng[1,2,6], Chih-Yen Tu[1,2,3]

Introduction: Transbronchial lung cryobiopsy (TBLC) has emerged as a new bronchoscopic procedure that can improve specimen quality to increase diagnostic yield in various diffuse parenchymal lung diseases (DPLDs). We evaluated the safety and feasibility of TBLC in combination with radial probe-endobronchial ultrasound (R-EBUS) to diagnose DPLDs without fluoroscopy.

Methods: Patients with DPLDs who underwent R-EBUS without fluoroscopy to locate target lesions and confirm the absence of adjacent vessels, followed by sampling with conventional transbronchial lung forceps biopsy (TBLB) and TBLC, were enrolled from January 2015 to March 2019.

Results: A total 21 patients with diffuse lung infiltrates and 13 patients with bilateral pulmonary nodules/masses were analyzed. The overall diagnostic rate was 76.4% (26/34), and the diagnostic yield increased from 44.1% with the TBLB to 70.6% after TBLC (p=0.023). Compared to TBLB, TBLC provided a larger specimen and sample volume (38 mm^3 vs 6 mm^3; p<0.001). Eleven patients who initially had non-diagnostic results by TBLB received a definite diagnosis after TBLC; eight of these patients were given a definite diagnosis of interstitial lung disease (ILD) (p<0.001).

Conclusion: Compared to TBLB with R-EBUS guidance, TBLC with R-EBUS guidance without fluoroscopy increased the diagnostic yield in patients with DPLDs, particularly in those with ILD. ***(Thorac Med 2024; 39: 106-118)***

Key words: Radial probe-endobronchial ultrasound, transbronchial lung cryobiopsy, transbronchial lung forceps biopsy, interstitial lung diseases, peripheral lung lesion

[1]Division of Pulmonary and Critical Care Medicine, Department of Internal Medicine, China Medical University Hospital, [2]School of Medicine, China Medical University. [3]Department of Life Science, National Chung Hsing University, [4]Department of Respiratory Therapy, China Medical University, [5]Graduate Institute of Clinical Medical Science, China Medical University, [6]Department of Internal Medicine, Hyperbaric Oxygen Therapy Center, China Medical University

Address reprint requests to: Dr. Wen-Chien Cheng, Department of Internal Medicine, China Medical University Hospital, No. 2, Yude Road, Taichung

Introduction

Transbronchial lung cryobiopsy (TBLC) has emerged as a new bronchoscopic procedure that can yield an improved specimen size and obtain crush artifact-free tissue compared with transbronchial lung biopsy (TBLB) performed with conventional forceps [1-4]. TBLC is used to obtain a specimen from the lung parenchyma, and is indicated for patients with diffuse parenchymal lung diseases (DPLDs). In the diagnosis of interstitial lung disease (ILD), Pajares *et al*. reported that TBLC provided a higher diagnostic yield than TBLB (74% vs. 34%) [5]. With regard to the application of TBLC for pulmonary masses or nodules, specimens obtained by TBLC have been shown to be consistently larger than those obtained by TBLB. This is preferential for mutation analysis and molecular testing, although no statistically significant difference has been reported in the diagnostic yield between TBLC and TBLB [6].

Although TBLC can provide a larger, artifact-free tissue sample for diagnosis, there have been concerns over a higher risk of bleeding and pneumothorax compared to TBLB [7]. In recent years, radial probe-endobronchial ultrasound (R-EBUS)-guided TBLC has been used to identify target lung parenchyma without adjacent blood vessels, and has been shown to reduce the risk of bleeding. However, few studies have assessed the feasibility and safety of R-EBUS-guided TBLC in the diagnosis of ILD and peripheral pulmonary lesions (PPLs). Berim *et al*. indicated that the simultaneous use of R-EBUS and fluoroscopy could reduce the risk of bleeding complications with TBLC in patients with suspected ILD [8]. In addition, Gnass *et al*. reported that the complication of pneumothorax occurred in 1 patient (5%) and mild bleeding in a few patients in diagnosing ILD with a combination of TBLC and R-EBUS, but there were no cases of moderate to severe bleeding [9]. The diagnostic yield of R-EBUS with TBLC in patients with ILD has been reported to be around 80% [9-10]. The rate of PPL diagnosis using R-EBUS with TBLC has been reported to range from 62.5% to 83%, with a moderate bleeding rate of 3% to 32% [11]. Abdelghani R *et al*. indicated that the diagnostic yield of R-EBUS with TBLC in subjects with DPLDs was 92.5 %, and the complication rate for pneumothorax and moderate bleeding was 5% and 12.5%, respectively [12].

Most previous studies have been limited by the lack of a control group. Only 1 study reported that R-EBUS with TBLC significantly increased the diagnostic yield in eccentrically and adjacently orientated PPLs to 75%, compared to 48% obtained via TBLB [13]. Therefore, we conducted this retrospective study of 34 patients with diffuse lung infiltrates or PPLs who underwent R-EBUS-guided TBLB, followed by R-EBUS-guided TBLC. The purpose of this study was to assess the efficacy and feasibility of R-EBUS-guided TBLC in the diagnosis of patients with diffuse lung infiltrates or PPLs, and to identify those patients who would benefit from R-EBUS-guided TBLC due to the larger diagnostic yield compared to R-EBUS-guided TBLB.

Patients and Methods

Between January 2015 and March 2019, 34 patients with diffuse lung infiltrates or PPLs who underwent R-EBUS to locate target lesions and confirm the absence of an adjacent vascular structure, followed by sampling with conven-

tional biopsy tools, including forceps, brushing and washing, and cryobiopsy, at our institution, were included in this study. Diffuse lung infiltrates on chest computed tomography (CT) images may present as ground glass opacities, reticular, and alveolar patterns. All procedures were performed in our bronchoscopy room, and bronchoscopy was performed under conscious sedation with pulse oximeter and electrocardiogram (EKG) monitoring. The clinical data of the patients, including age, sex, lesion location, pathological diagnosis, image size, image characteristics, specimen size, and complications were retrospectively analyzed. All authors had access to information that could identify individual participants after data collection. This study was approved by the China Medical University Hospital Institutional Review Board (CMUH103-REC1-112), and written consent was obtained from all patients.

All 34 patients underwent flexible bronchoscopy (BF-1T260; Olympus; Tokyo, Japan) with a transbronchial biopsy, and cryobiopsies were performed according to the standard protocol of China Medical University Hospital Interventional Pulmonology teams. The patients received local anesthesia with 2% xylocaine and conscious sedation with midazolam before the procedure. EBUS was performed using an endoscopic ultrasound system (EU-M30; Olympus) and a 20-MHz miniature radial probe (UM-S20–20R; Olympus). CT scans of all patients were performed prior to diagnostic bronchoscopy. Neither navigation bronchoscopy nor fluoroscopy was performed. The EBUS radial probe was inserted into the target bronchus according to the radiographic findings. Although the patients with DPLDs were undergoing TBLC, the use of fluoroscopy was suggested to reduce the possibility of a pneumothorax complication. However, fluoroscopy is not usually available in many institutions. We used R-EBUS to locate the best area to decrease the severity and the rate of complications.

The EBUS image presentations of the target lesions in diffuse lung infiltrates and PPLs were as follows: concentric, eccentric, adjacent isoechoic lesions, and blizzard patterns [14-15]. Once the target lesion had been identified on EBUS, the EBUS probe was marked with color tape against the orifice of the working channel of the bronchoscope. The R-EBUS probe was pulled out slowly. However, a guide sheath (GS) was not used in our clinical practice; therefore, the distance between the tip of the EBUS probe and the color tape was measured. We verified that the brushing, forceps, and cryoprobe were in the same location as the R-EBUS probe, based on the distance, and then sampling was performed using the traditional diagnostic method with a forceps biopsy and bronchus washing.

We then performed a cryobiopsy with a cryoprobe (ERBE Cryoprobe 1.9 mm diameter or 2.4 mm diameter), with a uniform freezing time of 4 seconds for each cryobiopsy. After freezing, the cryoprobe and bronchoscope were removed, with the frozen lung sample attached to the probe. The frozen samples were then thawed in normal saline and fixed in formalin. Each patient had 3 transbronchial biopsies of their lung lesions with forceps, and 1 to 2 with the cryoprobe. The bronchoscope was reintroduced immediately to assess bleeding at the biopsy site. Although the prophylactic placement of the Fogarty balloon or a bronchial blocker may mitigate the risk of bleeding during TBLC and increase the safety of the procedure, they were not available in our institution. We not only used R-EBUS guidance to choose the op-

timal area without a major vessel, but the prophylactic instillation of diluted norepinephrine was performed in most patients to reduc the rate of severe bleeding after the procedure.

The severity of bleeding was based on the Nashville Bleeding Scale, which is a new, simple, objective, and hierarchically-graded consensus classification for bleeding:

(1) Grade 1: Suctioning of blood required for less than 1 minute;

(2) Grade 2: Suctioning for more than 1 minute or repeat wedging of the bronchoscope for persistent bleeding or instillation of cold saline, diluted vasoactive substances or thrombin required;

(3) Grade 3: Selective intubation with an endotracheal tube (ETT) or balloon/bronchial blocker for less than 20 minutes, or premature interruption of the procedure;

(4) Grade 4: Persistent selective intubation >20 minutes or new admission to the ICU or PRBC transfusion or need of bronchial artery embolization or resuscitation [16].

After the procedure, the specimens were sent to the Department of Pathology where they were assessed by 2 independent pathologists. The final diagnosis was reached through multidisciplinary discussion, including experts in pulmonology, radiology, and lung pathology.

Statistical Analysis

The data were compiled and analyzed using commercial statistical software MedCalc version 15.6.1 (MedCalc, Mariakerke, Belgium). All continuous variables were reported as mean and standard deviation. Differences in continuous variables were compared using the Mann-Whitney U-test for non-normally distributed data. Categorical variables were reported as the number of patients and percentage. Differences in categorical variables were examined using the chi-square test or Fisher's exact test. McNemar's test was used to examine differences in diagnostic yield between forceps biopsies and cryobiopsies. Univariate and multivariate analyses were performed to identify the clinical factors associated with reaching a diagnosis of DPLDs after adding cryobiopsy. All tests of significance were 2-sided, and a p value ≤ 0.05 was considered to be statistically significant.

Results

Thirty-four patients (21 men and 13 women) with a mean age of 60 years were included in this retrospective study. Among them, 21 patients with diffuse lung infiltrates and 13 patients with bilateral PPLs were referred for R-EBUS-guided TBLC. A definite diagnosis after diagnostic bronchoscopy was established in 26 patients. Adenocarcinoma (9 patients) was the most common pathological diagnosis, followed by organizing pneumonia (7 patients). Invasive mucinous carcinoma, pulmonary alveolar proteinosis, and granulomatous inflammation were diagnosed in 2 patients each. Lymphoma, IgG4 disease, cryptococcus, and leiomyosarcoma were diagnosed in 1 patient each, and 8 patients had non-specific pathologic findings with chronic inflammation (Table 1). The locations of the biopsies are summarized in Table 2. The bilateral lower lobe (12 patients) was the most frequently biopsied site, followed by the right upper lobe (5 patients), lingual lobe (4 patients), and right middle lobe (1 patient).

Compared to TBLB with forceps, TBLC provided a larger specimen and sample volume (38 mm^3 vs 6 mm^3; $p < 0.001$) (Figure 1). Biopsy specimens obtained with the cryoprobe were considered to be diagnostic in 24 patients (24/34,

Table 1. Baseline Clinical Characteristics and Final Pathology Report of the Study Subjects

Variable	Value, N = 34
Age, years, median (IQR)	60 (52-70)
Sex (male), n (%)	21 (61.7)
Diffuse lung infiltration lesions, n (%)	21 (61.7)
Nodules or mass lesions, n (%)	13 (38.3)
Pathological diagnosis, n (%)	26 (76.4)
Invasive mucinous carcinoma	2 (5.8)
Adenocarcinoma	9 (26.4)
Lymphoma	1 (2.9)
Organizing pneumonia	7 (20.6)
Pulmonary alveolar proteinosis	2 (5.8)
IgG4 diseases	1 (2.9)
Cryptococcus	1 (2.9)
Granulomatous inflammation	2 (5.8)
Leiomyosarcoma	1 (2.9)
Pathological non-diagnosis, n (%)	8 (23.5)
Chronic inflammation	8 (23.5)

IQR: interquartile range

Table 2. Baseline Clinical Characteristics and Final Pathology Report of the Study Subjects

Location	N=34
Right upper lobe	
RB1	2
RB2	3
Right middle lobe	
RB4	1
Right lower lobe	
RB6	2
RB8	2
RB9	4
RB10	4
Left upper lobe	
LB4	4
Left lower lobe	
LB6	2
LB8	2
LB9	3
LB10	5

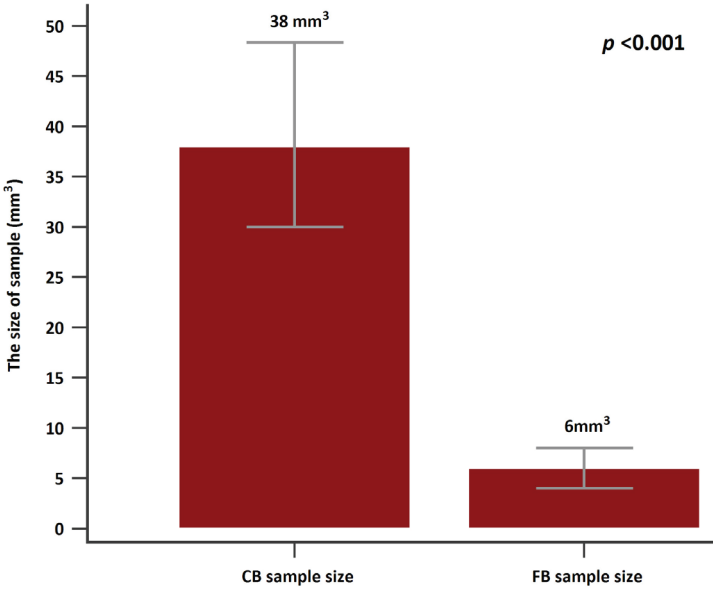

Fig. 2. CThe size of the biopsy specimens that were obtained with cryoprobe and forceps. Compared to TBLB with forceps, TBLC provided a larger specimen and sample volume (38 mm^3 vs 6 mm^3, $p < 0.001$).
CB: cryobiopsy; FB: forceps biopsy

70.6%), compared to 15 patients (15/34, 44.1%) with forceps biopsies. The diagnostic yield increased from 44.1% with the forceps biopsy to 70.6% after adding cryobiopsy (p = 0.023). Thirteen patients achieved a definite diagnosis using both forceps biopsy and cryobiopsy; however, 8 patients had non-diagnostic results even after a forceps biopsy and cryobiopsy. In 11 patients with initially non-diagnostic specimens obtained by forceps biopsy, a definite diagnosis was achieved after adding cryobiopsy. However, in 2 patients with initially definite diagnostic specimens obtained by forceps biopsy, non-diagnostic specimens were obtained after adding cryobiopsy (Table 3). Table 4 shows detailed information on sample size and the diagnosis of the 13 patients with inconsistent diagnostic results with forceps biopsy and cryobiopsy.

The study patients were divided into 2 groups: (1) those with initially non-diagnostic

Table 3. Diagnostic Yield of Crybiopsy (CB) and Forceps Biopsy (FB)

		Cryobiopsy (CB)	
Forceps Biopsy (FB)		**Diagnosed**	**Non-diagnosed**
	Diagnosed	**13**	**2**
	Undiagnosed	**11**	**8**

CB Diagnosed: 70.6%; FB Diagnosed: 44.1%; Δ = 26.47%; p = 0.023

Table 4. Detailed Information on Sample Size and Diagnosis of the 13 Patients with Inconsistent Diagnostic Results with Forceps Biopsy and Cryobiopsy. FB: Forceps Biopsy; CB: Cryobiopsy; PAP: Pulmonary Alveolar Proteinosis

FB samples (mm^3)	FB non-diagnosed	CB samples (mm^3)	CB diagnosed
8	Chronic inflammation	30	IgG4 disease
12	Chronic inflammation	36	Organizing pneumonia
1	No specific change	40	Organizing pneumonia
12	Chronic inflammation	6	Granulomatous disease
4	Chronic inflammation	50	PAP
1	Interstitial fibrosis	40	Organizing pneumonia
12	No diagnosis	45	Adenocarcinoma
8	Chronic inflammation	96	Organizing pneumonia
2	Chronic inflammation	36	Large B cell lymphoma
1	Chronic inflammation	9	PAP
10	Chronic inflammation	48	Organizing pneumonia
FB samples (mm^3)	**FB diagnosed**	**CB samples (mm^3)**	**CB non-diagnosed**
27	Fungal infection	72	Chronic inflammation
4	Adenocarcinoma	48	Interstitial fibrosis

specimens by forceps biopsy who then had a definite diagnosis after adding cryobiopsy; (2) those who still had the same diagnostic results or non-diagnostic specimens after adding cryobiopsy (Table 5). The only variable that was significantly different between these 2 groups was the diagnosis of ILD (13% vs 81.8%; $p < 0.001$). There were no significant differences in other variables, including initial image presentation (diffuse lung infiltration or nodules/masses), size of the target lesion on CT scan, characteristics of the EBUS image (concentric or eccentric/adjacent), diagnosis of malignant disease, and size of specimen (forceps biopsy or cryobiopsy) between the 2 groups. After univariate and multivariate analysis, the diagnosis of ILD was the only clinical factor related to having a diagnosis of DPLDs after adding cryobiopsy. These results suggested that adding cryobiopsy increased the diagnostic yield in patients with ILD.

With regard to the safety of the technique, 2 patients had pneumothorax which resolved after chest tube drainage, and the patients were subsequently discharged. In total, 5 (14.7%) patients had Grade 1 bleeding, and 28 (82.3%) had Grade 2 bleeding. All cases of bleeding were controlled by instillation of diluted norepinephrine or ice-cold saline (Table 6). No severe complications were recorded after the procedure.

Table 5. Clinical Basic Characteristics of These 2 Groups: (1) Those with Initially non-Diagnostic Specimens by Forceps Biopsy who Then had a Definite Diagnosis After Adding Cryobiopsy; (2) Those who Still had the Same Diagnostic Results or non-Diagnostic Specimens After Adding Cryobiopsy.

Clinical characteristics	No change with CB (n=23)	Change with CB (n=11)	*p*-value	Univariate analysis		Multivariate analysis	
				OR (95% CI)	*p*-value	OR (95% CI)	*p*-value
CT image characteristics			0.139	4.13 (0.73-23.4)	0.083		*P* value
Diffuse lung infiltrates	12 (52.2%)	9 (81.8%)					
Nodules or mass	11 (47.8%)	2 (18.2%)		124.073			0.012
Lesion size of biopsy (cm)	4.57 (2.48-5.58)	3.65 (2.05-4.87)	0.507	0.94 (0.69-1.27)	0.699		0.031
EBUS image characteristics			0.271	2.89 (0.50-16.58)	0.207	3.71 (0.34-40.01)	0.279
Concentric	14 (60.9%)	9 (81.8%)					
Eccentric/adjacent	9 (39.1%)	2 (18.2%)					
The final diagnosis							
Diagnosis of malignancy	11 (47.8%)	2 (18.2%)	0.139	0.24 (0.04-1.37)	0.085	-	-
Definite diagnosis of ILD	3 (13%)	9 (81.8%)	<0.001	30 (4.24-211.8)	<0.001	33.64 (4.75-272.4)	0.001
Sample size							
CB sample size (mm3)	36 (24-57.5)	40 (31.5-47.2)	0.926	0.99 (0.97-1.02)	0.739	1.01 (0.97-1.04)	0.713
FB sample size (mm3)	6 (4-9.5)	8 (1.3-11.5)	0.810	0.96 (0.85-1.07)	0.476	-	-

EBUS: endobronchial ultrasound; FB: forceps biopsy; CB: cryobiopsy; ILD: interstitial lung diseases; continue variable presented as median with interquartile range; DPLDs: diffuse pulmonary lung diseases; OR: odds ratio; CI: confidence interval

Table 6. Complications After Transbronchial Lung Forceps Biopsy and Transbronchial Lung Cryobiopsy

Patients, n=34	After biopsy
Complication	
Bleeding	
Grade 1	5 (14.7%)
Grade 2*	28 (82.3%)
Grade 3	0 (0%)
Grade 4	0 (0%)
Pneumothorax	2 (5.8%)

Grade 1: Suctioning of blood required for less than 1 minute.
Grade 2: Suctioning for more than 1 minute required or repeat wedging of the bronchoscope for persistent bleeding or instillation of cold saline, diluted vasoactive substances or thrombin.
Grade 3: Selective intubation with endotracheal tube (ETT) or balloon/bronchial blocker for less than 20 minutes, or premature interruption of the procedure.
Grade 4: Persistent selective intubation > 20 minutes or new admission to the ICU or PRBC transfusion or need for bronchial artery embolization or resuscitation.
*Prophylactic instillation of diluted norepinephrine was performed in most patients with mild bleeding.

Discussion

The current study showed that the addition of R-EBUS-guided TBLC to conventional TBLB increased the diagnostic yield from 44.1% to 70.6%, especially in patients with a diagnosis of ILD. In 11 patients with initially non-diagnostic specimens obtained by TBLB, a definite diagnosis was achieved after adding TBLC. Among these patients, 8 were ultimately diagnosed with ILD. Cryobiopsy provided larger tissue specimens than forceps biopsy (38 mm^3 vs 6 mm^3; $p < 0.001$), without uncontrolled complications such as near-fatal pneumothorax and bleeding.

Few studies have investigated R-EBUS-guided TBLC for diffuse lung infiltrates and PPLs. The novel method of combining R-EBUS and TBLC can be advantageous for patients with diffuse lung infiltrates and pulmonary masses/nodules by increasing the diagnostic yield. In 2013, Schuhmann *et al*. were the first to report the use of R-EBUS-guided TBLC in pulmonary masses/nodules. They reported that the specimen obtained by TBLC (11.17 mm^2) was significantly larger than that obtained by TBLB (4.69 mm^2) ($p < 0.001$). However, there was no significant difference in the diagnostic yield between TBLC (23/31; 74.2%) and TBLB (19/31; 61.3%) ($p = 0.42$) [6]. In addition, Armura *et al*. reported that TBLC could provide specimens of sufficient quantity and quality for DNA sequencing by Next Generation Sequencing (NGS), with diagnostic accuracy rates of 87% for TBLC and 82.6% for TBLB [17]. Hibare *et al*. reported diagnostic accuracy rates of 67.9% (19/28) in patients with PPLs with R-EBUS-guided TBLC and 75% (21/28) in those with R-EBUS-guided TBLB. The difference in diagnostic yield was not statistically significant ($p = 0.562$) [18]. However, Kho SS *et al*. reported that TBLC under R-EBUS guidance increased the diagnostic yield in eccentrically and adjacently orientated PPLs to 75%, compared to 48% obtained via forceps biopsy [13].

When noninvasive modalities such as laboratory data and imaging findings cannot be used to make a definite diagnosis, surgical lung biopsy (SLB) should be done following a multidisciplinary discussion on ILD, especially fibrotic ILD. TBLC has recently emerged as an alternative diagnostic tool, with lower mortality and morbidity compared with SLB [19], and a higher diagnostic yield than TBLB [5]. The diagnostic yield of TBLC needed to diagnose ILD has been reported to range from 66% to 86% [19-21]. A meta-analysis assessed the performance of TBLC for diagnosing diffuse lung in-

filtrate diseases, and showed a diagnostic yield of 72.9% with a mean tissue size of 23.4 mm2 [22]. The diagnostic yield seems to be reasonable, but safety concerns have been raised. Nevertheless, few studies have investigated R-EBUS-guided TBLC for ILD. Gnass *et al*. reported a diagnostic yield of 80% in patients with ILD using a combination of R-EBUS and TBLC [9]. Another study indicated that the diagnostic yield of R-EBUS with TBLC in patients with DPLDs was as high as 92.5% [12].

In the current study, the diagnostic yield increased from 44.1% with a forceps biopsy to 70.6% after adding cryobiopsy. In order to identify the patients who may benefit from TBLC, we divided them into 2 groups: (1) those with initially non-diagnostic specimens by forceps biopsy who then had a definite diagnosis after adding cryobiopsy; and (2) those who still had the same diagnostic results or non-diagnostic specimens after adding cryobiopsy. The only significant difference between the 2 groups was the proportion of ILD patients (81.8% in group 1 vs. 13% in group 2; $p < 0.001$). There were no significant differences in the type of image presentation (diffuse lung infiltrates or PPLs), characteristics of the EBUS image (concentric or eccentric/adjacent), lesion size, or tissue sample size, or in patients with lung malignancy between the 2 groups. Therefore, for patients suspected of having a diagnosis of ILD, cryobiopsy can increase the diagnostic yield. This is consistent with previous studies which showed a better diagnostic rate with TBLC than with TBLB in patients with ILD, but not in patients with pulmonary nodules/masses [6, 11, 23]. This may be because cryobiopsy provided a larger specimen than forceps biopsy in this study (38 mm3 vs 6 mm3; $p < 0.001$), which is also consistent with a previous study [22].

In the current study, 5 patients had non-specific pathological findings of chronic inflammation based on the forceps biopsy, and were ultimately diagnosed as having organizing pneumonia after adding cryobiopsy. We reviewed the pathologic picture of these patients, and the presence of Masson bodies in the cryobiopsy specimens was the key factor from which a definite diagnosis of organizing pneumonia was made. This can be explained by the fact that Masson bodies can be seen easily on larger cryobiopsy tissue specimens compared to forceps biopsy tissue specimens.

In reviewing the CT images of patients enrolled in our study, it was observed that those diagnosed with ILD presented various patterns, such as reticular, bilateral consolidations, or mass/nodules. The diverse range of CT image presentations in ILD might explain the absence of a significant difference in diagnostic yield between TBLB and TBLC, based on CT image characteristics. Although there was no statistically significant difference found in univariate analysis for CT image characteristics in diagnostic yield between TBLB and TBLC, a noticeable trend emerged. In patients who got different diagnoses between TBLB and TBLC, 81.8% exhibited diffuse lung infiltrates in CT images, while 18.2% showed nodules or masses in their CT images. It appeared that patients with CT images displaying diffuse lung infiltrates tended to benefit more in obtaining a diagnosis from TBLC. This outcome might be attributed to the limited number of patients in this study. A larger study with a higher number of cases is required for further investigation.

The complication rate of TBLC without R-EBUS for patients with ILD has been reported to be relatively high, with pooled estimates for moderate to severe bleeding and pneumo-

thorax of 39% and 12%, respectively [24]. Another study reported incidence rates of significant bleeding and pneumothorax of 14.2% and 9.4%, respectively [22]. Abdelghani R *et al*. reported the incidence of pneumothorax and moderate bleeding were 5% and 12.5%, respectively [12]. For patients with PPLs, the complication rate with TBLC has been reported to be relatively lower, compared to patients with ILD [11]. The purpose of combining R-EBUS guidance with TBLC is not only to reduce the bleeding rate by locating lung parenchyma without adjacent major vessels, but also to decrease the occurrence of pneumothorax.

Gnass *et al* reported a case series of 20 patients with ILD who underwent R-EBUS-guided TBLC, in which only 1 patient (1/20) had minor bleeding, and 1 (1/20) had pneumothorax [9]. In addition, the bleeding rate was lower than in those with ILD without R-EBUS-guided TBLC. In the current study, 2 patients (5.8%) had pneumothorax and required chest tube drainage, and 28 (82.3%) had Grade 2 bleeding, which was controlled by instillation of diluted norepinephrine or ice-cold saline. The complication rate in our study seems to be higher, which can be explained by the prophylactic instillation of diluted norepinephrine in the most of our patients, to reduce the severe bleeding after the procedure. Based on the newly developed bleeding scale (Nashville Bleeding Scale) [16], more of these patients were classified as having Grade 2 bleeding. In the current study, there were no near-fatal complications after receiving TBLC followed by TBLB with flexible bronchoscopy under R-EBUS guidance without fluoroscopy.

In this study, there were 2 patients in which only forceps biopsy was successful in making a definite diagnosis: 1 who was diagnosed with a fungal infection, and the other with adenocarcinoma. Both patients had larger specimens with cryobiopsy than with forceps biopsy. Dislocation of the cryoprobe is a possible explanation for these cases, because we did not recheck with EBUS before performing cryobiopsy. Therefore, we suspect that a technical error caused the negative cryobiopsy result in these 2 patients. In our protocol, we did not use a GS to locate the target lung lesion, which may have contributed to sampling errors. The use of TBLC or TBLB via a GS may overcome this issue.

There are several limitations to this study. First, it was performed at a single tertiary referral medical center and included a small number of patients. Therefore, the results may not be generalizable to other patient populations. Second, the study was retrospective in nature, and there may have been selection bias. Third, there was no control group because every patient received both a forceps biopsy and cryobiopsy under R-EBUS. Therefore, we could not differentiate safety data and ascribe the complication to one of the techniques. In addition, we could not conclude that R-EBUS-guided TBLB or TBLC could reduce the complication rate in patients with DPLDs. Fourth, prophylactic placement of a Fogarty balloon or bronchial blocker was recommended in TBLC in order to control bleeding, especially in cases with flexible bronchoscopy, when immediate tamponade was not possible [25-26]. However, the Fogarty balloon or a bronchial blocker were not available in our institution. To avoid severe bleeding, we not only used R-EBUS to locate the target lesions without a major blood vessel [27], but also used prophylactic instillation of diluted norepinephrine in the most of our patients. The life-threatening complication rate in

our study was low, and R-EBUS-guided TBLC appeared to be safe. Fifth, TBLC with fluoroscopic guidance is highly recommended to reduce the complication rate of pneumothorax [28], because we can know the proximity of the cryoprobe to the pleural surface, and the probe should be retracted 1 cm. However, fluoroscopy was not available in our institutions. We used R-EBUS to localize the optimal biopsy site by echogenic features. Only 2 patients had pneumothorax after the TBLC in our study. Chang *et al*. reported that R-EBUS-guided TBLC without fluoroscopy is a feasible technique to biopsy PPLs [10]. Finally, we did not use a GS to locate the target lung lesion in our protocol, which may have influenced the diagnostic rate with this novel method.

Conclusion

Compared to R-EBUS-guided TBLB, R-EBUS-guided TBLC in patients with DPLDs can increase the diagnostic yield due to the larger specimens and preserved architecture, particularly in patients with a diagnosis of ILD. The life-threatening complication rate was low in this study. R-EBUS guidance can be an alternative method to choose the optimal area for cryobiopsy at institutions without fluoroscopy. However, further large-scale prospective trials in a randomized setting are needed.

Acronyms

TBLC = transbronchial lung cryobiopsy; DPLDs = diffuse parenchymal lung diseases;

R-EBUS = radial probe-endobronchial ultrasound; TBLB = transbronchial lung forceps biopsy; ILD = interstitial lung disease; PPLs = peripheral pulmonary lesions; CT = computed tomography; EBUS = endobronchial ultrasound; GS= guide sheath; ETT= endotracheal tube.

Acknowledgements:

None

Funding:

None

Availability of data and materials:

The datasets used and/or analyzed during the current study are available from the corresponding author on a reasonable request.

Author contributions:

(I) Conception and design: CH Chen, CY Tu, BR Wu, WC Chen
(II) Administrative support: WC Liao, CY Tu, CH Chen,
(III) Provision of study materials or patients: CH Chen, WC Liao, CY Chen, BR Wu
(IV) Collection and assembly of data: WC Cheng, CH Chen, WC Chen
(IV) Data analysis and interpretation: CH Chen, WC Cheng
(V) Manuscript writing: YC Kuo, MF Shen, WC Cheng
(VI) Final approval of the manuscript: WC Cheng, MF Shen, BR Wu, WC Chen, WC Liao, CY Chen, CY Tu and CH Chen

Ethics approval and consent to participate:

The study has been approved by the China Medical University Hospital Institutional Review Board (CMUH103-REC1-112), and written consent was obtained from all patients.

Consent for publication:

Not applicable.

Competing interests:

The authors declare that they have no competing interests.

References

1. Franke K-J, Theegarten D, Von Weyhern CH, *et al*. Prospective controlled animal study on biopsy sampling with new flexible cryoprobes versus forceps: evaluation of biopsy size, histological quality and bleeding risk. Respiration 2010; 80(2): 127-132.
2. Hernández-González F, Lucena CM, Ramírez J, *et al*. Cryobiopsy in the diagnosis of diffuse interstitial lung disease: yield and cost-effectiveness analysis. Archivos de Bronconeumología (English Edition) 2015; 51(6): 261-267.
3. Fruchter O, Fridel L, Rosengarten D, *et al*.Transbronchial cryobiopsy in lung transplantation patients: first report. Respirology 2013; 18(4): 669-673.
4. Hagmeyer L, Theegarten D, Wohlschläger J, *et al*. The role of transbronchial cryobiopsy and surgical lung biopsy in the diagnostic algorithm of interstitial lung disease. Clin Respir J 2016; 10(5): 589-595.
5. Pajares V, Puzo C, Castillo D, *et al*. Diagnostic yield of transbronchial cryobiopsy in interstitial lung disease: a randomized trial. Respirology 2014; 19(6): 900-906.
6. Schuhmann M, Bostanci K, Bugalho A, *et al*. Endobronchial ultrasound-guided cryobiopsies in peripheral pulmonary lesions: a feasibility study. Eur Respir J 2014; 43(1): 233-239.
7. DiBardino DM, Haas AR, Lanfranco AR, *et al*. High complication rate after introduction of transbronchial cryobiopsy into clinical practice at an academic medical center. Ann Am Thorac Soc 2017; 14(6): 851-857.
8. Berim IG, Saeed AI, Awab A, *et al*. Radial probe ultrasound-guided cryobiopsy. J Bronchol Interv Pulmonol 2017; 24(2): 170-173.
9. Gnass M, Filarecka A, Pankowski J, *et al*. Transbronchial lung cryobiopsy guided by endobronchial ultrasound radial miniprobe in interstitial lung diseases: preliminary results of a prospective study. Pol Arch Intern Med 2018; 128(4): 259-262.
10. Chang CH, Lee CS, Li SH, *et al*. Feasibility of radial endobronchial ultrasound-guided bronchoscopic cryobiopsy without fluoroscopy for lung parenchymal lesions. Can Respir J 2017; 2017: 7170687.
11. Gupta A, Youness H, Dhillon SS, *et al*. The value of using radial endobronchial ultrasound to guide transbronchial lung cryobiopsy. J Thorac Dis 2019; 11(1): 329-334.
12. Abdelghani R, Thakore S, Kaphle U, *et al*. Radial endobronchial ultrasound-guided transbronchial cryobiopsy. J Bronchol Intervent Pulmonol 2019; 26: 245-249.
13. Kho SS, Chan SK, Yong MC, *et al*. Performance of transbronchial cryobiopsy in eccentrically and adjacently orientated radial endobronchial ultrasound lesions. ERJ Open Res 2019; 5(4): 00135-2019.
14. Chen A, Chenna P, Loiselle A, *et al*. Radial probe endobronchial ultrasound for peripheral pulmonary lesions, a 5-year institutional experience. Ann Am Thorac Soc 2014; 11:578-582.
15. Izumo T, Sasada S, Chavez C, *et al*. Radial endobronchial ultrasound images for ground-glass opacity pulmonary lesions. Eur Respir J 2015; 45: 1661-1668
16. Folch EE, Mahajan AK, Oberg CL, *et al*. Standardized definitions of bleeding after transbronchial lung biopsy: a Delphi Consensus Statement from the Nashville Working Group. Chest 2020; 158(1): 393-400.
17. Arimura K, Tagaya E, Akagawa H, *et al*. Cryobiopsy with endobronchial ultrasonography using a guide sheath for peripheral pulmonary lesions and DNA analysis by next generation sequencing and rapid on-site evaluation. Respir Investig 2019; 57(2): 150-156.
18. Hibare KR, Goyal R, Nemani C, *et al*. Radial endobronchial ultrasound for the diagnosis of bronchoscopically invisible lesions: first case series from India. Lung India 2017; 34(1): 43-46.

19. Ravaglia C, Bonifazi M, Wells AU, *et al*. Safety and diagnostic yield of transbronchial lung cryobiopsy in diffuse parenchymal lung diseases: a comparative study versus video-assisted thoracoscopic lung biopsy and a systematic review of the literature. Respiration 2016; 91(3): 215-227.
20. Ramaswamy A, Homer R, Killam J, *et al*. Comparison of transbronchial and cryobiopsies in evaluation of diffuse parenchymal lung disease. J Bronchol Interv Pulmonol 2016; 23(1): 14-21.
21. Bango-Alvarez A, Ariza-Prota M, Torres-Rivas H, *et al*. Transbronchial cryobiopsy in interstitial lung disease: experience in 106 cases - how to do it. ERJ Open Res 2017; 3(1): 00148-2016.
22. Sethi J, Ali MS, Mohananey D, *et al*. Are transbronchial cryobiopsies ready for prime time?: a systematic review and meta-analysis. J Bronchol Interv Pulmonol 2019; 26(1): 22-32.
23. Brar G, Chee A, Hergott C, *et al*. Incremental yield of cryobiopsy on peripheral endobronchial ultrasound sampling of peripheral lung nodules. Chest 2017; 152(4): A862.
24. Johannson KA, Marcoux VS, Ronksley PE, *et al*. Diagnostic yield and complications of transbronchial lung cryobiopsy for interstitial lung disease. A systematic review and metaanalysis. Ann Am Thorac Soc 2016; 13(10): 1828-1838.
25. Colella S, Haentschel M, Shah P, *et al*. Transbronchial lung cryobiopsy in interstitial lung diseases: best practice. Respiration 2018; 95(6): 383-391.
26. Hagmeyer L, Theegarten D, Wohlschlager J, *et al*. Transbronchial cryobiopsy in fibrosing interstitial lung disease: modifications of the procedure lead to risk reduction. Thorax 2019, 74(7): 711-714.
27. Hetzel J, Maldonado F, Ravaglia C, *et al*. Transbronchial cryobiopsies for the diagnosis of diffuse parenchymal lung diseases: expert statement from the cryobiopsy working group on safety and utility and a call for standardization of the procedure. Respiration 2018; 95(3): 188-200
28. Dhooria S, Mehta RM, Srinivasan A, *et al*. The safety and efficacy of different methods for obtaining transbronchial lung cryobiopsy in diffuse lung diseases. Clin Respir J 2018; 12(4): 1711-1720.

Does High-Dose Intravenous Vitamin C Improve the Outcomes of Patients with Septic Shock? A Case Series Report

Juo-Chen Ting[1], Chieh-Jen Wang[1,*], Chao-Hsien Chen[1], Jou-Chun Wu[1], Mei-ling Lin[2], Tai-Ting Su[2], Chang-Yi Lin[1]

Background and objective: Septic shock remains a major cause of morbidity and mortality in intensive care units, despite the availability of therapeutic interventions. Some preliminary studies have suggested that high doses of intravenous vitamin C (IVVC) combined with hydrocortisone and thiamine may improve clinical outcomes. However, subsequent randomized trials have reported conflicting results. The aim of this study was to present our experience in using high-dose IVVC for patients with septic shock.

Methods: In this retrospective observational study, we enrolled patients diagnosed with septic shock who received high-dose IVVC within 3 days of the diagnosis. The primary outcomes were hospital mortality and severity of organ dysfunction on Day 3.

Results: A total of 26 patients were enrolled. These patients had higher mortality than expected and limited improvement in organ function on Day 3 after enrollment. Moreover, patients who received IVVC ≥ 6 g/day had worse outcomes.

Conclusion: The routine use of high-dose vitamin C is not recommended in patients with septic shock. ***(Thorac Med 2024; 39: 119-128)***

Key words: Vitamin C; thiamine; hydrocortisone; critical illness; septic shock; mortality

Introduction

The mortality rate of septic shock patients remains high, despite the availability of several interventions [1]. Patients with sepsis have reduced serum levels of antioxidants, most notably vitamin C [2]. Physiologically, vitamin C downregulates pro-inflammatory cytokines, maintains the endothelial barrier, and facilitates the production of catecholamines, vasopressin, and cortisol [3]. Considering its low level in critically ill patients, vitamin C supplementation in patients with septic shock could theoretically be beneficial. Malik *et al*. [4] first reported the therapeutic efficacy of high-dose intravenous vitamin C (IVVC) in combination with thiamine and hydrocortisone in severe

[1]Division of Pulmonary, Department of Internal Medicine, MacKay Memorial Hospital, Taipei City, Taiwan, [2]Department of Nursing, MacKay Memorial Hospital, New Taipei City, Taiwan
Address reprint requests to: Dr. Chieh-Jen Wang, Division of Pulmonary, Department of Internal Medicine, MacKay Memorial Hospital, Taipei City, Taiwan

sepsis patients. They found that this combination therapy could reduce hospital mortality and prevent progressive organ dysfunction. However, subsequent randomized-controlled trials (RCTs) [5-9] have reported conflicting results. Several RCTs [6-9] showed no significant reduction in mortality, and a large RCT [5] even reported worse outcomes in patients with septic shock who received high-dose IVVC. In contrast, recent meta-analyses [10-14] have shown that high-dose IVVC as monotherapy may be associated with improved overall survival. Due to these conflicting results, the use of IVVC remains controversial.

At MacKay Memorial Hospital (MMH), the combination of IVVC, thiamine, and steroids, referred to as the SBC combination, is used in shock resuscitation for selected patients. The Shockway algorithm shown in Figure 1 is the standard management protocol for patients with circulatory shock at our hospital. Briefly, all patients with shock and/or metabolic failure receive adequate fluid resuscitation and vasopressor/inotropic support until these interventions fail to resolve the shock status. Patients remaining at this stage are considered refractory to usual circulatory manipulation, and subsequently the SBC combination becomes a treatment option. In this study, we retrospectively analysed the clinical outcomes of septic shock patients who received high-dose IVVC.

Methods

In this retrospective observational study, we enrolled patients diagnosed with septic shock who received high-dose IVVC (defined as ≥ 1 g per day). Septic shock was defined as having an infection leading to shock status with lactate ≥ 2 mmol/L despite adequate fluid resuscitation, and requiring vasopressors for hemodynamic support [15]. Patients not meeting the definition of septic shock or having concomitant shock due to other etiologies were excluded. Patients receiving IVVC beyond 3 days after the onset of septic shock and those who were not cared for by internal medicine specialists were also excluded.

The primary outcomes were hospital mortality and severity of persistent organ dysfunction (defined as the Sequential Organ Failure Assessment (SOFA) score on Day 3). The secondary outcomes were length of intensive care unit (ICU) stay among those who survived, duration of vasopressor use, and use of continuous renal replacement therapy (CRRT). Changes in the partial pressure of arterial oxygen (PaO_2)/fraction of inspired oxygen (FiO_2) ratio from Day 0 to Day 3 were also used to evaluate organ dysfunction.

The chi-squared test or Fisher's exact test was used to compare the frequencies of categorical variables. Continuous variables with a normal distribution were reported as mean ± standard deviation, and non-normally distributed variables were reported as median (interquartile range). The normality of the distribution of continuous variables was examined using the Shapiro–Wilk test. Two normally distributed continuous variables were compared using independent samples t-tests or paired t-tests, if related. The Mann-Whitney U test and Wilcoxon test were used to compare 2 groups of non-normally distributed variables. All p-values were 2-sided, and a value < 0.05 was considered statistically significant. All analyses were performed using MedCalc version 20.016 for Windows (MedCalc Software Ltd, Ostend, Belgium).

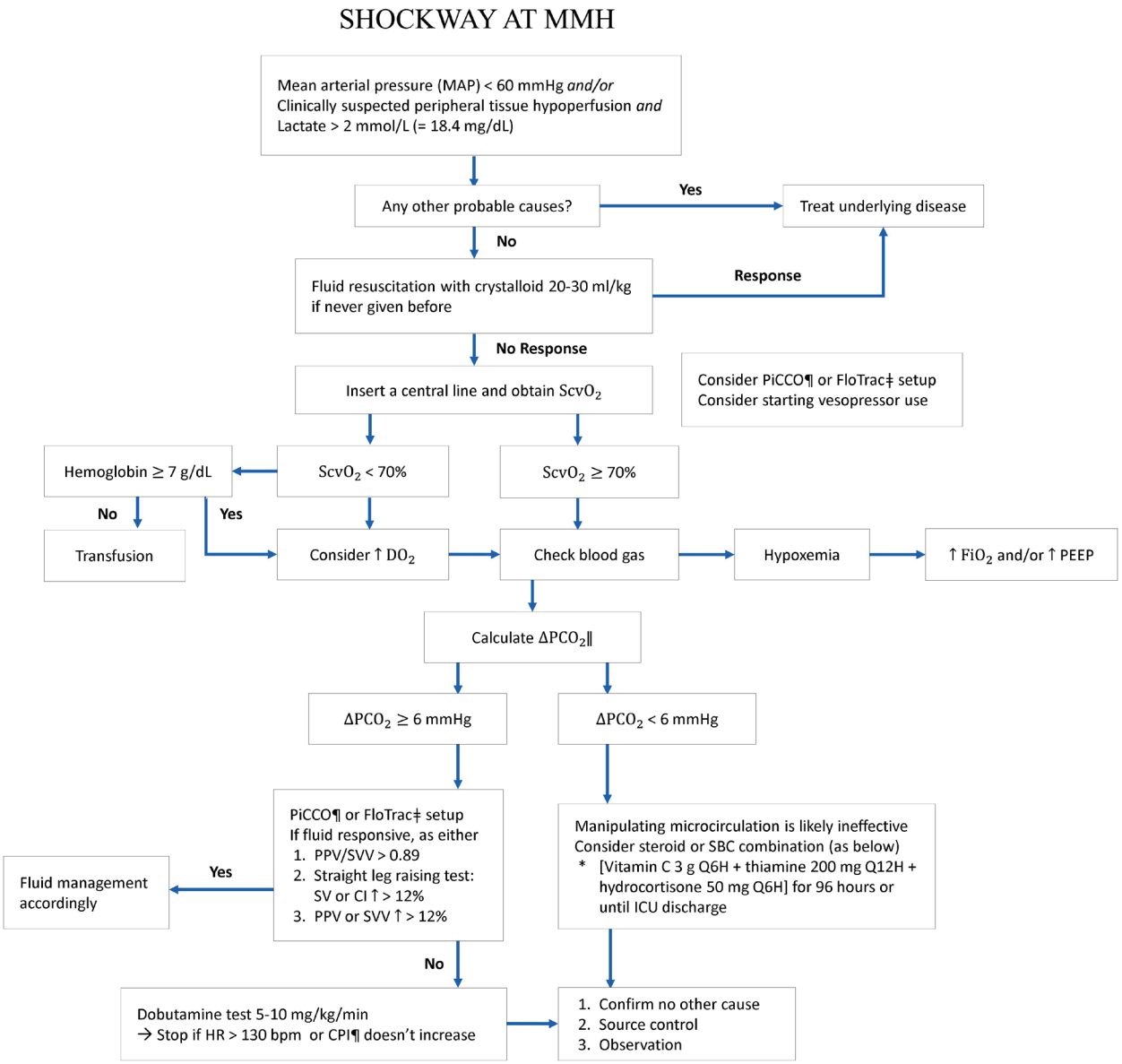

Fig. 1. Shockway Algorithm. Shock patients who are refractory to usual circulatory manipulation would be considered to receive the SBC combination*. Acronyms: $ScvO_2$, central venous oxygen saturation; DO_2, oxygen delivery; FiO_2, fraction of inspired oxygen; PEEP, positive end expiratory pressure; Q6H, every 6 hours; Q12H, every 12 hours.

* SBC combination = [Vitamin C 3 g Q6H + thiamine 200 mg Q12H + hydrocortisone 50 mg Q6H] for 96 hours or until ICU discharge.

¶ PiCCO (Pulse index Continuous Cardiac Output) is a cardiac output monitor that combines pulse contour analysis and a transpulmonary thermodilution technique. Cardiac output is the product of the heart rate (HR) and the stroke volume (SV), and cardiac index (CI) is the cardiac output divided by the body surface area. Stroke volume variation (SVV) and pulse pressure variation (PPV) are percentage values predicting fluid responsiveness. Cardiac power index (CPI) is the product of pressure (MAP) and flow (CI), representing the power of left ventricular cardiac output.

‡ FloTrac is a cardiac output monitor that uses pulse contour analysis to calculate cardiac output and other derived parameters, including stroke volume (SV), stroke volume variation (SVV), and pulse pressure variation (PPV).

‖ ΔPCO_2 is the central venous-to-arterial CO_2 difference, which is calculated from simultaneous sampling of central venous blood from a central vein catheter and arterial blood. An increased ΔPCO_2 ($\geq$ 6 mmHg) suggests that blood flow might not be sufficient to remove global CO_2 production from peripheral circulation, and thus could be used to guide fluid management.

Results

From January 1, 2021 to July 29, 2022, 61 patients who received high-dose IVVC for various purposes were identified in the MMH database. Thirty-five of these patients did not meet the inclusion criteria and were excluded. Among the 26 enrolled patients, 12 received IVVC < 6 g/day, and 14 received IVVC ≥ 6 g/day (see Figure 2). Steroids and thiamine were administered to most patients, except for 1 patient who did not receive thiamine and 3 who did not receive either. The patients' characteristics are presented in Table 1 and the clinical outcomes are shown in Table 2. All of the patients received mechanical ventilation on ICU admission. The hospital mortality rate was 73.1%, with a median change in SOFA score on Day 3 of only 1.3. The patients who died tended to be younger, have a higher SOFA score and lower inflammatory markers on day 0, and receive a higher dose of IVVC (see Table 1). However, none of these reached statistical significance. The demand for vasopressors gradually decreased and the PaO_2/FiO_2 ratio gradually increased from Day 0 to Day 3 (see Figure 3). When comparing the patients who received IVVC ≥ 6 g/day and < 6 g/day, there were no significant differences in baseline age, sex, comorbidities, and disease severity (SOFA score and Acute Physiologic and Chronic Health Evaluation [APACHE] II score), but a higher mortality rate (85.7%, p=0.1904), longer vasopressor use (72.5 days, p=0.1984), and longer ICU stay (17 days, p=0.3809) were found in those who received IVVC ≥ 6 g/day (Figure 4). Again, none of these reached statistical significance.

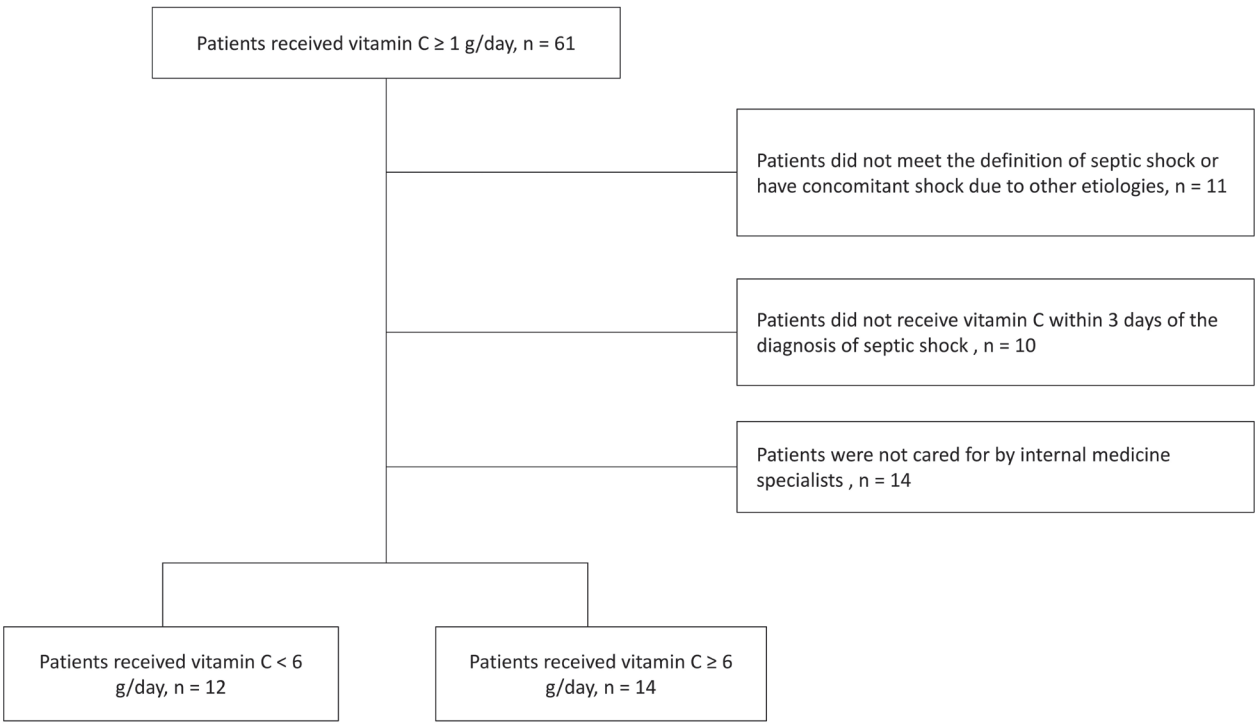

Fig. 2. Study flowchart

Table 1. Patient Characteristics

	Total (n=26)	Survivors (n=7)	Non-survivors (n=19)	*p* value
Age, year, mean ± SD	67.8±10.3	74.1±9.4	65.5±9.9	0.0579
Male/female, no.	15/11	4/3	11/8	
SOFA score, mean ± SD	10.8±3.1	9.9±1.3	11.2±3.5	0.1677
APACHE II score, mean ± SD	25.7±4.8	25.6±5.5	25.7±4.6	0.92
Dose of vitamin C, g/day, median (IQR)	6.0 (2.0-8.0)	2.0 (2.0-5.3)	6.0 (2.1-11.0)	0.0948
Comorbidity, no. (%)				
Hypertension	13 (50.0%)	4 (57.1%)	9 (47.4%)	>0.9999
Diabetes mellitus	6 (23.1%)	1 (14.3%)	5 (26.3%)	>0.9999
CKD stage 5 or ESRD	2 (7.7%)	0 (0.0%)	2 (10.5%)	>0.9999
COPD	2 (7.7%)	0 (0.0%)	2 (10.5%)	>0.9999
Coronary artery disease	4 (15.4%)	2 (28.6%)	2 (10.5%)	0.287
Heart failure	2 (7.7%)	2 (28.6%)	0 (0.0%)	0.0646
Cerebrovascular disease	2 (7.7%)	0 (0.0%)	2 (10.5%)	>0.9999
Liver cirrhosis	2 (7.7%)	1 (14.3%)	1 (5.3%)	0.4738
Cancer	10 (38.5%)	3 (42.9%)	7 (36.8%)	>0.9999
Laboratory data				
CRP, mg/dL, mean ± SD	19.8±13.7	23.1±10.3	18.4±14.9	0.461
WBC, 10^3/uL, median (IQR)	14.55 (4.70-16.8)	15.3 (14.67-20.72)	10.10 (12.25-16.70)	0.0994
Procalcitonin, ng/mL, median (IQR)	15.9 (1.7-61.0)	20.5 (4.0-129.1)	9.3 (1.7-58.5)	0.495
Lactate, mg/dL, median (IQR)	31.8 (24.5-77.8)	41.3 (24.9-59.6)	31.7 (24.6-83.0)	0.8851
Infection focus, no (%)				
Pneumonia	14	2 (28.6%)	12 (63.2%)	
Intra-abdominal infection	9	4 (57.1%)	5 (26.3%)	
Urinary tract infection	3	1 (14.3%)	2 (10.5%)	

Acronyms: SD, standard deviation; SOFA, Sequential Organ Failure Assessment; APACHE, Acute Physiologic and Chronic Health Evaluation; IQR, interquartile range; CKD, chronic kidney disease; ESRD, end-stage renal disease; COPD, chronic obstructive pulmonary disease; ABG, arterial blood gas; CRP, C-reactive protein; WBC, white blood cell.

* SOFA scores were calculated from the worst values corresponding to 6 organ systems, ranging from 0 to 24, with higher scores indicating more severe organ dysfunction.

¶ APACHE II scores range from 0 to 71, with higher scores indicating greater disease severity and a higher risk of death.

Table 2. Primary and Secondary Outcomes

Primary Outcomes	**Total (n = 26)**
Hospital mortality, no. (%)	19 (73.1)
Change in SOFA score on day 3, mean ± SD	1.3 ± 5.0
Secondary Outcomes	
ICU LOS, median (IQR), day	15 (8.8-25)
Duration of vasopressor use, median (IQR), hour	54 (34-91)
CRRT use, no. (%)	8 (30.8)

Acronyms: SOFA, Sequential Organ Failure Assessment; SD, standard deviation; ICU, intensive care unit; LOS, length of stay; IQR, interquartile range; CRRT, continuous renal replacement therapy.

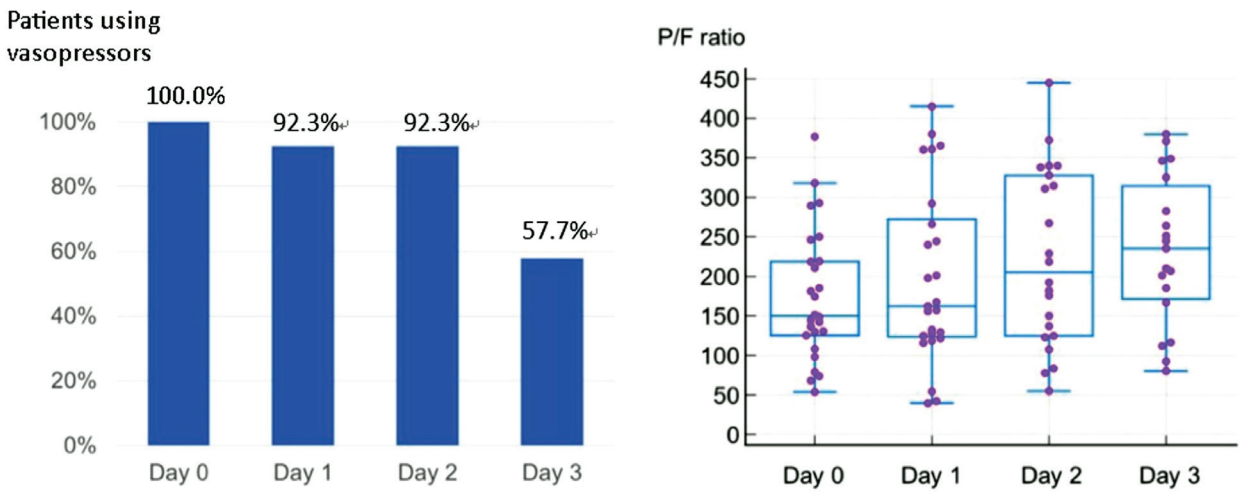

Fig. 3. Left, percentage of vasopressor use. Right, PiO_2/FiO_2 (P/F) ratio from Day 0 to Day 3, median and interquartile range.

Discussion

The mortality rate among our patients was high, and there was limited improvement in the SOFA score on Day 3, reflecting minimal effects on organ improvement. One possible explanation for the poor outcomes may be related to patient selection. The enrolled patients followed the Shockway algorithm during hospitalization, indicating that they had refractory septic shock despite adequate fluid resuscitation and vasopressor support before IVVC treatment. This may have contributed to selection bias, and consequently the higher mortality rate. Nevertheless, our findings are consistent with recent RCTs [5-9], which demonstrated no beneficial effect with vitamin C use, whether as monotherapy or in combination therapy, in adult patients with septic shock.

To date, the LOVIT trial [5] is the largest RCT on IVVC in septic patients. It enrolled 863 patients and randomized them to receive

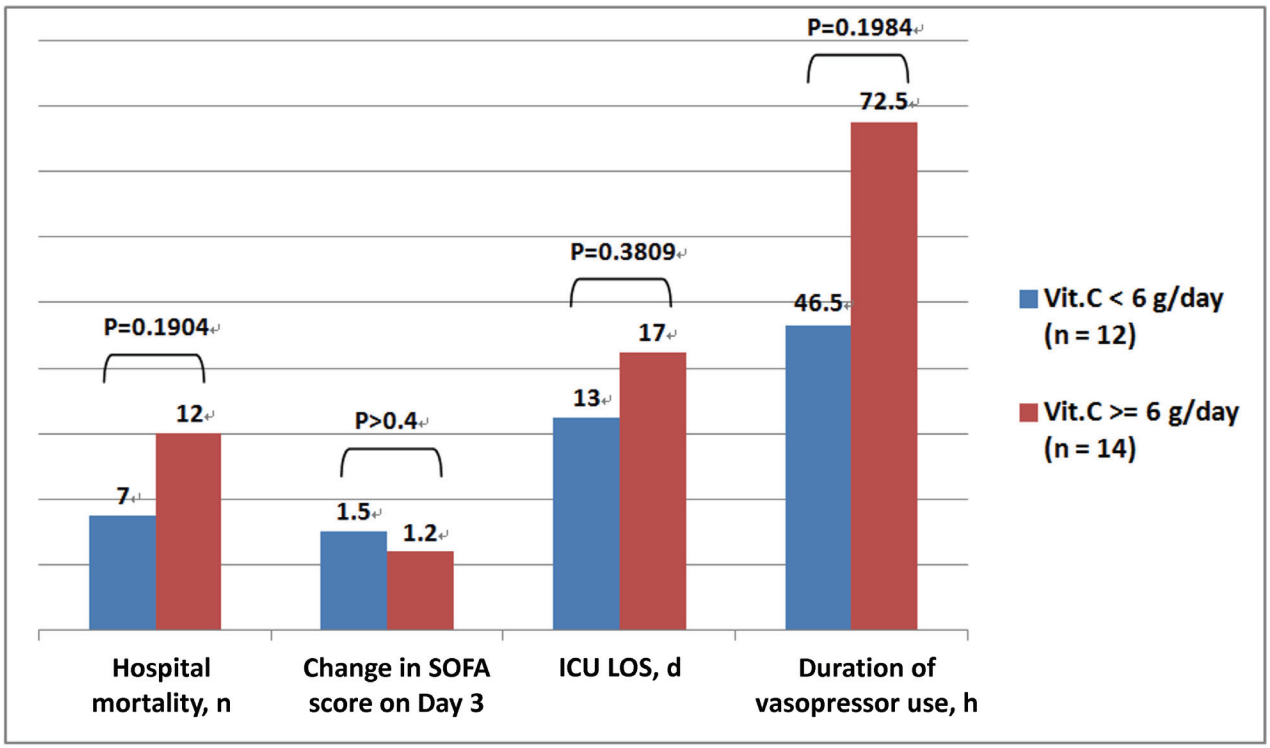

Fig. 4. Comparison of patients who received vitamin C < 6 g/day and those who received ≥ 6 g/day. This shows a higher mortality rate, longer vasopressor use, and longer ICU stay for those receiving vitamin C of ≥ 6 g/day, though none achieved statistical significance. Acronyms: SOFA, Sequential Organ Failure Assessment; ICU, intensive care unit; LOS, length of stay; Vit.C, vitamin C.

either 200 mg/kg/day IVVC or placebo for 4 days. They found that the patients who received IVVC had a higher risk of death or persistent organ dysfunction at 28 days than those who received the placebo. However, recent meta-analyses [10-14] have suggested that IVVC as monotherapy was associated with a significant reduction in overall mortality. Due to these conflicting results, the use of IVVC remains controversial. Hence, the current Surviving Sepsis campaign guidelines [16] do not recommend IVVC in adults with sepsis or septic shock. The European Society for Clinical Nutrition and Metabolism (ESPEN) guideline [17] on clinical nutrition in intensive care also does not recommend IVVC without proof of vitamin C deficiency. The American Society for Parenteral and Enteral Nutrition (ASPEN) guidelines [18] do not specifically comment on the supplementation of single vitamins, but a more detailed consideration of this topic has been proposed.

Theoretically, vitamin C supplementation should have many beneficial effects in critically ill patients [3], however real-world data do not support its use. The possible side effects of vitamin C include nephrolithiasis [19], acute kidney injury [20], acute hemolysis [21], and hypoglycemia [22]. However, since very few events have been reported [23], these complications are less likely to contribute to the worse outcomes in IVVC treatment, as demonstrated by the LOVID trial [5]. Some researchers have proposed the idea of a ‘‘rebound effect’’ due to the abrupt termination of high-dose IVVC

[24-25]. Hemila and Chalker [26] conducted a secondary analysis of the LOVIT trial [5], and found that the increased mortality in the vitamin C arm was not explained by ongoing vitamin C administration, but by the abrupt termination of vitamin C treatment. This suggests that high-dose vitamin C per se may not be harmful, and that a tapered dose is possibly needed following high-dose administration of vitamin C. Further studies are warranted to verify this issue.

The debate over whether combination therapy or vitamin C monotherapy is superior also remains controversial. In experimental settings, adding steroids to IVVC has shown a synergistic effect in reducing inflammation by increasing the expression of sodium-coupled vitamin C transporter 2, thereby facilitating the uptake of vitamin C into cells [27-28]. The addition of thiamine to the combination aims to prevent oxalate accumulation, a risk factor for nephrolithiasis secondary to calcium oxalate stones [29]. Thiamine deficiency is also common in septic patients and is associated with increased mortality [30]. Therefore, combination treatment was initially adopted by Malik *et al* [4], and later in several RCTs [7-9]. However, recent meta-analyses [10-14] have shown a mortality benefit only with IVVC monotherapy, but not combination therapy. In addition, Lee and colleagues [11] found that this mortality benefit was observed only in patients with a higher baseline mortality risk. In other words, IVVC monotherapy may be beneficial only when the patient is severely ill. Even though our patients had a very high baseline risk of mortality, as indicated by an average SOFA score > 10 on Day 0, there was barely any survival benefit following IVVC, possibly because the patients received combination therapy, rather than vitamin C monotherapy. Nevertheless, future studies are needed to confirm the treatment effect of IVVC in patients with different baseline risks of mortality.

In this study, we observed that patients who received IVVC ≥ 6 g/day had an increased mortality rate and prolonged organ dysfunction compared to those who received IVVC < 6 g/day. This raises the question of the optimal dose in high-dose IVVC therapy. Previous studies have used heterogeneous methodologies and variable dosing, such as 50 mg/kg every 6 hours [5], 1.5-2 g every 6 hours [7-9], or a 1 g bolus followed by continuous infusion at 0.25 g/h [6], with durations ranging up to 4-5 days or until discharge from the ICU or death [5-9]. Subgroup analyses in recent meta-analyses [10-11] have failed to demonstrate different treatment effects based on the dose, timing, and duration of IVVC treatment. Nevertheless, a component network meta-analysis [14] conducted to assess whether vitamin C at various doses could improve patient outcomes compared very high-dose (≥ 12 g/day), high-dose (< 12 g/day, ≥ 6 g/day), and non-high-dose (< 6 g/day) vitamin C treatment, and found that high-dose and very-high-dose vitamin C were associated with lower mortality, a result in contrast to our findings. However, the certainty was low due to the small size of the study population in these 2 groups. This suggests that the effect of IVVC in critically ill patients has yet to be determined and might be dose-dependent.

There are several limitations to this study. First, it was a retrospective study with a small sample size. Second, we did not exclude patients receiving palliative care, such as those who refused hemodialysis for acute renal failure. Third, as mentioned earlier, the enrolled patients had a high risk of mortality before IVVC treatment, leading to a certain degree of selection bias. Finally, the enrolled patients did

not strictly receive the standard SBC regimen, allowing them to receive a variable dose of vitamin C, as long as it was ≥ 1 g per day.

In conclusion, we enrolled patients with septic shock who received high-dose IVVC, and found no improvement in mortality after treatment, especially in those who received IVVC ≥ 6 g/day. Improvement in organ dysfunction was observed; however, it did not reach statistical significance. Therefore, we conclude that the routine use of vitamin C in patients with septic shock is not recommended. Nevertheless, it remains possible that a clinically defined subgroup would respond to vitamin C treatment, given proper timing, dosing, and treatment course. Even though many studies have been conducted to explore the use of vitamin C, many issues remain unresolved, and further investigations are warranted.

Acknowledgements:

We are grateful to Dr. Malcolm Higgins for proofreading of the manuscript.

References

1. Liu V, Escobar GJ, Greene JD, *et al*. Hospital deaths in patients with sepsis from 2 independent cohorts. JAMA 2014 Jul 2; 312(1): 90-2. doi: 10.1001/jama.2014.5804. PMID: 24838355.
2. Carr AC, Rosengrave PC, Bayer S, *et al*. Hypovitaminosis C and vitamin C deficiency in critically ill patients despite recommended enteral and parenteral intakes. Crit Care 2017 Dec 11; 21(1):300. doi: 10.1186/s13054-017-1891-y. PMID: 29228951; PMCID: PMC5725835.
3. Wilson JX. Mechanism of action of vitamin C in sepsis: ascorbate modulates redox signaling in endothelium. Biofactors 2009 Jan-Feb; 35(1):5-13. doi: 10.1002/biof.7. PMID: 19319840; PMCID: PMC2767105.
4. Marik PE, Khangoora V, Rivera R, *et al*. Hydrocortisone, vitamin C, and thiamine for the treatment of severe sepsis and septic shock: a retrospective before-after study. Chest 2017; 151(6): 1229-1238. doi:10.1016/j.chest.2016.11.036
5. Lamontagne F, Masse MH, Menard J, *et al*. Intravenous vitamin C in adults with sepsis in the intensive care unit. N Engl J Med 2022; 386(25):2387-2398. doi:10.1056/NEJMoa2200644
6. Wacker DA, Burton SL, Berger JP, *et al*. Evaluating vitamin C in septic shock: a randomized controlled trial of vitamin C monotherapy. Crit Care Med 2022; 50(5):e458-e467. doi:10.1097/CCM.0000000000005427
7. Fujii T, Luethi N, Young PJ, *et al*. Effect of vitamin C, hydrocortisone, and thiamine vs hydrocortisone alone on time alive and free of vasopressor support among patients with septic shock: the VITAMINS Randomized Clinical Trial. JAMA 2020; 323(5):423–431. doi: 10.1001/jama.2019.22176
8. Sevransky JE, Rothman RE, Hager DN, *et al*. Effect of vitamin C, thiamine, and hydrocortisone on ventilator- and vasopressor-free days in patients with sepsis: the VICTAS Randomized Clinical Trial. JAMA 2021; 325(8): 742-750. doi:10.1001/jama.2020.24505
9. Lyu QQ, Zheng RQ, Chen QH, *et al*. Early administration of hydrocortisone, vitamin C, and thiamine in adult patients with septic shock: a randomized controlled clinical trial. Crit Care 2022 Sep 28; 26(1):295. doi: 10.1186/s13054-022-04175-x. PMID: 36171582; PMCID: PMC9520942.
10. Patel JJ, Ortiz-Reyes A, Dhaliwal R, *et al*. IV vitamin C in critically ill patients: a systematic review and meta-analysis. Crit Care Med 2022; 50(3): e304-e312. doi:10.1097/CCM.0000000000005320
11. Lee ZY, Ortiz-Reyes L, Lew CCH, *et al*. Intravenous vitamin C monotherapy in critically ill patients: a systematic review and meta-analysis of randomized controlled trials with trial sequential analysis. Ann Intensive Care 2023 Mar 7; 13(1): 14. doi: 10.1186/s13613-023-01116-x. PMID: 36882644; PMCID: PMC9990974.
12. Radke DI, Homayr AL, Stoppe C, *et al*. Vitamin C in critical illness: end of the story or still a place? Curr Opin Crit Care 2023 Aug 1; 29(4): 339-345. doi: 10.1097/MCC.0000000000001054. Epub 2023 Jun 9. PMID: 37306524.
13. Wen C, Li Y, Hu Q, *et al*. IV vitamin C in sepsis: a latest

systematic review and meta-analysis. Int J Clin Pract 2023 Jan 24; 2023:6733465. doi: 10.1155/2023/6733465. PMID: 36743822; PMCID: PMC9889164.

14. Fujii, T., Salanti, G., Belletti, A. *et al*. Effect of adjunctive vitamin C, glucocorticoids, and vitamin B1 on longer-term mortality in adults with sepsis or septic shock: a systematic review and a component network meta-analysis. Intensive Care Med 2022; 48:16–24. https://doi.org/10.1007/s00134-021-06558-0
15. Singer M, Deutschman CS, Seymour CW, *et al*. The third international consensus definitions for sepsis and septic shock (Sepsis-3). JAMA 2016; 315(8):801–810. doi:10.1001/jama.2016.0287
16. Evans L, Rhodes A, Alhazzani W, *et al*. Surviving sepsis campaign: international guidelines for management of sepsis and septic shock 2021. Intensive Care Med 2021 Nov; 47(11):1181-1247. doi: 10.1007/s00134-021-06506-y. Epub 2021 Oct 2. PMID: 34599691; PMCID: PMC8486643.
17. Montejo JC, Pichard C, Preiser JC, *et al*. ESPEN guideline on clinical nutrition in the intensive care unit. Clin Nutr 2019 Feb; 38(1): 48-79. doi: 10.1016/j.clnu.2018.08.037. Epub 2018 Sep 29. PMID: 30348463.
18. Compher C, Bingham AL, McCall M, *et al*. Guidelines for the provision of nutrition support therapy in the adult critically ill patient: The American Society for Parenteral and Enteral Nutrition. JPEN J Parenter Enteral Nutr 2022 Jan; 46(1):12-41. doi: 10.1002/jpen.2267. Epub 2022 Jan 3. Erratum in: JPEN J Parenter Enteral Nutr. 2022 Aug;46(6):1458-1459. PMID: 34784064.
19. de Grooth HJ, Manubulu-Choo WP, Zandvliet AS, *et al*. Vitamin C pharmacokinetics in critically ill patients: a randomized trial of four IV regimens. Chest 2018 Jun; 153(6):1368-1377. doi: 10.1016/j.chest.2018.02.025. Epub 2018 Mar 6. PMID: 29522710.
20. Kellum JA, Lameire N, Aspelin P, *et al*. KDIGO clinical practice guideline for acute kidney injury. Kidney Int Suppl 2012; 2:Suppl 1: 1-38.
21. Rees DC, Kelsey H, Richards JD. Acute haemolysis induced by high dose ascorbic acid in glucose-6-phosphate dehydrogenase deficiency. BMJ 1993 Mar 27; 306(6881):841-2. doi: 10.1136/bmj.306.6881.841. PMID: 8490379; PMCID: PMC1677333.
22. Tang Z, Du X, Louie RF, *et al*. Effects of drugs on glucose measurements with handheld glucose meters and a portable glucose analyzer. Am J Clin Pathol 2000 Jan; 113(1): 75-86. doi: 10.1309/QAW1-X5XW-BVRQ-5LKQ. PMID: 10631860.
23. Yanase F, Fujii T, Naorungroj T, *et al*. Harm of IV high-dose vitamin C therapy in adult patients: a scoping review. Crit Care Med 2020; 48(7): E620-8.
24. Anderson TW, Suranyi G, Beaton GH. The effect on winter illness of large doses of vitamin C. Can Med Assoc J 1974 Jul 6; 111(1): 31-6. PMID: 4601508; PMCID: PMC1947567.
25. Omaye ST, Skala JH, Jacob RA. Plasma ascorbic acid in adult males: effects of depletion and supplementation. Am J Clin Nutr 1986 Aug; 44(2): 257-64. doi: 10.1093/ajcn/44.2.257. PMID: 3728363.
26. Singer P, Blaser AR, Berger MM, *et al*. Abrupt termination of vitamin C from ICU patients may increase mortality: secondary analysis of the LOVIT trial. Eur J Clin Nutr 2023 Apr; 77(4): 490-494. doi: 10.1038/s41430-022-01254-8. Epub 2022 Dec 20. PMID: 36539454; PMCID: PMC10115628.
27. Barabutis N, Khangoora V, Marik PE, *et al*. Hydrocortisone and ascorbic acid synergistically prevent and repair lipopolysaccharide-induced pulmonary endothelial barrier dysfunction. Chest 2017 Nov; 152(5): 954-962. doi: 10.1016/j.chest.2017.07.014. Epub 2017 Jul 21. PMID: 28739448; PMCID: PMC5812759.
28. Fujii T, Deane AM, Nair P. Metabolic support in sepsis: corticosteroids and vitamins: the why, the when, the how. Curr Opin Crit Care 2020 Aug; 26(4):363-368. DOI: 10.1097/mcc.0000000000000736. PMID: 32487845.
29. Donnino MW, Andersen LW, Chase M, *et al*. Center for Resuscitation Science Research Group. Randomized, double-blind, placebo-controlled trial of thiamine as a metabolic resuscitator in septic shock: a pilot study. Crit Care Med 2016 Feb; 44(2):360-7. doi: 10.1097/CCM.0000000000001572. PMID: 26771781; PMCID: PMC4754670.
30. Fujii T, Sevransky J. Thiamine for septic shock: take your vitamins? Am J Respir Crit Care Med 2023 Sep 1; 208(5): 513-515. doi: 10.1164/rccm.202307-1140ED. PMID: 37490623; PMCID: PMC10492244.

A Small Pleural Solitary Fibrous Tumor Masquerading as Thymoma

Chia Liu[1], Yi-Chen Yeh[2], Chia-Hung Wu[3,4], Han-Shui Hsu[1,5]

Solitary fibrous tumors (SFTs) are rare neoplasms that can originate from various sites in the body, including the pleura, pericardium, and mediastinum. Although most SFTs are benign and asymptomatic, local invasion, recurrence, or metastasis may occur in some cases. To classify SFTs, a scoring system has been developed, which categorizes tumors into 3 groups based on the patient's age, tumor size, and presence or absence of mitosis and necrosis. In this case report, we described a 41-year-old female patient who was incidentally found to have a 2.8-cm SFT in contact with the anterior chest wall, pericardium, and aorta. The location of the tumor initially raised suspicion of a thymoma. However, intraoperative findings revealed that the tumor originated from the lung, and subsequent pathological analysis following its excision confirmed it to be a SFT. This case highlights the importance of considering SFTs in the differential diagnosis of thoracic neoplasms. ***(Thorac Med 2024; 39: 129-133)***

Key words: Solitary fibrous tumor, thymoma.

Introduction

Thoracic solitary fibrous tumors (SFTs) usually arise from the pleura, and their symptoms depend on the tumor's size and location. They can be asymptomatic or cause dyspnea, chest pain, and chest tightness [1]. Paraneoplastic syndromes are rare. When a tumor arises at the mediastinal side of the pleura, differentiating it from a mediastinal tumor is challenging, due to the overlapping features and equivocal morphology. If located at specific sites, it can also mimic a neurogenic tumor or pulmonary malignancy.

Herein, we present the case of a patient with a tumor that was incidentally found within the upper anterior thorax; the first impression was a thymoma. The tumor was later diagnosed as a SFT after surgical excision.

[1]Division of Thoracic Surgery, Department of Surgery, Taipei Veterans General Hospital; Taipei, Taiwan, [2]Department of Pathology and Laboratory Medicine, Taipei Veterans General Hospital; Taipei, Taiwan, [3]Department of Radiology, Taipei Veterans General Hospital; Taipei, Taiwan, [4]School of Medicine, National Yang-Ming Chiao Tung University, Taipei, Taiwan, [5]Institute of Emergency and Critical Care Medicine, National Yang-Ming Chiao Tung University, Taipei, Taiwan
Address reprint requests to: Dr. Han-Shui Hsu, Division of Pulmonary, Department of Internal Medicine, MacKay Memorial Hospital, Taipei City, Taiwan

Case Report

A 41-year-old female patient had no prior medical history, and denied exposure to risk factors such as smoking, tuberculosis, or asbestos. However, a routine chest radiograph during a medical checkup detected a 2.8-cm, well-defined, radiopaque lesion that overlapped the right border of the right atrium and ascending aorta, and no apparent silhouette was observed. The lesion was located in the retrosternal space on the right lateral chest radiograph (Figure 1A, B). However, physical examination results were unremarkable. A post-contrast medium enhanced computed tomography (CT) scan of the chest was carried out, which revealed a soft tissue lesion measuring approximately 2.7 x 2.7 x 2.9 cm in size, with a broad base on the mediastinal side. Other benign lesions originating from the pleura could not be excluded due to relative hyper-attenuation in the pre-contrast phase (Figure 1C, D). The differential diagnosis included lymphoma, germ cell tumor, spindle cell carcinoma, metastatic tumor, or other pleural-originated tumors. Lactate dehydrogenase, alpha-fetoprotein beta-human chorionic gonadotropin, acetylcholine receptor autoantibodies and the thyroid function test were all within a normal range.

Surgical resection was performed for both diagnostic and curative purposes. The patient underwent uniportal video-assisted thoracoscopic surgery via a 3-cm incision at the right 5th intercostal space in the midaxillary line for tumor resection. The tumor was an exophytic mass located in the right upper lobe of the lung, adjacent to the mediastinum, but without invasion (Figure 2A). The tumor and adjacent lung parenchyma were resected using an endoscopic stapler. The pathology report revealed a 3.8 x 3.5

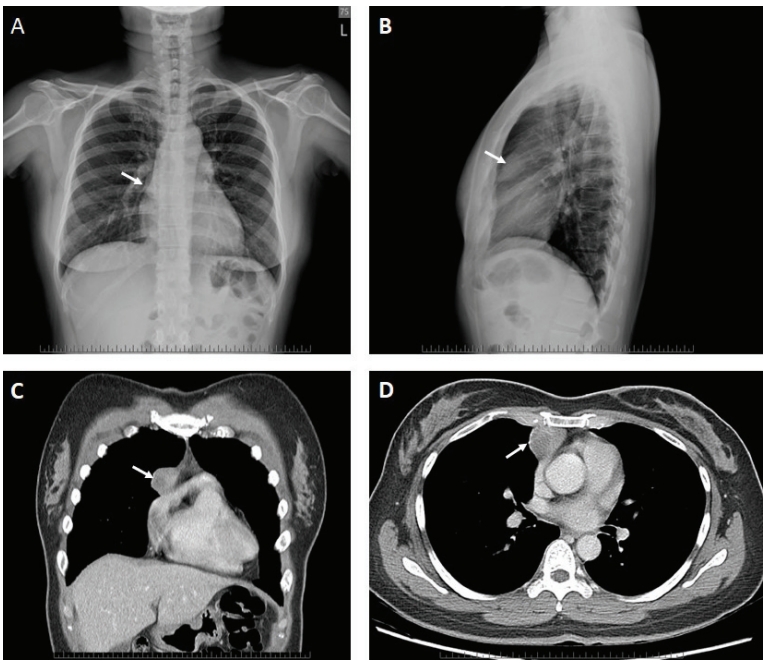

Fig. 1. (A) Pre-operative chest radiograph revealed a well-demarcated radiopaque lesion that overlapped the right border of the right atrium and ascending aorta. (B) Right lateral chest radiograph showed a retrosternal lesion. Coronal (C) and Axial (D) views of the CT scan of the chest revealed a soft tissue lesion, with a broad base on the mediastinal side.

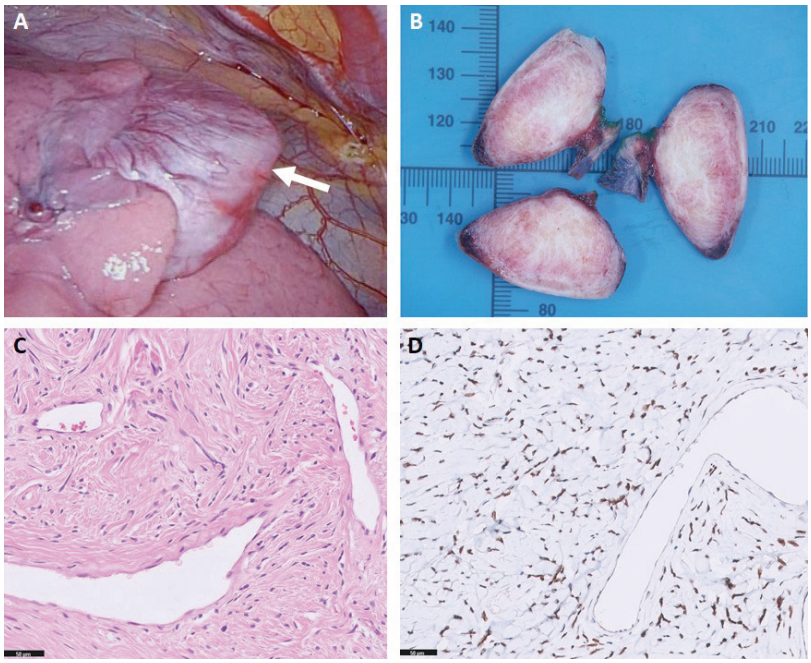

Fig. 2. (A) Thoracoscopic view of the tumor, without connection to the mediastinum. (B) The greyish-white, rubbery to firm tumor. (C) Hematoxylin–eosin, original magnification x200 of the tumor. (D) STAT6 stain, original magnification x200 of the tumor.

x 1.8 cm, greyish-white, rubbery to firm tumor (Figure 2B), which was well-circumscribed and composed of haphazardly arranged elongate spindle cells with low to moderate cellularity, minimal cellular atypia, abundant rope-like stromal collagen, and staghorn-shaped vasculature. Mitotic figures and necrosis were not detected. The neoplastic cells showed cluster of differentiation 34 (CD34) and signal transducer and activator of transcription 6 (STAT6) positivity. The histopathological diagnosis was consistent with a SFT (Figure 2C, D). Based on the risk stratification model for SFTs, the tumor was categorized as belonging to a low metastatic risk group.

Discussion

SFTs were first described by Klemperer in 1931; they usually occur after the fifth decade of life, and develop equally among men and women [2]. The tumors can develop in the pleura, lung parenchyma, pericardium, and mediastinum, including the extrathoracic organs. The vast majority of SFTs of the pleura arise from the visceral pleura. In exceedingly rare instances, SFTs can originate from the lung parenchyma [3-4]. SFTs of the pleura comprise 5% of all pleural tumors, ranking second after mesothelioma. Malignant SFTs, though extremely rare, account for 10–15% of SFTs of pleural cases. Accurate diagnosis of and effective treatment for SFTs are crucial for the well-being of these patients [5].

On chest radiography, the tumors usually appear as well-defined masses that contact the pleura and may present an "incomplete border sign." On chest CT, the small intrathoracic SFT presents as a homogeneous, well-circumscribed, non-invasive, lobular soft-tissue mass adjacent

to the chest wall or within a fissure, forming an obtuse angle with the pleural surface [6-8].

SFTs are characterized by prominent fibrous tissue, which results in low-to-intermediate signal intensity on T1-weighted images, a low signal on T2-weighted images, and poor enhancement on fluorodeoxyglucose-positron emission tomography (FDG-PET). A high T2 signal may indicate hypervascularity, cystic degeneration, hemorrhage, or necrosis. Magnetic resonance imaging (MRI) can aid in the diagnosis of SFTs [6-7].

The treatment of choice for both benign and malignant SFTs is complete resection with a 1-2-cm surgical margin. Pre-operative needle biopsy is not necessary for respectable thoracic SFTs. For small SFTs originating from the visceral pleura, wedge resection of the adjacent pulmonary parenchyma is recommended, while lobectomy or pneumonectomy is indicated for large or sessile tumors [9-10]. Localized pleurectomy is required for SFTs growing from the parietal pleura. There is no clear evidence to support adjuvant therapy, but image follow-up is essential, and recurrent metastases in the lung or pleura should be resected, if possible.

Previously, SFTs of the pleura were called localized mesotheliomas, but the nomenclature has been amended due to their mesenchymal rather than mesothelial origin. SFTs are immunoreactive with CD34 and bcl-2, but lack expression for cytokeratin and S-100 protein. In the past, the diagnosis of SFT heavily relied on the detection of CD34 expression. The literature reports the incidence of CD34-positive SFTs ranging from 90% to 95%. In addition, within the subset of CD34-positive SFTs, some cases may exhibit focal or patchy CD34 expression, which could be overlooked in small biopsy specimens. The loss of CD34 expression has been linked to poorly differentiated components in an otherwise typical SFT, and in SFTs characterized as "dedifferentiated" [11]. STAT6 serves as a highly sensitive and nearly perfectly specific immunohistochemical marker for SFT, offering valuable assistance in distinguishing this tumor type from histologic mimics [12-13].

Commonly used criteria for malignancy include high cellularity with crowding and overlapping of nuclei, high mitotic activity of more than 4 mitotic figures per 10 high-power fields, and pleomorphism [14]. The risk stratification model for SFTs by Demicco, *et al*. is a scoring system that classifies tumors into 3 categories based on the patient's age, tumor size, and presence or absence of mitosis and necrosis. The study reported that no metastases occurred in the low-risk group, but the 5-year metastatic risk was 73% for high-risk patients [15]. In the case of our patient, who was under 55 years old, a score of 0 points was assigned for age. The tumor size, measuring less than 4.9 cm, also received a score of 0 points. Notably, there was no observed mitotic activity (0/10 HPF) and an absence of necrosis (<10%), resulting in 0 points for both criteria. Considering these factors, the patient's risk stratification score was 0, indicating a low-risk classification, according to the model.

Conclusion

In conclusion, small intrathoracic SFTs may closely resemble various other thoracic neoplasms, depending on their location. Despite the potential for malignancy, biopsy is not always performed prior to surgical excision. Therefore, clinicians must include SFTs in their differential diagnosis and consider the possibility of malignancy when developing a treatment plan.

References

1. De Perrot M, Fischer S, Brundler MA, *et al*. Solitary fibrous tumors of the pleura. Ann Thorac Surg 2002; 74(1): 285-93.
2. Klemperer P, Coleman BR. Primary neoplasms of the pleura. A report of five cases. Am J Ind Med 1992; 22(1): 1-31.
3. Khouzam MS, Khouzam N. Malignant solitary fibrous tumor of the pleura. J Cardiothorac Surg 2022; 17(1): 92.
4. Sexton G, McLoughlin J, Burke L, *et al*. Solitary fibrous tumour of mediastinum: an often asymptomatic neoplasm. BMJ Case Rep 2021; 14(8): e241223.
5. Zhang J, Liu J, Zhang Z, *et al*. Solitary fibrous tumors of the chest: an analysis of fifty patients. Front Oncol 2021; 11: 697156.
6. Altinok T, Topcu S, Tastepe AI, *et al*. Localized fibrous tumors of the pleura: clinical and surgical evaluation. Ann Thorac Surg 2003; 6(3): 892-5.
7. Chick JF, Chauhan NR, Madan R. Solitary fibrous tumors of the thorax: nomenclature, epidemiology, radiologic and pathologic findings, differential diagnoses, and management. AJR Am J Roentgenol 2013; 200(3): W238-48.
8. Luciano C, Francesco A, Giovanni V, *et al*. CT signs, patterns and differential diagnosis of solitary fibrous tumors of the pleura. J Thorac Dis 2010; 2(1): 21-5.
9. Mitchell JD. Solitary fibrous tumor of the pleura. Semin Thorac Cardiovasc Surg 2003; 15(3): 305-9.
10. Ajouz H, Sohail AH, Hashmi H, *et al*. Surgical considerations in the resection of solitary fibrous tumors of the pleura. J Cardiothorac Surg 2023; 18(1): 79.
11. Dermawan JK, Rubin BP, Kilpatrick SE, *et al*. CD34-negative solitary fibrous tumor: a clinicopathologic study of 25 cases and comparison with their CD34-positive counterparts. Am J Surg Pathol 2021; 45(12): 1616-25.
12. Doyle LA, Vivero M, Fletcher CD, *et al*. Nuclear expression of STAT6 distinguishes solitary fibrous tumor from histologic mimics. Mod Pathol 2014; 27(3): 390-5.
13. Tariq MU, Din NU, Abdul-Ghafar J, *et al*. The many faces of solitary fibrous tumor; diversity of histological features, differential diagnosis and role of molecular studies and surrogate markers in avoiding misdiagnosis and predicting the behavior. Diagn Pathol 2021; 16(1): 32.
14. England DM, Hochholzer L, McCarthy MJ. Localized benign and malignant fibrous tumors of the pleura. A clinicopathologic review of 223 cases. Am J Surg Pathol 1989; 13(8): 640-58.
15. Demicco EG, Wagner MJ, Maki RG, *et al*. Risk assessment in solitary fibrous tumors: validation and refinement of a risk stratification model. Mod Pathol 2017; 30(10): 1433-42.

Solitary Fibrous Tumor of Pleura, Complicated with Hemothorax and Pulmonary Embolism: A Case Report

Yi-Chun Yang[1], Shu-Farn Tey[2], I-Chuang Liao[3]

Solitary fibrous tumors (SFTs) are rare neoplasms, with an estimated frequency of 2.8 per 100,000 individuals, and account for less than 5% of pleura tumors. Most SFTs are benign, but there is still a 10~20% malignancy rate.

Here, we reported the case of a 75-year-old female diagnosed with SFT of the pleura, complicated with hemothorax and pulmonary embolism.

SFTs grow slowly, so most patients are asymptomatic until the tumors become large enough to compress the adjacent lung. A few patients may present with paraneoplastic syndrome, such as Doege–Potter syndrome [DPS] and hypertrophic pulmonary osteoarthropathy.

Despite its low incidence, malignant SFTs have a high recurrence rate (63%), even after complete resection, and a poor prognosis. Adjuvant chemotherapy should be administered, although the efficacy is limited.

The complications of hemothorax and pulmonary embolism are less mentioned in other case reports. For hemothorax, hemostasis followed by staged tumor resection seems to be a better strategy. For pulmonary embolism, tumors with heart involvement should be ruled out. Also, SFTs may originate from the intima of the pulmonary artery, mimicking pulmonary embolism. ***(Thorac Med 2024; 39: 134-141)***

Key words: Solitary fibrous tumors (SFTs), hemothorax, pulmonary embolism

Introduction

Solitary fibrous tumors (SFTs) are rare neoplasms, with an estimated frequency of 2.8 per 100,000 individuals, and account for less than 5% of pleural tumors. While SFTs are commonly found as intra-thoracic tumors, primarily in the pleura, approximately 50% of them arise outside the thorax, including the brain, liver, prostate, and bones. SFTs predominantly occur in middle-aged adults (50s-70s), and have an equal distribution between genders [1- 2].

Pleural SFTs typically present as painless masses that grow slowly, and are often incidentally detected through chest X-rays. However, in some cases, patients may experience symp-

[1]Department of Internal Medicine, [2]Division of Chest Medicine, [3]Division of Pathology, Chi Mei Hospital, Tainan City, Taiwan
Address reprint requests to: Dr. Shu-Farn Tey, Division of Chest Medicine, Department of Internal Medicine, Chi Mei Hospital, No.901, Zhonghua Rd., Yongkang Dist., Tainan City 710, Taiwan (R.O.C.)

toms of airway obstruction when the tumors reach a significant size, especially > 10 cm, and cause compression of the adjacent trachea and lung parenchyma [3]. In this report, we describe the case of a large pleural SFT complicated with massive hemothorax and pulmonary embolism, which are uncommon complications of this type of tumor.

Case Report

A 75-year-old woman, without a specific medical history, presented with progressive dyspnea and intermittent chest pain for 1 month. At our emergency department, her GCS level was E4V5M6. Her vital signs were as follows: body temperature of 36.2 o C, heart rate of 137 bpm, respiratory rate of 24 breaths per minute, and blood pressure of 142/86mmHg. During chest auscultation, decreased breathing sounds were noted at the left lung field. Chest X-ray (Figure.1) revealed left lung atelectasis with left-sided pleural effusion. Laboratory data, including tumor markers such as CEA and SCC Ag, were within normal range, but lactate levels were elevated. Computed tomography (CT) scan of the chest (Figure 2) showed a well-defined, heterogeneous, large LUL tumor (measuring 11cm x 8cm) with mediastinal compression and massive hemothorax. An echo-guided pigtail drainage tube then was inserted. Much serosanguineous fluid with a high hematocrit ratio (pleural fluid to blood: 58%) was extracted. Cytological analysis of the pleural effusion did not reveal malignant cells.

The patient continued to experience dyspnea accompanied by oxygen desaturation, and the effectiveness of the pigtail drainage tube was limited. A CT angiography revealed pulmonary embolism in the interlobular to segmental branches of the right lower lung (Figure 3). Due to the presence of massive hemothorax and poor drainage function, video-assisted thoracic surgery (VATS) was performed for decortication and chest tube drainage. During the surgery, no pleural seeding or active bleeder was observed, but there was slow oozing of blood from the surface of the tumor. Considering the relatively high risk associated with tumor resection, the patient's family, after discussion with the chest surgeon, agreed to a staged surgery.

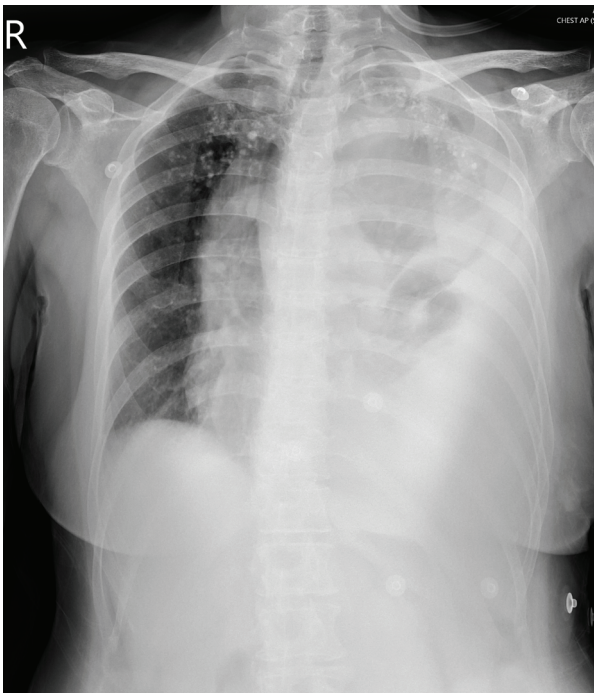

Fig. 1. Chest X-ray PA view revealed left lung atelectasis with massive left-sided pleural effusion, tracheal deviation to the right side, and calcified granuloma at bilateral upper lung fields, favoring old TB

CT-guided biopsy of the left upper lung tumor was conducted, and the pathological examination revealed spindle-shaped cells with a low mitotic rate. These cells were arranged in a patternless distribution and showed positive staining for CD34 and STAT-6 markers. Based on these findings, a diagnosis of benign solitary

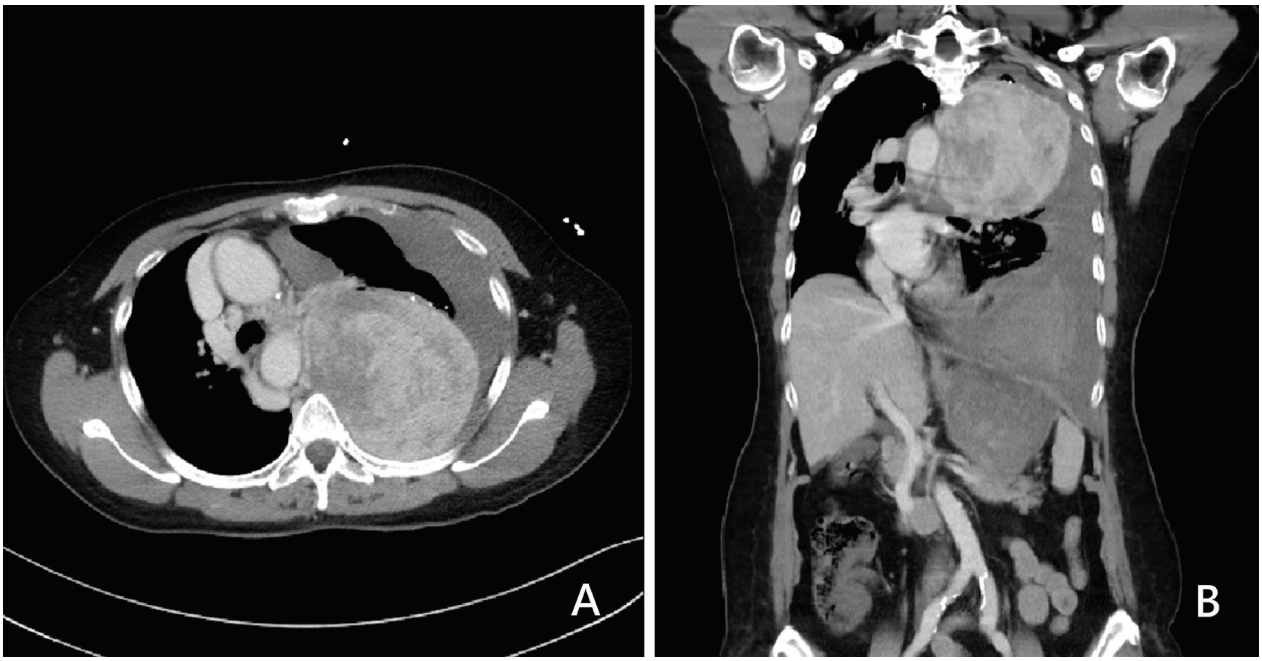

Fig. 2. Chest CT horizontal (A) and coronal (B) views with contrast, showing a well-defined, heterogeneous, large LUL tumor (measuring 11 cm x 8cm) with mediastinal compression and massive hemothorax.

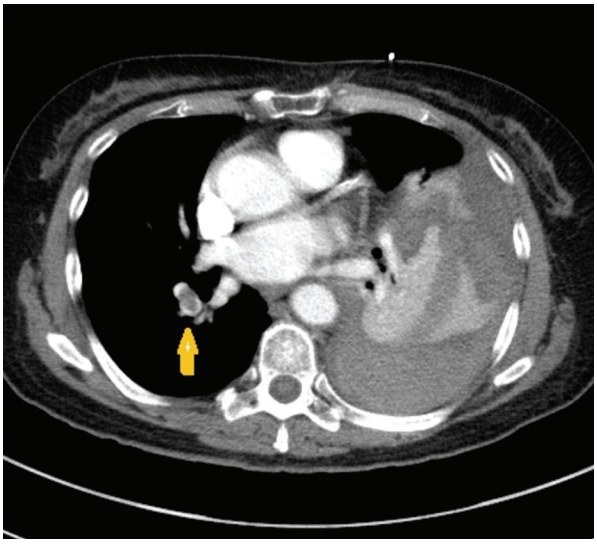

Fig. 3. CT angiography showed a pulmonary embolism in the right lower lung interlobular to segmental branches.

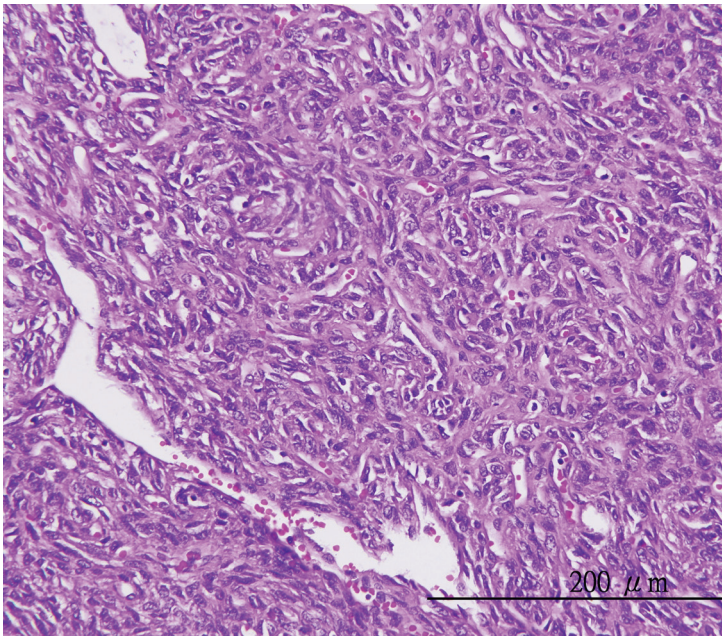

Fig. 4. Pathological examination revealed the tumor to be composed of spindle cells separated by collagen fibers, forming a patternless architecture. Dilated vessels were noted, with some of them revealing a branching staghorn appearance. There was only mild nuclear atypia, and no tumor necrosis or increased mitotic figures

fibrous tumor was reached (Figures 4, 5, 6).

Following the completion of all invasive procedures, we prescribed rivaroxaban for the treatment of pulmonary embolism, as it was confirmed that there was no bleeding tendency.

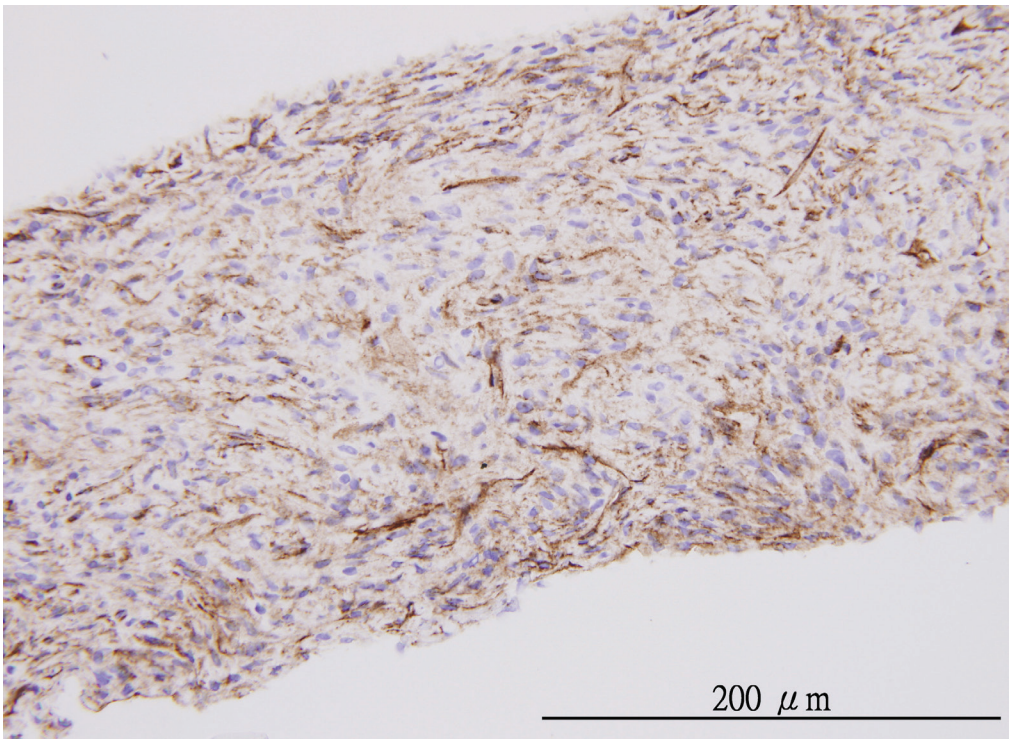

Fig. 5. Immunohistochemical examination revealed tumor cells with cytoplasmic staining of CD34.

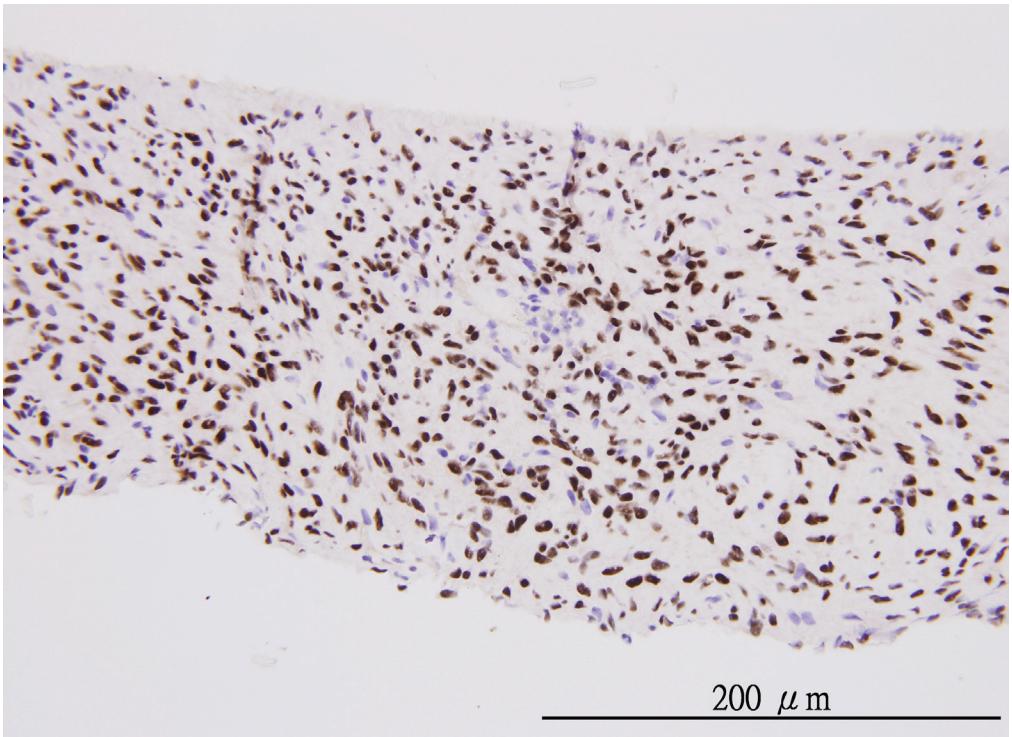

Fig. 6. Immunohistochemically, the tumor cells showed nuclear staining of STAT-6. This, combined with the results in Figure 5, confirmed the diagnosis of solitary fibrous tumor.

One month later, the patient underwent left pneumonectomy without any complications. Since then, she has been regularly followed up at our outpatient department, and no signs of tumor recurrence were detected during the follow-up visits.

Discussion

Histology and genetic features

SFTs originate from mesenchymal cells. Initially, these tumors were primarily described in relation to the pleura, mediastinum, and serosal surfaces. However, it was subsequently discovered that they can arise in various anatomical locations, including the brain, lungs, pleura, liver, pancreas, kidneys, prostate, and bones, among others. The visceral pleura is the most common site of origin of intrathoracic SFTs, accounting for approximately 80% of cases. However, pleural SFTs make up less than 5% of all tumors originating from the pleura [1].

To accurately differentiate SFTs from other pleural tumors, a comprehensive approach involving clinical, histomorphological, immunohistochemical, and molecular features is necessary [4].

Histologically, SFTs feature spindle-shaped cells with low mitotic rates (< 4 mitoses per 10 high-power fields), arranged in a patternless distribution with varying amounts of collagen and reticular fibers. Sarcomatoid carcinoma and mesothelioma display similar morphological features, making them important differential diagnoses in the pleura [4]. Hence, immunohistochemical staining is necessary. The expression of STAT6 and CD34 plays a crucial role in confirming the diagnosis of SFTs [4-5].

From the genetic perspective, a characteristic feature of SFTs is the fusion of the neighboring NGFI-A binding protein 2 (NAB2) and signal transducer and activator of transcription 6, interleukin-4 induced (STAT6) genes on chromosome 12q13. This specific fusion event, known as NAB2-STAT6 fusion, is instrumental in the diagnosis of SFTs. The expression of nuclear STAT6 serves as a valuable marker for identifying this fusion [6].

A study conducted by Huang *et al*. investigated 52 cases of SFT and reported that the NAB2ex4-STAT6ex2/3 fusion variant was the most common fusion type observed in intrapulmonary SFTs. Though the fusion variants are significantly associated with tumor location, they do not appear to be correlated with disease free survival [6].

Clinical Manifestations

The clinical manifestations of SFTs are influenced by the size and location of the tumors. Patients with small-sized SFTs are often asymptomatic, and the tumors are typically discovered incidentally through chest radiographs. However, as the tumors grow larger and exert pressure on the surrounding lung parenchyma or bronchi, various symptoms may arise. These can include cough, dyspnea (shortness of breath), chest tightness, fever, and weight loss. If the parietal pleura is involved, patients may experience chest pain [7-8]. Besides, some patients with SFTs may present with paraneoplastic syndromes, such as hypertrophic pulmonary osteoarthropathy and Doege–Potter syndrome [DPS].

Hypertrophic pulmonary osteoarthropathy is the most common paraneoplastic syndrome observed in patients with SFTs, with an incidence rate reported to be around 35% [8]. The exact mechanism is not fully understood, but it is believed to be associated with the accumula-

tion of hepatocyte growth factors and hyaluronic acid. The syndrome is characterized by finger clubbing, hypertrophic changes in the skin, and periosteal bone changes [10]. Clinically, hypertrophic skin changes can manifest as deepening of facial skin folds, furrowing of the brow with noticeable sebaceous hyperplasia, and thickened eyelids with ptosis. Bone changes may lead to painful periostitis and arthritis [11].

DPS occurs due to excessive production of the prohormone of insulin-like growth factor, known as big IGF2, by the tumors. Patients with DPS may present with recurrent and refractory hypoglycemia. Larger tumors, especially those measuring over 10cm, have been reported to have a higher incidence rate of DPS. Laboratory data of patients with DPS typically show an increased IGF2:IGF1 ratio, which is clinically significant when it exceeds 10 [10-11].

Large SFTs complicated by tumor rupture or bleeding leading to hemothorax, as observed in our patient, have been reported in only a few studies [12-15]. The spontaneous rupture of superficial vessels on the tumor surface may be attributed to the shear force generated during rapid tumor expansion. In such cases, the recommended management approach is transthoracic drainage followed by elective tumor resection, unless the patient's vital signs are unstable. Detailed investigation is crucial, particularly for large SFTs located near vital organs and blood vessels [15].

In addition to hemothorax, our patient also experienced pulmonary embolism. It is well established that malignancy is strongly associated with an increased risk of pulmonary embolism. Cancers with a higher malignant potential, particularly those in stage IV, tend to have a higher incidence of thromboembolic events. However, pulmonary embolism in the context of SFTs is rare. Only 1 case report has described a patient with malignant SFT complicated by tumor emboli, resulting in severe limb ischemia. The reported case involved an advanced-stage SFT that invaded the left ventricle of the heart, which was believed to be the cause of recurrent tumor embolism [16]. Furthermore, 2 case reports from China have mentioned primary SFTs originating from the intima of the pulmonary arteries, mimicking pulmonary embolism [17-18]. These cases suggest the possibility of primary or metastatic SFTs affecting the pulmonary arteries and impairing pulmonary circulation. Although the pathology results for our patient indicated a benign tumor, long-term follow-up and comprehensive evaluation will be necessary to monitor any potential complications or disease progression.

Treatment and surveillance

Most SFTs are benign and grow slowly. Otherwise, there is a 10~20% malignancy rate [19]. Differentiating between benign and malignant SFTs can be challenging, until the tumors display aggressive behavior, such as frequent recurrence and metastasis, which may occur more than 5 years after the initial presentation [20]. Histological characteristics, including: (1) a high mitotic count (> 4 mitoses per 10 high-power fields), (2) varying degrees of pleomorphism, (3) high cellularity, (4) presence of necrosis and hemorrhage, (5) stromal or vascular invasion, and (6) a significant increase in the Ki-67 index (Ki-67/MIB-1 proliferation index > 10%), are used to determine malignant SFTs [19,21].

Complete surgical tumor resection is considered the gold standard treatment for SFTs. Benign pleural SFTs have a high cure rate, with only an 8% local recurrence rate. On the other

hand, malignant SFTs have a higher recurrence rate of 63% [19]. The majority of recurrences occur within the first 2 years after tumor resection. [22].

Currently, there are no widely accepted guidelines specifically addressing the optimal frequency of surveillance for SFTs. Posttreatment surveillance plans are based on guidelines for soft tissue sarcoma from the National Comprehensive Cancer Network (NCCN) [23]. Patients are stratified into low, intermediate, and high-risk groups based on factors such as mitotic count, necrosis, and sex. For low-risk patients, it is recommended to have a CT scan or chest radiograph every 6 months for the first 3 years, followed by yearly surveillance up to year 10. Intermediate- and high-risk patients are advised to undergo chest CT every 3 to 4 months for the first 2 years, followed by surveillance every 6 months for the next 3 years, and then annually up to year 20.

Following surgical treatment for malignant SFTs, systemic chemotherapy with an anthracycline-based regimen is commonly recommended, although its efficacy is limited. However, emerging evidence from case reports and clinical trials suggests that anti-angiogenic agents and immune checkpoint inhibitors may have therapeutic benefits for malignant SFTs [24]. Larger studies or randomized trials are needed to confirm the efficacy and safety of these novel agents.

Conclusion

Our patient presented with the uncommon complications of hemothorax and pulmonary embolism, which are not frequently reported in other case studies. Managing hemothorax involves achieving hemostasis followed by staged tumor resection, which has shown promising results. For pulmonary embolism, it is crucial to rule out heart involvement and consider the possibility of SFTs originating from the pulmonary artery intima, mimicking pulmonary embolism.

Paraneoplastic syndromes, including DPS, should be considered and promptly managed to address associated symptoms, such as refractory hypoglycemia. Complete surgical tumor resection remains the mainstay of treatment for SFTs, and adjuvant chemotherapy is recommended for malignant cases, even though they have a high recurrence rate and poor prognosis. The efficacy and safety of novel agents, such as anti-angiogenic agents and immune checkpoint inhibitors, are still being studied, and require further research to establish their role in the management of malignant SFTs.

References

1. Kouki HS, Koletsis EN, Zolota V, *et al*. Solitary fibrous tumor of the lung. Gen Thorac Cardiovasc Surg 2008 May; 56(5): 249-51.
2. Zhang J, Liu J, Zhang Z, *et al*. Solitary fibrous tumors of the chest: an analysis of fifty patients. Front Oncol 2021 Jul 1; 11: 697156.
3. Wang Y, Xu Y, Li R, *et al*. Rapidly growing giant solitary fibrous tumor of the pleura: a case report and review of the literature. Int J Clin Exp Pathol 2020 Sep 1;13(9):2363-2368.
4. Tariq MU, Din NU, Abdul-Ghafar J, *et al*. The many faces of solitary fibrous tumor; diversity of histological features, differential diagnosis and role of molecular studies and surrogate markers in avoiding misdiagnosis and predicting the behavior. Diagn Pathol 2021; 16(1): 32.
5. Kuroki S, Ayabe T, Gi T, *et al*. Intrapulmonary solitary fibrous tumor coexisting with lung adenocarcinomas. Surg Case Rep 2022 Aug 2; 8(1): 150.
6. Huang SC, Li CF, Kao YC, *et al*. The clinicopathological

significance of NAB2-STAT6 gene fusions in 52 cases of intrathoracic solitary fibrous tumors. Cancer Med 2016 Feb; 5(2): 159-68.

7. Furukawa N, Hansky B, Niedermeyer J, *et al*. A silent gigantic solitary fibrous tumor of the pleura: case report. J Cardiothorac Surg 2011 Sep 29; 6: 122.
8. Mejías-Lafontaine E, Galarza S, Gonzalez-Cancel I, *et al*. Digital clubbing as first sign of giant solitary fibrous tumor. A case report. J Surg Case Rep 2021 Aug 4;2021(8): rjab337.
9. Fridlington J, Weaver J, Kelly B, *et al*. Secondary hypertrophic osteoarthropathy associated with solitary fibrous tumor of the lung. J Am Acad Dermatol 2007 Nov;57(5 Suppl): S106-10.
10. Karki A, Yang J, Chauhan S, *et al*. Paraneoplastic syndrome associate with solitary fibrous tumor of pleura. Lung India 2018 May-Jun; 35(3): 245-247.
11. Fort-Culillas R, Barahona San Millán R, Garcia-Fructuoso I, *et al*. Doege-Potter syndrome in a facial solitary fibrous tumor: diagnose and clinical management discussion. Clin Case Rep 2021; 9: e04291.
12. Leng XF, Xian L, Qin JJ, *et al*. Malignant solitary fibrous tumour of pleura accompanied with first symptoms of chest pain and hemoptysis: a case report. Ann Thorac Cardiovasc Surg 2012; 18: 251-5.
13. Negri G, Bandiera A, Ciriaco P, *et al*. Solitary fibrous tumour of the pleura presenting as a spontaneous massive hemothorax. Surg Res Pract 2014; 2014: 139404.
14. Asai K, Suzuki K, Shimota H, *et al*. Solitary fibrous tumour of pleura with hemothorax at the thoracic apex. Jap J Thor Cardiovas Surg 2003; 51(9): 434-7.
15. Tan JHY, Hsu AAL. Challenges in diagnosis and management of giant solitary fibrous tumour of pleura: a case report. BMC Pulm Med 2016; 16(1): 114.
16. Bodapati S, Shafa AM, Zamora Salazar C, *et al*. Critical limb ischemia as a rare presentation of malignant solitary fibrous tumor of the pleura. Am J Case Rep 2022 May 31; 23: e935445.
17. Li B, Mao MM, Adhikari BK, *et al*. Primary solitary fibrous tumour in the pulmonary artery: a case report. J Int Med Res 2020 Mar; 48(3): 300060520911273.
18. Luo R, Xu H, Zhang P, *et al*. Rare solitary fibrous tumor in the pulmonary artery mimicking pulmonary embolism. Circ Cardiovasc Imaging 2017 May; 10(5): e005933.
19. Khouzam MS, Khouzam N. Malignant solitary fibrous tumor of the pleura. J Cardiothorac Surg 2022 May 3; 17(1): 92.
20. Gholami S, Cassidy MR, Kirane A, *et al*. Size and location are the most important risk factors for malignant behavior in resected solitary fibrous tumors. Ann Surg Oncol 2017; 24(13): 3865. Epub 2017 Oct 16.
21. Wang YX, Zhong Y, Fan SS, *et al*. Solitary fibrous tumors of the lung: a clinicopathological analysis of 52 cases. Curr Oncol 2023 Feb 1; 30(2): 1784-1793.
22. De Perrot M, Fischer S, Bründler MA, *et al*. Solitary fibrous tumors of the pleura. Ann Thorac Surg 2002; 74: 285-93.
23. National Comprehensive Cancer Network (NCCN). NCCN clinical practice guidelines in oncology. Available at: https://www.nccn.org/professionals/physician_gls
24. De Bernardi A, Dufresne A, Mishellany F, *et al*. Novel therapeutic options for solitary fibrous tumor: antiangiogenic therapy and beyond. Cancers (Basel) 2022 Feb 20; 14(4): 1064.

Sequential Presentation of T790M Mutation and Small Cell Transformation as Acquired Resistance to Tyrosine Kinase Inhibitor in an EGFR-Mutant Non-Small-Cell Lung Adenocarcinoma Patient

Kuan-Hua Chen[1], Chiao-Hung Wang[2]

Patients with epithelial growth factor receptor (EGFR)-positive non-small-cell lung cancer (NSCLC) have shown a remarkable response to EGFR tyrosine kinase inhibitors (TKIs), compared to standard cytotoxic chemotherapy. EGFR-TKIs are the first-line therapy for metastatic NSCLC patients due to the higher response rate and better tolerability. However, these patients may eventually have disease progression. Repeated biopsy from patients who have disease progression can help the clinician confirm the mechanism of resistance, and are useful for further treatment planning. We described the case of an 81-year-old woman who had NSCLC and developed acquired resistance to TKI with 2 different mechanisms, which enabled the disease to continue progression despite a change to second-line TKI therapy. This case emphasized the importance of repeated biopsy when the disease progresses. We also conducted a literature review on the mechanisms and possible treatment options for these patients. ***(Thorac Med 2024; 39: 142-151)***

Key words: metastatic non-small cell lung cancer, acquired resistance to TKI therapy, T790M gatekeeper mutation, small cell transformation

Introduction

Patients with non-small-cell lung cancer (NSCLC) who are positive for epithelial growth factor receptor (EGFR) have demonstrated a remarkable response to EGFR tyrosine kinase inhibitors (TKIs), compared to standard cytotoxic chemotherapy. Based on data showing the efficacy of several agents in patients with EGFR mutations, the National Comprehensive Cancer Network (NCCN) NSCLC panel recommends EGFR mutation testing for patients with metastatic NSCLC. Targeted therapy for the specific oncogene is the first-line treatment for patients with metastatic NSCLC and a targetable driver oncogene, as it offers a higher response rate (e.g., osimertinib, 80%) in the first-line setting and better tolerability. However, these patients inevitably experience disease progression after a median time of about 12 months [1].

[1]Division of Chest Medicine, Department of Internal Medicine, Taipei City Hospital, Renai Branch, [2]Division of Chest Medicine, Department of Internal Medicine, Taipei City Hospital, Renai Branch
Address reprint requests to: Dr. Kuan-Hua Chen, Division of Chest Medicine, Department of Internal Medicine, Taipei City Hospital, Renai Branch 10 Fl., No. 76, Jingfu St., Wenshan Dist., Taipei City 116, Taiwan (R.O.C)

Repeated biopsy samples from patients with EGFR-positive NSCLC who experienced disease progression have revealed several mechanisms of acquired resistance to EGFR-TKIs. These mechanisms include the emergence of the EGFR T790 gatekeeper mutation, amplification of MET, HER2, or MAPK, mutation of PIK3CA or BRAF, and even histological transformation from adenocarcinoma to small cell lung cancer (SCLC). Recent discussions have focused on the possible mechanisms underlying the transformation from NSCLC to the SCLC phenotype after TKI therapy. Conventionally, SCLC was believed to develop from neuroendocrine cells of the central airways, while adenocarcinoma originated from alveolar type II cells. However, some studies have suggested that alveolar type II cells may serve as common precursors for both SCLC and adenocarcinoma [2]. This finding could explain the presence of histological transformation as acquired resistance.

Case Report

In September 2019, an 81-year-old ethnic Chinese woman with no smoking history presented with a 5-kg weight loss over the past month. She also experienced nausea without vomiting for 2 weeks. There was no apparent cough, dyspnea, or increased sputum at that time. A chest radiograph in September 2019 (Fig. 1) revealed a retrocardiac tumor mass, which was initially missed. She was diagnosed with acute gastroenteritis, but a physical examination showed no significant abnormalities. Laboratory findings showed 2+ occult blood in the stool. Therefore, examinations were conducted to exclude malignancies of the gastrointestinal tract, including abdominal ultrasound, panendoscopy, and colonoscopy, which only revealed a renal cyst and hiatal hernia. However, the symptoms persisted despite supportive care.

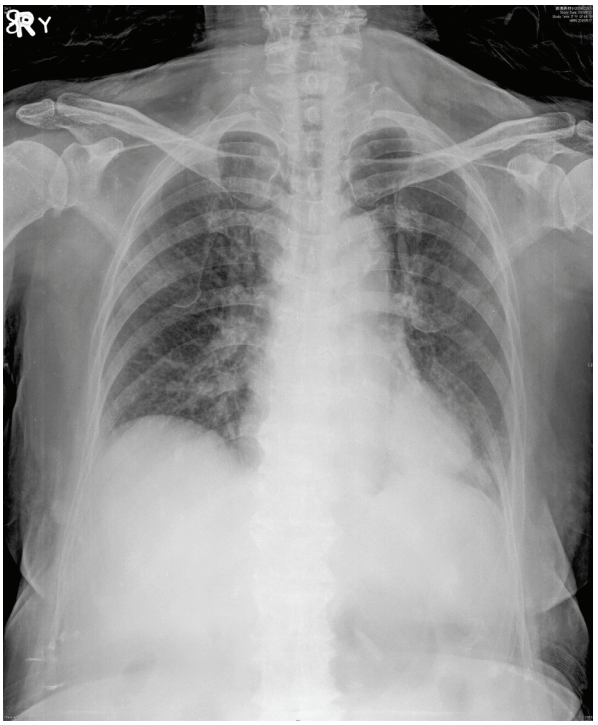

Fig. 1. Chest radiograph showed a retrocardial tumor mass that was missed initially in September 2019.

Due to the persistence of symptoms, the attending physician arranged a contrast-enhanced abdominal computed tomography (CT) scan, which revealed a lobulated 5.9-cm mass in the left lower lobe, along with enlarged lymph nodes in the right retrocrural and paraesophageal regions, and a small amount of left-sided pleural effusion (Fig. 2). In November 2019, the patient underwent a CT-guided biopsy of the left lower lobe mass, which confirmed the diagnosis of lung adenocarcinoma. The biopsy also detected an EGFR mutation of an exon 19 deletion. Subsequently, brain magnetic resonance imaging (MRI) and positron emission tomography (PET) scans were performed for surveillance of distant metastases, revealing

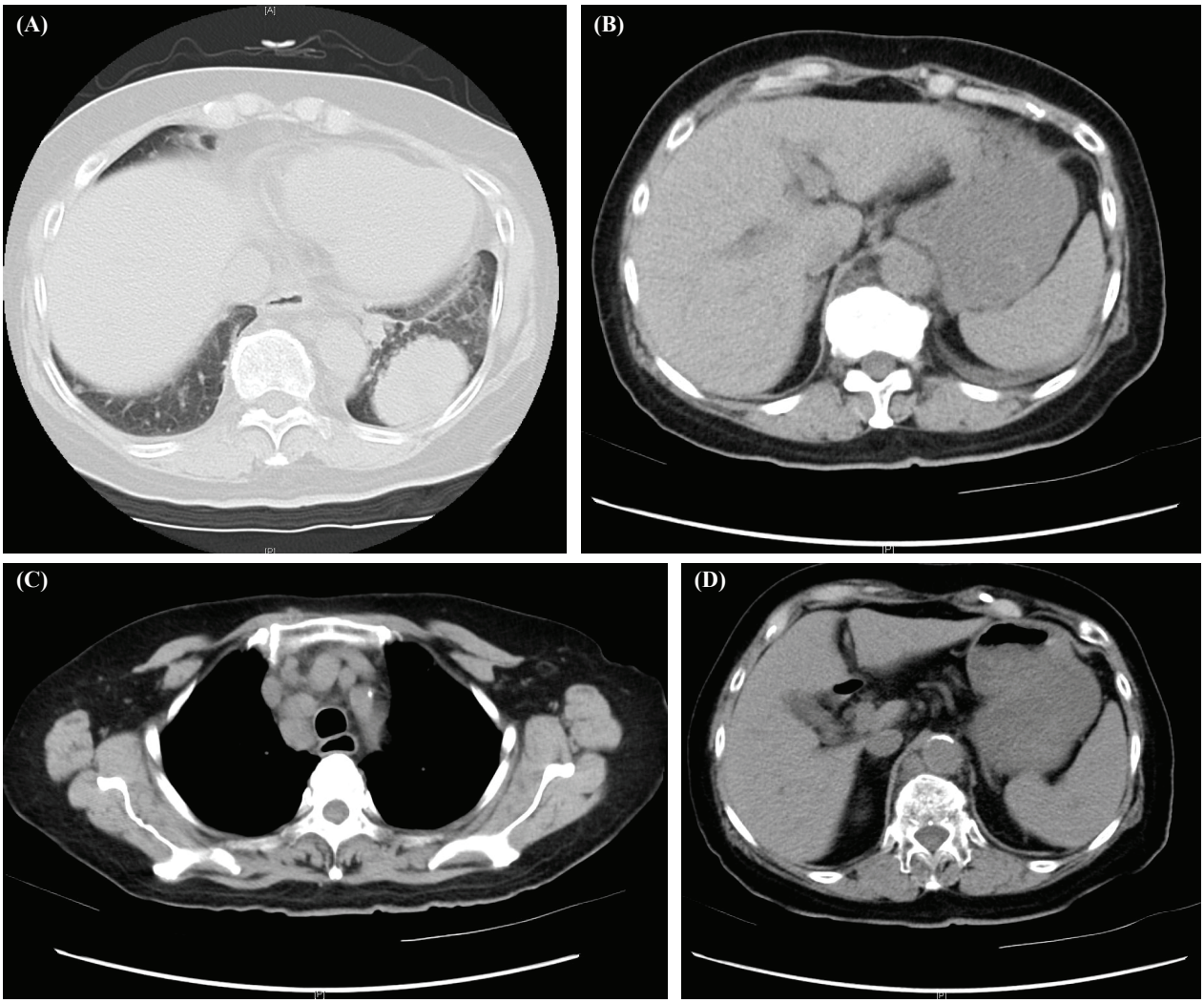

Fig. 2. (A) Chest computed tomography showed a left lower lobe mass lesion, about 5.9 cm, with a 1.4-cm satellite nodule around the mass. (B) A small amount of left-side pleural effusion was found, as well as (C) an enlarged right paratracheal lymph node. (D) An enlarged lymph node at the right retrocrural region, measuring 1 x 1 cm, favored distant lymph node metastasis.

multiple brain metastases in the cerebellum and hypermetabolism in the right retrocrural lymph node (Fig. 3). The final diagnosis was stage IV left lung adenocarcinoma with an EGFR exon 19 deletion (cT3N3M1b).

The patient was initially treated with erlotinib plus bevacizumab. However, in December 2019, due to the development of multiple oral ulcers and acneiform skin lesions, erlotinib was switched to gefitinib. Subsequent follow-up brain MRI and chest CT in January 2020 showed a partial response in cerebellar metastasis and the primary lesion, respectively, after 3 months of treatment with the first-generation EGFR-TKI.

However, the serially followed up carcinoembryonic antigen (CEA) levels showed a gradual increase since then. After 7 months of progression-free survival (PFS), disease progression was confirmed by chest CT in June 2020, revealing an increase in the size of the left lower lobe tumor (Fig. 4), an increase in

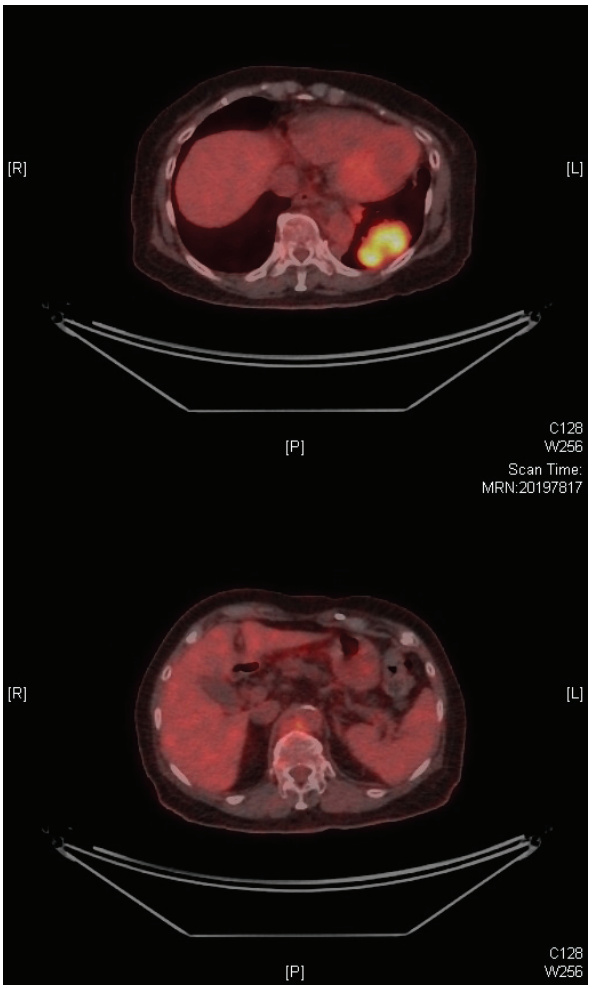

Fig. 3. PET scan showed (A) a left lower lobe tumor with heterogeneously intense hypermetabolism, and (B) mild hypermetabolism at the right retrocrural lymph node.

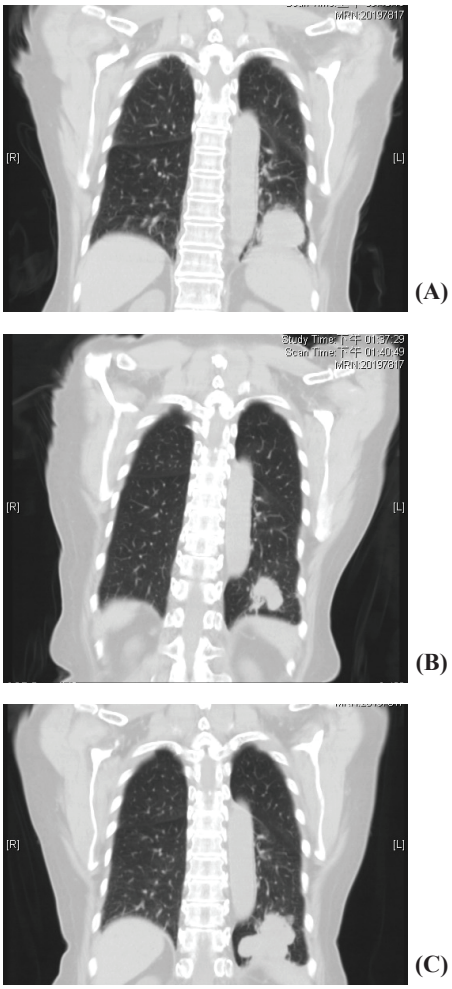

Fig. 4. (A) Chest computed tomography coronal section at the initial diagnosis, (B) after 3 months of EGFR-TKI treatment, and (C) at follow-up showing progression in 2020.

the number of bilateral lung-to-lung metastases, and an increase in the size of the small neck lymph nodes. However, the brain MRI showed a slight decrease in the size of the cerebellar metastasis. A repeated biopsy of the left lower lobe mass was performed on July 20, 2020, which identified the EGFR T790M mutation. Subsequently, the patient was treated with osimertinib. However, in October 2020, after 2 months of treatment with osimertinib, the patient experienced right-side face and upper limb swelling for 1 week. Chest X-ray revealed a mediastinal mass (Fig. 5), and contrast-enhanced chest CT showed a 7-cm mass in the right upper mediastinum, compressing the bilateral brachiocephalic vein and superior vena cava (SVC), but with a mild decrease in the size of the left lower lobe lung cancer (Fig. 6). A further tissue biopsy of the right upper mediastinal mass was performed, and the histologic analysis favored small cell lung cancer. The immunohistochemical staining results were as

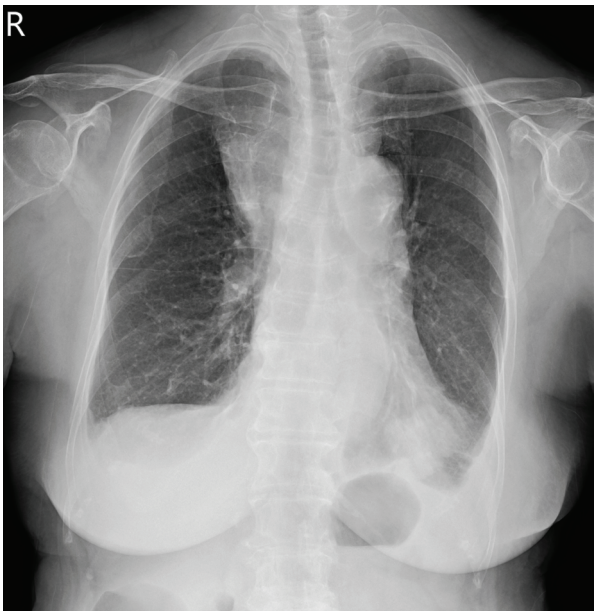

Fig. 5. Chest X-ray in October 2020, showing right upper lung zone opacities.

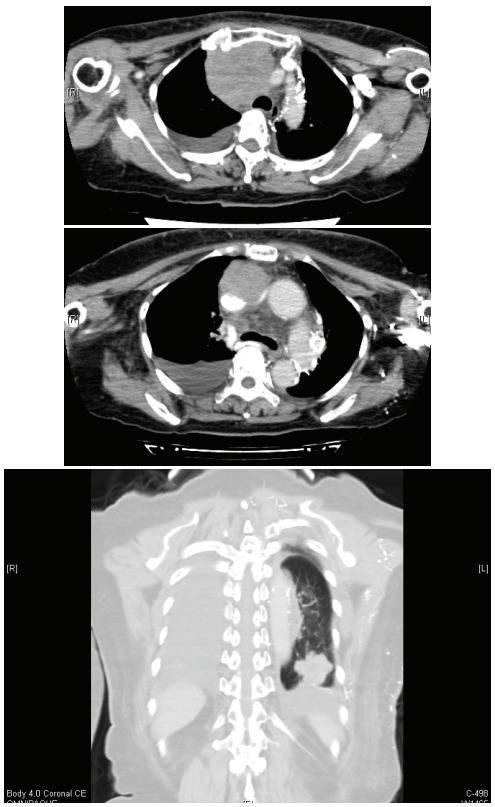

Fig. 6. Chest computed tomography in October 2020 found an enlarged mediastinal mass that compressed the SVC, and resulted in SVC syndrome. (A, B) Right-side pleural effusion was also present. (C) The left lower lobe tumor seem mildly decreased in size.

follows: TTF-1: negative; CD56: positive; chromogranin A: negative; synaptophysin: partially positive; P40: negative.

Thereafter, chemotherapy with a first cycle of etoposide and carboplatin was prescribed, along with concurrent radiotherapy. The SVC syndrome gradually regressed after chemotherapy. Osimertinib was discontinued due to the transformation to small cell carcinoma, as it did not meet the application criteria for osimertinib under the patient's Taiwan health insurance. Despite receiving the second cycle of etoposide with carboplatin in November 2020, a follow-up brain MRI revealed an increase in the size of the cerebellar metastasis and the identification of new bony metastases. Due to progressive dyspnea and consciousness disturbances, the patient was subsequently referred to hospice care and passed away in February 2021. A summarized time course is provided in the Supplemental file.

Discussion

We reported a case of lung cancer that underwent histological transformation from adenocarcinoma to small cell carcinoma following sequential treatment with a first-generation EGFR-TKI and second-line treatment with osimertinib.

Although first- and second-generation EGFR-TKIs have shown high response rates, resistance typically develops within an average of 12 months [1]. Repeated biopsies have revealed various mechanisms of acquired resistance to EGFR TKIs. The most common mechanism is the presence of a T790M mutation in the EGFR gene, which increases the receptor's affinity for ATP and allows for sustained EGFR signaling, despite the presence of the inhibitor. T790M

mutations are reported in approximately 50-60% of resistant tumor samples [3-4]. Other resistance mechanisms, accounting for 15-20% of cases, involve bypassing the requirement for EGFR signaling. These mechanisms include amplification of MET and HER2, as well as histological transformation from EGFR-mutant adenocarcinoma to SCLC, which accounts for 5-15% of cases.

The histological transformation to SCLC as an acquired resistance mechanism to EGFR-TKIs was first described in 2006. However, our understanding of how this transformation occurs and leads to resistance is still incomplete. There is ongoing debate regarding the mechanism of SCLC transformation -- whether it is simply an escape resistance mechanism or a result of misdiagnosis with a combined histology of NSCLC and SCLC.

Two large case series have evaluated the frequency of lung cancer with a combined histology of NSCLC and SCLC [5]. The first series analyzed 176 patients with SCLC, of whom 17 (10%) had an NSCLC component (7 of these patients were initially diagnosed with NSCLC). The second series analyzed 429 patients with SCLC, of whom 9 (2%) had an NSCLC component. In the second series, 6 of these 9 patients with an NSCLC component underwent repeat biopsy, which revealed a dominant histology of 3 SCLC, 2 adenocarcinoma, and 1 squamous cell carcinoma. It is possible that this transformation represents a change from 1 phenotype to another. However, another possibility is that the initial core needle biopsy used for diagnosis did not provide a sufficient sample to determine the presence of combined histology.

However, there are studies that support the notion that the transformation is not solely caused by combined histology. In a case series by Sequist LV, *et al*. [3], repeat biopsies were performed on tumors with EGFR-TKI resistance, and genomic sequencing of EGFR was also conducted. The biopsy samples that transformed into SCLC still retained the original EGFR activating mutation, indicating that there were no independent de novo cancers, but rather a transformed phenotype as a mechanism of resistance to treatment. This suggests that the transformation is not solely a result of combined histology, but rather a mechanism of resistance.

Another reason why combined histology at the initial diagnosis is less likely is that most patients respond well to EGFR-TKIs for several months, and up to years thereafter. If combined histology was present at the initial diagnosis, there would likely be more substantial tumor growth at the time of SCLC diagnosis.

The transformation to SCLC can occur not only as a resistance mechanism to EGFR-TKIs, but also in cases of resistance to conventional chemotherapy or radiotherapy [6]. In addition, synchronous development of adenocarcinoma and SCLC has been observed in EGFR-mutant tumors prior to treatment with an EGFR-TKI [7].

Genomic analysis of tumors that undergo transformation to SCLC as an acquired resistance mechanism to TKIs can provide valuable insights. In adenocarcinoma, there is a high prevalence of KRAS and EGFR mutations. EGFR mutations and ALK translocations account for approximately 30-50% of adenocarcinoma cases in non-smokers, with variations seen among different races. On the other hand, in SCLC, large-scale genome-sequencing projects have shown a high prevalence of TP53 and RB1 mutations, while known oncogenic drivers in adenocarcinoma, such as EGFR or KRAS,

are not significantly mutated [8]. Inactivation of RB1 plays a key role in the development of SCLC, and RB1 mutations have been found in 100% of human SCLC tumors sequenced in these projects. This phenomenon has also been confirmed in the transformation from adenocarcinoma to SCLC, where repeat biopsy samples from patients with EGFR-mutant adenocarcinoma transformed to SCLC revealed a 100% loss of RB1 [9].

With regard to whether there is a common origin for adenocarcinoma and SCLC, histologically, SCLC is believed to originate from neuroendocrine cells within the distal part of the conducting airway, and adenocarcinoma is thought to derive from alveolar type II cells. However, some animal studies on lung cancer have suggested a shared ancestry between certain SCLC and NSCLC subtypes. Targeted deletion of TP53 and RB1 in alveolar type II cells of mice resulted in the development of SCLC, indicating a possible link between alveolar type II cells and SCLC development [10].

Activation of EGFR signaling is believed to be crucial for the differentiation of alveolar cells, and blocking EGFR signaling can halt alveolar cell proliferation [11]. This is why EGFR-mutant lung cancers tend to be well-differentiated adenocarcinomas. However, with the use of EGFR-TKIs, the differentiation may be blocked. In the presence of additional genetic events such as RB1 inactivation, alveolar type II cells may subsequently transform into SCLC and become independent of EGFR signaling. Conversely, if other resistance pathways develop, such as the EGFR T790M gatekeeper mutation, EGFR signaling can be regained, and the resistant cells may maintain the adenocarcinoma histology.

The prognosis of SCLC transformed from adenocarcinoma is generally poorer than that of primary SCLC with extensive disease, with a median survival ranging from 8 to 13 months [12, 13]. The time from the first diagnosis of lung adenocarcinoma to the onset of SCLC transformation is often longer (median 19 months, range 1-61 months) than the PFS reported in patients treated with TKIs in prospective clinical trials (8-11 months). To identify this poor prognostic situation during TKI therapy, repeat biopsies may be necessary when tumors do not respond as initially expected or when responses among different lesions are discordant. Rapid increases in serum neuron-specific enolase (NSE) levels and a poor response to EGFR-TKIs may also indicate the possibility of transformation to SCLC from adenocarcinoma [14].

Case reports and literature reviews have discussed patients who experienced histological transformation from NSCLC to SCLC, highlighting the complex and unique nature of these types of lung cancer. In the case report by Hong E, *et al*. [15], a 54-year-old man with EGFR-mutant NSCLC carrying an exon 19 deletion developed acquired resistance to gefitinib. Liquid biopsy at that time detected the T790M mutation, but the patient showed a mixed response after 1 month of osimertinib treatment, with progression in the main tumor and disappearance of other pulmonary metastases. Tissue biopsy of the progressing tumor site after 3 months of osimertinib revealed small cell transformation. Genetic analysis showed a persistent EGFR exon 19 deletion, RB1 mutation, and TP53 mutation, but no T790M mutation, which may account for the mixed response observed in the patient. Treatment was then shifted to chemotherapy with etoposide and carboplatin, similar to the treatment approach for de novo

SCLC. This mixed response reveals that acquired resistance can involve both on-target and off-target mechanisms, and can occur simultaneously.

The treatment course of the patient described in the report by Hong E, *et al* (15) was similar to that of our patient. Initially, they both had a favorable response to first-generation TKI treatment (the patient in Hong's report had a PFS of 10.5 months, while our patient had 7 months of PFS). Following disease progression, the patient in Hong's report underwent liquid biopsy, which revealed the presence of a T790M mutation. In our case, however, we performed a repeat tissue biopsy of the primary tumor, which had increased in size after progression, and this biopsy revealed the presence of the T790M mutation. In both cases, the patients had a mixed treatment response to osimertinib. In Hong's report, the primary tumor continued to grow despite the disappearance of other metastatic lung lesions, leading to a biopsy that confirmed histological transformation. In our case, the patient presented with SVC syndrome and a new mediastinal mass lesion, which was biopsied and revealed small cell carcinoma. Due to the small cell histology, further next-generation sequencing was not performed, and it is unknown whether the T790M mutation was present.

Both patients received conventional chemotherapy consisting of etoposide with platinum, as typically administered for de novo SCLC. In Hong's report, the patient achieved a PFS of 5 months with this regimen. However, our patient had a PFS of only 2 months, and brain and bone metastases developed along with a deterioration of consciousness, leading to a shift in the treatment strategy towards hospice care. In contrast, the patient in Hong's report underwent a fourth-line treatment with docetaxel and carboplatin, combined with anlotinib, resulting in an additional 3 months of PFS. Following progression, the patient also underwent a fourth biopsy of the same tumor, which revealed poorly differentiated mixed histological subtypes of adenocarcinoma and SCLC. Neither of these 2 patients received combination therapy with osimertinib after the histological transformation.

Treatment options for patients with transformed SCLC after failure of EGFR-TKIs include chemotherapy with etoposide and platinum, which is considered the first-line treatment choice. EGFR-TKIs combined with chemotherapy have also been suggested to have a role in the post-transformation therapy regimen. The case series by Mambetsariev I, *et al*. reported that some patients with EGFR-mutated lung adenocarcinoma who transformed to SCLC continued to use EGFR-TKIs in combination with chemotherapy or as maintenance therapy for more than 12 months after small cell carcinoma transformation [16].

In addition, several novel treatments have been reported for transformed SCLC, including BCL-2 inhibitors, agents targeting RB1 loss, and anti-angiogenic therapy. In this section, we will discuss these promising treatments [17].

BCL-2 inhibitors: The BCL-2 family proteins play a crucial role in regulating mitochondrial apoptosis and act as anti-apoptotic proteins. Previous studies have shown that targeting BCL-2 can be an effective treatment strategy for SCLC. One such inhibitor is ABT-263, an orally bioavailable BCL-2 family protein inhibitor. ABT-263 blocks BCL-2 and induces cell apoptosis. A study has demonstrated that SCLC transformed cell lines exhibit a higher response rate to ABT-263 than EGFR-TKI-resistant NSCLC cell lines with the T790M resis-

tance mutation [19]. However, further clinical trials are necessary to assess the efficacy and safety of ABT-263 in transformed SCLC.

Agents targeting RB1 loss: Several potential agents, including AURKA inhibitors, have been suggested to target RB1 loss in transformed SCLC cells. RB1 loss leads to dependence on AURKA, as observed in independent CRISPR/Cas9 and drug screening assays using RB1-deficient classical SCLC cell lines. AURKA inhibitors have the potential to target RB1-deficient SCLC cells in transformed SCLC. A phase 1/1b clinical trial (NCT04085315) currently is underway to evaluate the combination of the AURKA inhibitor alisertib with osimertinib for metastatic EGFR-mutant lung cancer. Although data collection for this trial will be ongoing until 2025, preliminary findings suggest that alisertib + osimertinib may result in clinically meaningful disease control in EGFR-mutant lung adenocarcinoma patients whose disease is resistant to osimertinib monotherapy. However, further analysis and additional clinical trials are required to establish the efficacy and safety of this combination therapy for transformed SCLC [20].

Anti-angiogenic therapy: This treatment is often combined with chemotherapy, EGFR-TKIs, or both. Studies have demonstrated the effectiveness of anlotinib in treating transformed SCLC patients, resulting in longer overall survival compared to those who did not receive anti-angiogenic agents [18]. Another study validated these findings in EGFR-mutant transformed SCLC patients, showing an objective response rate of 66.7% and a median PFS [21].

In conclusion, the transformation from adenocarcinoma to SCLC can manifest as an acquired resistance mechanism to TKIs. Our case highlights the occurrence of 2 distinct acquired resistance mechanisms during TKI treatment, and underscores the significance of repeated biopsies in NSCLC patients experiencing disease progression. In addition, despite not being covered by health insurance in Taiwan, the combination of chemotherapy and EGFR-TKI may still play a role as a treatment option after transformation to SCLC.

References

1. Engelman JA, Janne PA. Mechanisms of acquired resistance to epidermal growth factor receptor tyrosine kinase inhibitors in non-small cell lung cancer. Clin Cancer Res 2008; 14(10): 2895-9.
2. Oser MG, Niederst MJ, Sequist LV, *et al*. Transformation from non-small cell lung cancer to small-cell lung cancer: molecular drivers and cells of origin. Lancet Oncol 2015; 16: e165-72.
3. Sequist LV, Waltman BA, Dias-Santagata D, *et al*. Genotypic and histological evolution of lung cancers acquiring resistance to EGFR inhibitors. Sci Transl Med 2011; 3: 75ra26.
4. Yu HA, Arcila ME, Rekhtman N, *et al*. Analysis of tumor specimens at the time of acquired resistance to EGFR-TKI therapy in 155 patients with EGFR-mutant lung cancers. Clin Cancer Res 2013; 19: 2240-47.
5. Adelstein DJ, Tomashefski JF Jr, Snow NJ, *et al*. Mixed small cell and non-small cell lung cancer. Chest 1986; 89: 699-704.
6. Norkowski E, Ghigna MR, Lacroix L, *et al*. Small-cell carcinoma in the setting of pulmonary adenocarcinoma: new insights in the era of molecular pathology. J Thorac Oncol 2013; 8: 1265-71.
7. Peifer M, Fernandez-Cuesta L, Sos ML, *et al*. Integrative genome analyses identify key somatic driver mutations of small-cell lung cancer. Nat Genet 2012; 44: 1104-10.
8. Rudin CM, Durinck S, Stawiski EW, *et al*. Comprehensive genomic analysis identifies SOX2 as a frequently amplified gene in small-cell lung cancer. Nat Genet 2012; 44: 1111-6.
9. Niederst MJ, Sequist LV, Poirier JT, *et al*. RB loss in

resistant EGFR mutant lung adenocarcinomas that transform to small-cell lung cancer. Nat Commun 2015; 6: 6377.

10. Sutherland KD, Proost N, Brouns I, *et al*. Cell of origin of small cell lung cancer: inactivation of Trp53 and Rb1 in distinct cell types of adult mouse lung. Cancer Cell 2011; 19: 754-4.
11. Desai TJ, Brownfield DG, Krasnow MA. Alveolar progenitor and stem cells in lung development, renewal and cancer. Nature 2014; 507: 190-94.
12. Roca E, Gurizzan C, Amoroso V, *et al*. Outcome of patients with lung adenocarcinoma with transformation to small-cell lung cancer following tyrosine kinase inhibitors treatment: a systematic review and pooled analysis. Cancer Treat Rev 2017; 59: 117-22.
13. Sculier JP, Chansky K, Crowley JJ, *et al*. The impact of additional prognostic factors on survival and their relationship with the anatomical extent of disease expressed by the 6th Edition of the TNM Classification of Malignant Tumors and the proposals for the 7th Edition. J Thorac Oncol 2008; 3: 457-66.
14. Liu Y. Small cell lung cancer transformation from EGFR-mutated lung adenocarcinoma: a case report and literatures review. Cancer Biol Ther 2018; 19(06): 445-9.
15. Hong E, Chen XE, Mao J, *et al*. Sequential occurrence of T790M mutation and small cell lung cancer transformation in EGFR-positive lung adenocarcinoma: a case report. World J Clin Cases 2022 Mar 26; 10(9): 2836-43.
16. Mambetsariev I, Arvanitis L, Fricke J, *et al*. Small cell lung cancer transformation following treatment in EGFR-mutated non-small cell lung cancer. J Clin Med 2022 Mar 5; 11(5): 1429.
17. Yin X, Li Y, Wang H, *et al*. Small cell lung cancer transformation: from pathogenesis to treatment. Semin Cancer Biol 2022 Nov; 86(Pt 2): 595-06.
18. Wang S, Xie T, Hao X, *et al*. Comprehensive analysis of treatment modes and clinical outcomes of small cell lung cancer transformed from epidermal growth factor receptor mutant lung adenocarcinoma. Thorac Cancer 2021 Oct; 12(19): 2585-93.
19. Niederst MJ, Sequist LV, Poirier JT, *et al*. RB loss in resistant EGFR mutant lung adenocarcinomas that transform to small-cell lung cancer. Nat. Commun. 6 (2015) 6377.
20. Collin MB, Matthew AG, *et al*. Phase I study of the aurora kinase A inhibitor alisertib in combination with osimertinib in EGFR-mutant lung cancer. Journal of Clinical Oncology 39, no. 15_suppl (May 20, 2021) 9074-9074
21. Wang W, Xu C, Chen H *et al*. Genomic alterations and clinical outcomes in patients with lung adenocarcinoma with transformation to small cell lung cancer after treatment with EGFR tyrosine kinase inhibitors: a multicenter retrospective study. Lung Cancer 155 (2021) 20-7.

Colonic Tuberculosis in an Immunocompetent Patient: A Case Report

Tan-Ching Lan[1], Ya-Ju Wu[2], Shian-Chiw Ko[1]

Tuberculosis is a major public health problem worldwide. The pathogen is *Mycobacterium tuberculosis*, which can infect any part of the body. Lung parenchyma is the most commonly infected site, while infections in the abdomen are relatively uncommon. In general, abdominal tuberculosis lacks special clinical manifestations and is easily confused with other diseases. Tuberculosis should be incorporated into the differential diagnosis in areas of high prevalence, such as Taiwan. Mycobacterial culture remains the gold standard for diagnosis. Here, we reported the case of an asymptomatic and immunocompetent patient who was diagnosed with colonic tuberculosis. Microbiologic evidence gained from colonic tissue led to the final diagnosis. ***(Thorac Med 2024; 39: 152-157)***

Key words: Extrapulmonary tuberculosis (EPTB), tuberculosis (TB), *Mycobacterium tuberculosis*

Introduction

Tuberculosis (TB) is a wide-spreading infectious disease, and the pathogen is Mycobacterium tuberculosis(MTB). The route of transmission is mainly through air droplets when the infected persons cough or talk. Approximately 25% of the world's population is infected by MTB, but only 5-15% of those will actually develop active TB disease. According to the World Health Organization (WHO), 10 million people are newly diagnosed with active TB and about 1.5 million people die each year due to the disease [1]. In Taiwan, there were 7,062 new TB cases in 2021. The incidence rate was 30.1 per 100,000 population and the mortality rate was 1.9 per 100,000 population [2].

TB is classified as either pulmonary or extrapulmonary TB (EPTB), based on the infected organs. Lung parenchyma is the most commonly infected site, and cases with pulmonary involvement are defined as pulmonary TB. Ac-

[1]Division of Chest Medicine, ChiMei Hospital, Tainan City, Taiwan, [2]Department of Pathology, ChiMei Hospital, Tainan City, Taiwan
Address reprint requests to: Dr. Shian-Chin Ko, Division of Chest Medicine, Department of Internal Medicine, Chi Mei Hospital, No.901, Zhonghua Rd., Yongkang Dist., Tainan City 710, Taiwan (R.O.C.)

cording to WHO classification criteria, EPTB means infections in organs outside the lung parenchyma [1]. For infected patients, early diagnosis and prompt anti-TB treatment are most important. MTB can infect any part of the body, but infections in the abdomen are uncommon. Abdominal TB lacks specific clinical symptoms and radiological findings. In these cases, we may face the problem of obtaining adequate specimens for microbiologic or histopathologic confirmation. Therefore, reaching a timely and accurate diagnosis of abdominal TB is often a predicament in clinical practice [3-7].

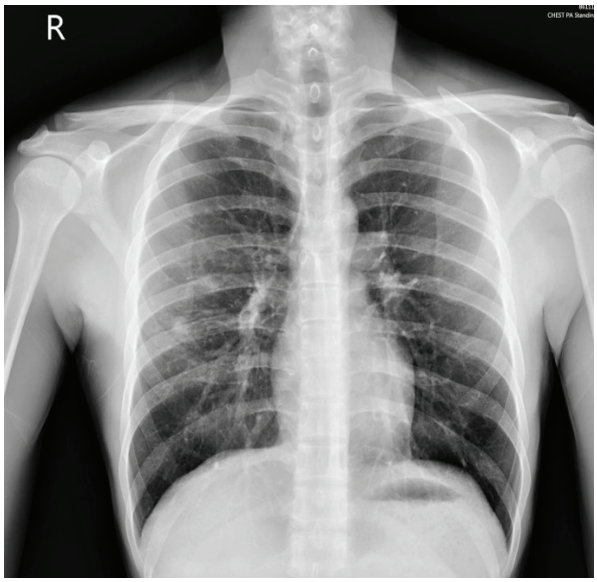

Fig. 1. CXR in March 2022 showed a nodular opacity at the right middle lung field.

Case Report

A 33-year-old male presented to the family medicine department in our hospital for a physical check-up in early March 2022. Chest radiography (CXR) showed a nodular opacity at the right middle lung field (Figure 1). Colonoscopy showed colitis with multiple ulcerations, with polypoid lesions at the cecum and proximal ascending colon (Figure 2). The histopathology of the colonic ulcers revealed chronic active colitis with focal erosion and non-caseating granulomas (Figure 3). The special stains, including periodic acid-schiff stain(PAS), acid-fast stain(AFS), and cytomegalovirus(CMV) immunohistochemical stain, were negative (Figure 4). The colonic specimen was also sent for mycobacterial culture, based on the gastroenterologist's experience, and the microbiologic analysis revealed the presence of MTB. There-

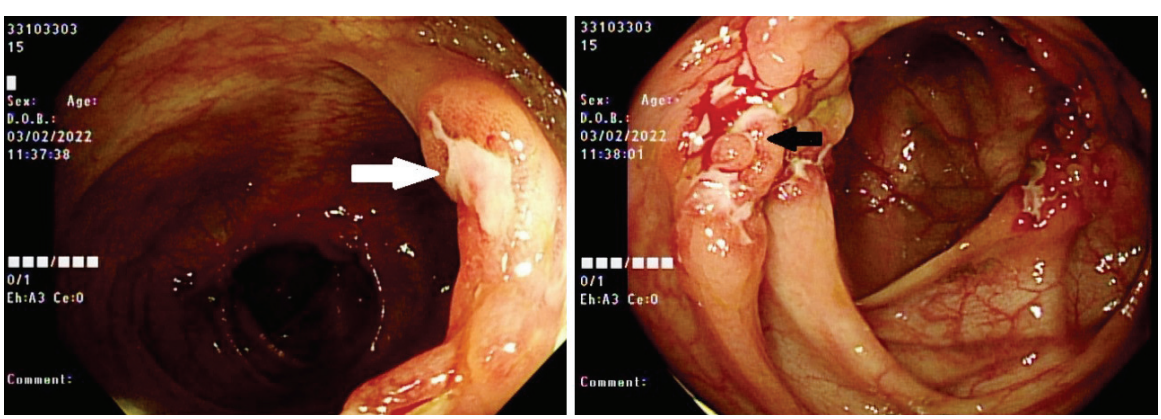

Fig. 2. Colonoscopy showed multiple ulcerations with polypoid lesions at the proximal ascending colon (white arrow head) and cecum, including the ileocecal valve (black arrow head).

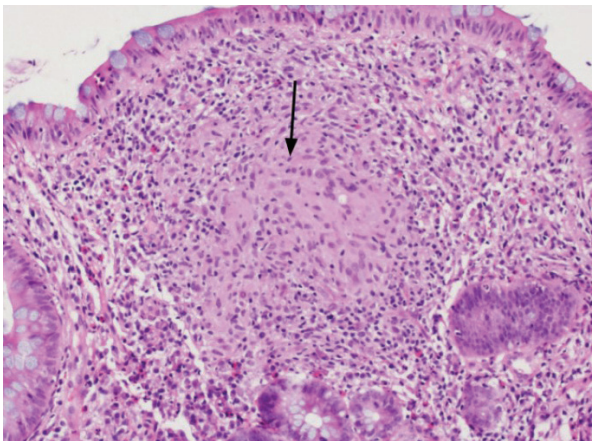

Fig. 3. Under hematoxylin-eosin stain, electronic microphotography (x200) showed colonic mucosa with non-caseating granulomas (black arrow head) and epithelioid histiocytes aggregation in the lamina propria.

fore, the patient was referred to the chest department for treatment of extrapulmonary TB.

Tracing back the patient's history, lung nodules had been detected at a previous examination. Initial chest computed tomography (CT) in December 2019 disclosed a cluster of small nodules in the superior segment of the right lower lobe (RLL), and the largest nodule had cavitation (Figure 5A). He was advised to visit the chest clinic due to a suspicion of mycobacterial infection. However, the patient was lost to follow-up, so no further workup was performed.

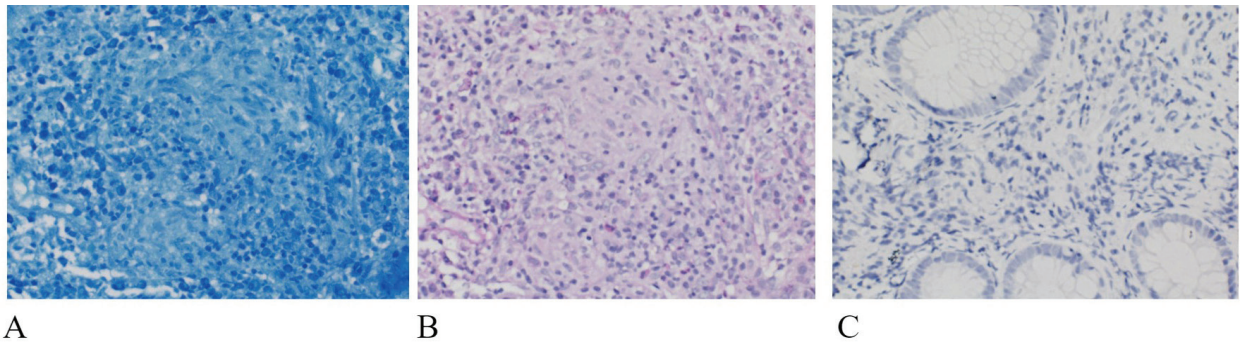

Fig. 4. The electronic microphotography (x 400) showed that colonic specimens were negative on AFS (A), PAS stain (B) and CMV immunohistochemical stain (C).

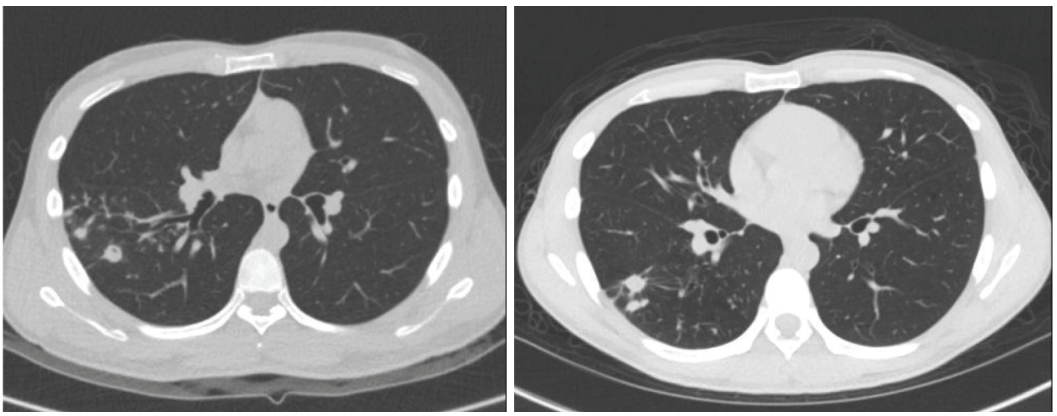

Fig. 5. (A) Chest-CT in 2019 showed a cluster of random-sized nodules in the superior segment of the RLL. The largest nodule had a diameter < 1 cm and internal cavitation (white arrow). (B) Chest-CT in 2022 showed resolution of the previous lung nodules. However, new tree-in-bud lesions and a subpleural nodular lesion, up to 1.5-cm in size with irregular outlines, were detected.

Upon admission to the chest department in late March 2022, the patient denied any symptoms of fever, anorexia, cough, dyspnea, abdominal pain, distension, bloody stool or change in bowel habits. He was of normal weight, with a body mass index of 18.3kg/m2. There was no major medical disorder, such as hypertension, liver cirrhosis, renal impairment or diabetes mellitus. The TB contact was his grandmother, who had pulmonary TB after complete treatment 8 years ago, and the patient mentioned no abnormalities found at that time. He was afebrile, with a pulse rate of 75 beats/min regularly, a respiratory rate of 18 breaths/min, and blood pressure of 121/62 mmHg. Physical examinations were unremarkable. The hemogram and biochemistry were within normal limits. The serological test for human immunodeficiency virus was negative. Chest CT in March 2022 showed resolution of previous lung lesions. However, new clusters of small nodular lesions and tree-in-bud opacities were seen in the superior segment of the RLL (Figure 5B). Mycobacterial infection in the lung was still suspected. Since the largest pulmonary nodule was up to 1.5 cm in size and with an irregular outline, CT-guided fine needle biopsy was performed. The pathological finding revealed fibrous tissue only. AFS and mycobacterial culture of 3 specimens of sputum were negative. Although no active pulmonary TB was found, inactive pulmonary TB was highly suspected.

Overall, microbiologic evidence led to the final diagnosis of colonic TB. Four-drug combined anti-TB therapy (isoniazid, rifampin, ethambutol, pyrazinamide) was initiated. The drug susceptibility test showed that the MTB isolate was susceptible to all first-line anti-TB drugs. He completed a 9-month course of anti-TB therapy successfully.

Discussion

There are apparently fewer cases of EPTB than of pulmonary TB. In 2021, it was estimated that 8% to 23% of TB cases were extrapulmonary. This estimate varied by region and made up an average of 17% of total TB cases notified by the WHO [1]. One report from 1997 that collected data in Taiwan, described a 1:9 ratio of EPTB to pulmonary TB [8]. However, the proportion of EPTB in Taiwan was as high as 23% to 27%, according to Taiwan's National Health Insurance (NHI) data collected from 1996 to 2003 [9]. Based on the higher proportion of EPTB in Taiwan, we should be aware of extrapulmonary presentations of TB.

The main mechanisms of extrapulmonary infection are mycobacterial transmission from lung parenchyma to other organs through the bloodstream or lymphatic systems. Other possible mechanisms are primary infection of extrapulmonary organs or contagious spread from adjacent organs. For example, gastrointestinal mucosa can be infected with MTB by polluted food. The common sites of EPTB are lymph nodes and pleura, while infections in the abdomen are rare [3-7,10-12]. Abdominal TB lacks special clinical manifestations. The common systemic symptoms are fever, weight loss, night sweats and anorexia. Symptoms localized to the abdomen include abdominal pain, distension, nausea, vomiting, diarrhea, and blood in the stool. Commonly infected sites in the abdomen are the ileocecal valve, the colon and the peritoneum. On colonoscopy, the presence of ulcerations is a common finding. Other endoscopic abnormalities include erythema, erosions, nodules, pseudopolyps, and strictures [4, 6, 13-14].

Analysis of TB-related ascites reveals protein of more than 2.5 g/dl, white cell counts of 500-1,500 per cubic mm with predominant lymphocytes, and a serum-ascites albumin gradient less than 1.1g/dL. In addition, a systematic review described the high specificity of adenosine deaminase (ADA). ADA measurement of more than 39 IU/L in ascites fluid suggests a diagnosis of peritoneal TB [4,6,15-16].

Abdominal CT is another frequently-used diagnostic tool. Peritoneal involvement can be identified by ascites and a thickened peritoneum with a smooth or nodular surface. Lymph nodal involvement commonly appears as enlarged, necrotic lesions with peripheral enhancement. Intestinal TB can appear with bowel wall thickening and strictures. Mass-like lesions, probably caused by thickening of the ileocecal valve and enlarged lymph nodes, are uncommon and sometimes misidentified as malignancy [17, 18].

We should maintain a high level of clinical suspicion for EPTB, because it always lacks specific manifestations. Microbiological analysis is important to confirm the diagnosis. Clinical symptoms, pathological examinations and images are also used to support the clinical diagnosis. The hallmark of histopathological analysis is caseous granulomas, while chronic inflammation with non-caseous granulomas is the usual presentation. Microbiological analysis includes AFS, gene examinations and mycobacterial culture. If AFS is positive, it is necessary to differentiate MTB from nontuberculous mycobacteria. The gold standard of diagnosis is mycobacterial culture, but the final result is reported weeks later [3,4,6]. GeneXpert-MTB/RIF is a rapid nucleic acid amplification assay to detect MTB. A systematic review of GeneXpert-MTB/RIF reported that sensitivity varied across different extrapulmonary specimens (31%~97%). Specificity was ≧ 98% in cerebrospinal fluid, pleural fluid, urine and peritoneal fluid [19]. Therefore, GeneXpert-MTB/RIF is a useful tool to confirm an EPTB diagnosis rapidly, but a negative result can not entirely exclude the possibility of MTB infection.

According to the Taiwan Guidelines for TB Diagnosis & Treatment (7thed.), the main management for EPTB is medical treatment. The general therapeutic course is 4-drug combined anti-TB therapy with isoniazid, rifampin, ethambutol, pyrazinamide for 2 months, then 2-drug combined anti-TB therapy with isoniazid and rifampin for the next 4 to 7 months, if the drug susceptibility test shows no resistance. The duration of 2-drug combined anti-TB therapy should be extended for infections in the skeleton or central nervous system. The indications for corticosteroid therapy are involvement of the pericardium and the central nervous system. The main role of surgical intervention is biopsy. For abdominal TB, surgery can be considered in cases with complications, such as obstruction, fistula, and perforation. Most colorectal TB lesions show resolution with complete mucosal healing after as few as 2 months of anti-TB therapy. Therefore, there is no requirement to repeat colonoscopy when the patient is asymptomatic after treatment [3-6].

In conclusion, abdominal TB is easily confused with other diseases. The low incidence, atypical symptoms and nonspecific imaging findings are diagnostic challenges. We reported an immunocompetent patient who was asymptomatic and was diagnosed with colonic TB through microbiological evidence of colonic tissue. Prior self-healing pulmonary TB and mycobacterial transmission to the gastrointestinal tract were suspected. Mycobacterial culture

is the gold standard of diagnosis and should be performed in a timely manner to prevent a delay in diagnosis. EPTB always has a good response to anti-TB drugs. Therefore, the most important issue of abdominal TB is getting an accurate diagnosis early.

References

1. World Health Organization. Global tuberculosis report 2021. Available at https://www.who.int/teams/global-tuberculosis-programme/tb-reports/global-tuberculosis-report-2021. Accessed January 30, 2023.
2. Taiwan Centers for Disease Control. Available at https://daily.cdc.gov.tw/stoptb/Indicator.aspx. Accessed February 07, 2023.
3. Taiwan Guidelines for TB Diagnosis & Treatment (7E). Available at https://www.tspccm.org.tw/media/12044. Accessed January 28, 2023.
4. Debi U, Ravisankar V, Prasad KK, *et al*. Abdominal tuberculosis of the gastrointestinal tract: revisited. World J Gastroenterol. 2014; 20(40): 14831-14840.
5. Niţu FM, Călăraşu C, Nemeş RM, *et al*. Concomitant lung and intestinal tuberculosis - a case report. Rom J Morphol Embryol. 2019; 60(2): 717-721.
6. Al-Zanbagi AB, Shariff MK, Gastrointestinal tuberculosis: a systematic review of epidemiology, presentation, diagnosis and treatment. Saudi J Gastroenterol 2021; 27(5): 261-274.
7. Ramirez-Lapausa M, Menendez-Saldana A, Noguerado-Asensio A, Extrapulmonary tuberculosis: an overview. Rev Esp Sanid Penit 2015; 17: 3-11.
8. Yu MC, Suo J, Bai KJ, *et al*. 臺灣地區的肺外結核. 胸腔醫學. 1997: 99-104.
9. Hsu YC, Yang MH, Chen YH, *et al*. 台灣1996-2003年肺外結核病流行病學特性分析. 疫情報導. 2007; 第23卷第8期 231-242頁.
10. Sotgiu G, Falzon D, Hollo V, *et al*. Determinants of site of tuberculosis disease: an analysis of European surveillance data from 2003 to 2014. PLoS One 2017; 12: e0186499.
11. Cherian JJ, Lobo I, Sukhlecha A, *et al*. Treatment outcome of extrapulmonary tuberculosis under Revised National Tuberculosis Control Programme. Indian J Tuberc 2017; 64: 104-8.
12. Pang Y, An J, Shu W, *et al*. Epidemiology of extrapulmonary tuberculosis among inpatients, China, 2008-2017. Emerg Infect Dis 2019; 25: 457-64.
13. Cho JK, Choi YM, Lee SS, *et al*. Clinical features and outcomes of abdominal tuberculosis in southeastern Korea: 12 years of experience. BMC Infect Dis 2018; 18: 699.
14. Chien K, Seemangal J, Batt J, *et al*. Abdominal tuberculosis: A descriptive case series of the experience in a Canadian tuberculosis clinic. Int J Tuberc Lung Dis 2018; 22: 681-5.
15. Sanai FM, Bzeizi KI. Systematic review: tuberculous peritonitis -- presenting features, diagnostic strategies and treatment. Aliment Pharmacol Ther 2005; 22: 685-700.
16. Riquelme A, Calvo M, Salech F, *et al*. Value of adenosine deaminase (ADA) in ascitic fluid for the diagnosis of tuberculous peritonitis: A meta-analysis. J Clin Gastroenterol 2006; 40: 705-10.
17. Lee WK, Van Tonder F, Tartaglia CJ, *et al*. CT appearances of abdominal tuberculosis. Clin Radiol 2012; 67: 596-604.
18. Deshpande SS, Joshi AR, Deshpande SS, *et al*. Computed tomographic features of abdominal tuberculosis: Unmask the impersonator! Abdom Radiol (NY) 2019; 44: 11-21.
19. Kohli M, Schiller I, Dendukuri N, *et al*. Xpert MTB/RMP assay for extrapulmonary tuberculosis and rifampicin resistance. Cochrane Database Syst Rev 2018; 8(8): CD012768.

Primary Pulmonary Adenoid Cystic Carcinoma with Tracheal Invasion and Total Obstruction of the Left Main Bronchus – A Case Report

Chao-Wen Lu[1,2,3], Min-Shu Hsieh[3,4], Hsao-Hsun Hsu[4,5]

Primary pulmonary adenoid cystic carcinoma (ACC) is a rare pulmonary malignancy. With its slow-growing nature, it is difficult to diagnose until the disease progresses to an advanced stage. We reported the case of a 68-year-old woman who presented with a 1-year history of chest discomfort. After serial examinations, an ACC with tracheal invasion and total obstruction of the left main bronchus was identified. Based on the preoperative assessment of the patient, left pneumonectomy with partial resection of the trachea and bronchoplasty were deemed feasible. A final pathological examination revealed an ACC with a mixed cribriform and tubular pattern. *MYB* breakage was confirmed via fluorescence in situ hybridization. Since the resection margins were tumor-free, no adjuvant therapy was necessary. No tumor recurrence was noted on the follow-up chest computed tomography. This case highlights the challenges in diagnosing and treating primary pulmonary ACCs. Surgery remains its mainstay treatment modality. ***(Thorac Med 2024; 39: 158-164)***

Key words: adenoid cystic carcinoma, anterolateral thoracotomy, pneumonectomy

Introduction

Primary airway cancers comprise less than 1% of all pulmonary malignancies [1-4]. Squamous cell carcinoma (SqCC) is the most common primary tracheal tumor, followed by adenoid cystic carcinoma (ACC) [4]. ACC is a salivary gland-type tumor of the lung characterized by 3 distinct architectures: tubular, cribriform, and solid [5-6]. The presence of a solid pattern is associated with distant metastasis and a poorer prognosis [5]. ACC usually grows slowly and remains undetected for many years until it reaches an advanced stage [5].

Complete surgical resection is the primary treatment modality for ACCs. However, R0 resection may be challenging, and may be associated with severe complications due to the central location of the airway [3]. Promising prognoses can still be achieved using R1 resection

[1]Department of Surgery, National Taiwan University Hospital Yun Lin Branch, Yunlin 640, Taiwan. [2]Graduate Institute of Pathology, National Taiwan University College of Medicine, Taipei 100, Taiwan. [3]Department of Pathology, National Taiwan University Cancer Center, Taipei 106, Taiwan. [4]Department of Surgery, National Taiwan University Hospital & College of Medicine, Taipei 100, Taiwan. [5]National Taiwan University Cancer Center, Taipei 106, Taiwan

Address reprint requests to: Dr. Hsao-Hsun Hsu, Department of Surgery, College of Medicine, National Taiwan University. No. 7 Zhongshan South Road, Zhongzheng Dist., Taipei City 100225, Taiwan (R.O.C.)

with adjunctive therapies such as radiotherapy [4, 6-7]. We report a case of ACC arising from the left main bronchus, with total obstruction of the left lung.

Case Presentation

A 68-year-old woman was regularly followed up at our outpatient clinic for hypertension and asthma. She had a 1-year history of chest discomfort, with left lung collapse on chest radiography (Figure 1A). Chest computed tomography (CT) revealed a large tumor obstructing the left main bronchus, leading to the total collapse of the left lung (Figure 1B and 1C). Bronchoscopy revealed an endotracheal tumor extending from the left main bronchial orifice to the level above the carina (Figures 2A and 2B). Esophagogastroduodenoscopy ultrasound revealed a 38.2 × 62.6-mm hypoechoic heterogeneous lesion at the para-esophageal space near the aorta, approximately 28-30 cm below the incisors. Fine-needle biopsy via esophagogastroduodenoscopy confirmed an ACC, characterized by mixed tubular and cribriform patterns with biphasic p63 staining and diffuse SOX10 expression. Brain and bone CT revealed no distant metastases.

Echocardiography revealed a normal left ventricular ejection fraction (87.0%) with mild to moderate tricuspid regurgitation (TR max pressure gradient: 20.5 mmHg). A pulmonary function test was not performed. Despite complete obstructive collapse of the left lung, the patient was able to maintain normal daily activity. Therefore, based on the adequate heart function and fair clinical presentation, we concluded that the patient would be able to maintain her normal daily activity after a left pneumonectomy. After discussion with the patient and her family, the left pneumonectomy and carinal resection with bronchoplasty were performed.

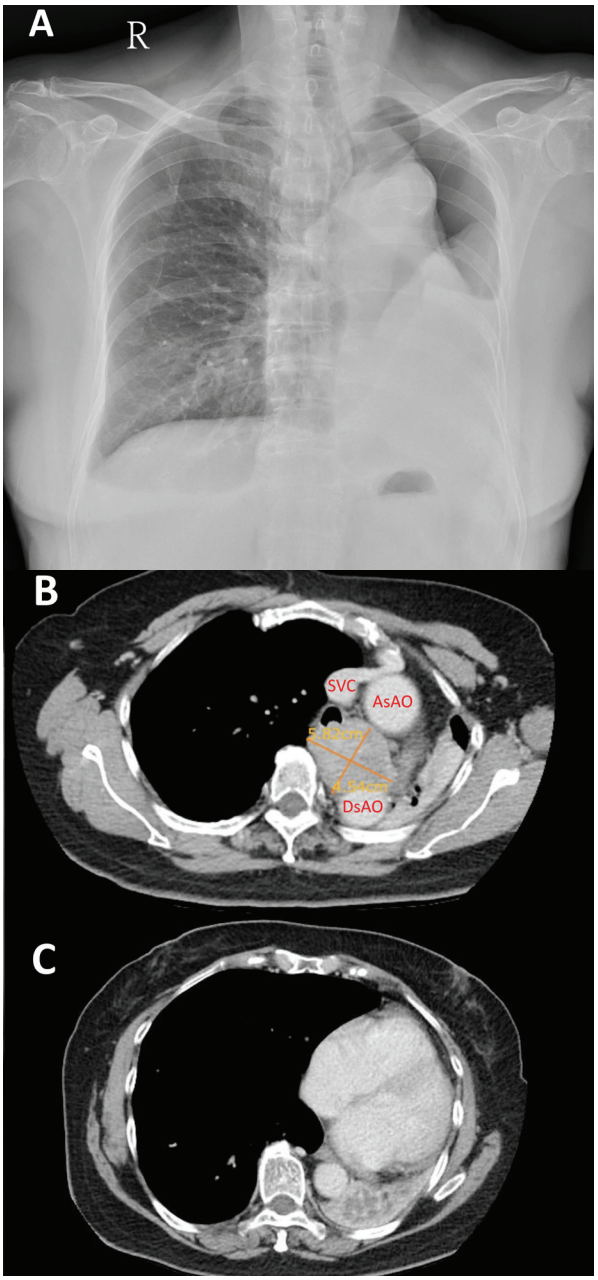

Fig. 1. (A) Chest radiography showing a collapsed left lung. (B) Computed tomography (CT) scan showing a mass obstructing the left main bronchus. (C) CT showing a completely collapsed left lung. SVC, superior vena cava; AsAO, ascending aorta; Ds AO, descending aorta.

Intraoperatively, a solid and firm tumor, invading the trachea, was found in the left main

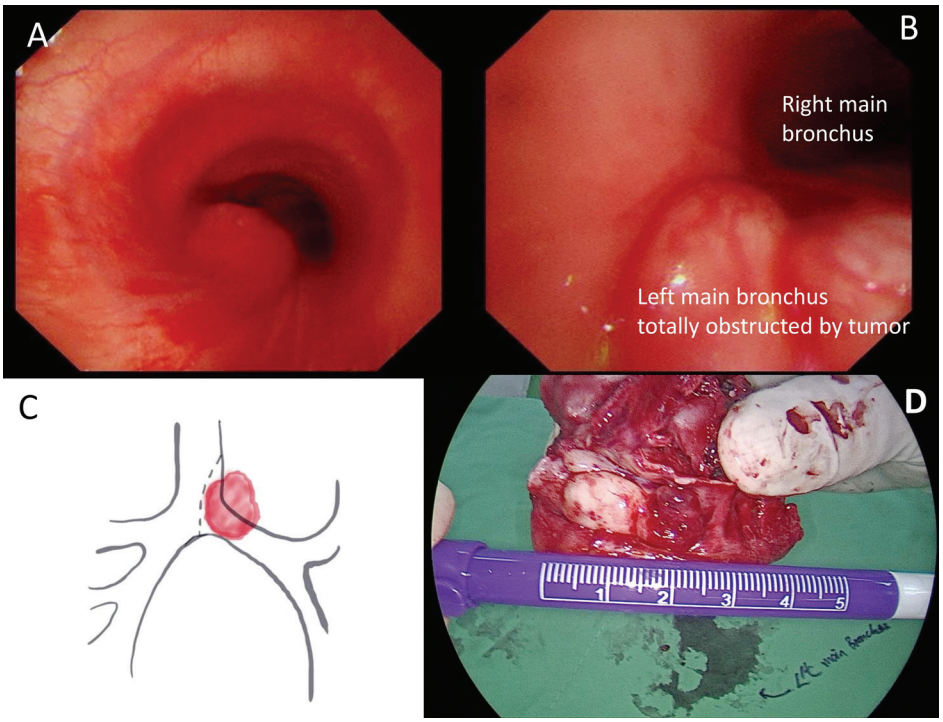

Fig. 2. (A) Bronchoscopy showing tumor invasion into the trachea. (B) The tumor completely obstructed the left main bronchus orifice. (C) Schematic picture of the left main bronchus resection with partial tracheal resection. (D) Total obstruction of the left main bronchus.

bronchus (Figures 2C and 2D). Pulmonary artery pressure was not elevated after clamping the left main pulmonary artery. The left side of the heart was compressed for better tumor exposure, and venoarterial extracorporeal membrane oxygenation (VA-ECMO) was used to maintain normal blood pressure. The tumor was removed by means of a left main bronchus resection, with partial tracheal resection, and without injury to the recurrent nerve. The trachea was repaired using a 4-0 PDS with an interrupted style. A pericardial flap was used to cover the anastomosis site. Then, we checked the air leak using the water sealing method. No air leakage from the repaired site was seen. A 28 Fr chest tube was set at the posterior aspect of the left thoracic cavity, and the wound was closed in layers. The total blood loss was 350 mL, and the total operative time was 491 min. Intraoperative VA-ECMO was successfully discontinued.

The patient was transferred to the intensive care unit for postoperative surveillance. No right ventricular dilatation or elevation of central venous pressure was observed, and the Swan-Ganz catheter was removed on postoperative day 3. As the patient began to walk and demonstrated good tolerance, prostaglandin E1 infusion was gradually tapered.

Consultation with an otolaryngologist was required due to the development of hoarseness and left vocal cord palsy. After spontaneous improvement of the hoarseness, watchful waiting was implemented. The chest tube was clamped on the 8th postoperative day, and successfully removed the following day. On postoperative day 10, the patient was transferred to the general ward under relatively stable conditions. The

patient was successfully discharged on postoperative day 17.

Pathological examination revealed a 6 × 6 × 4.8 cm ACC, with mixed cribriform and tubular patterns (Figure 3). No solid components were observed. Perineural invasion was also observed. MYB rearrangement was confirmed using fluorescence in situ hybridization (FISH) (Figure 4). The section margins were tumor-free, and the pathological stage was T3N0M0.

The patient was regularly followed up with a bronchoscopic examination and chest CT, without adjuvant therapy (Figure 5). She has remained disease-free and has been able to independently perform her activities of daily living for 17 months.

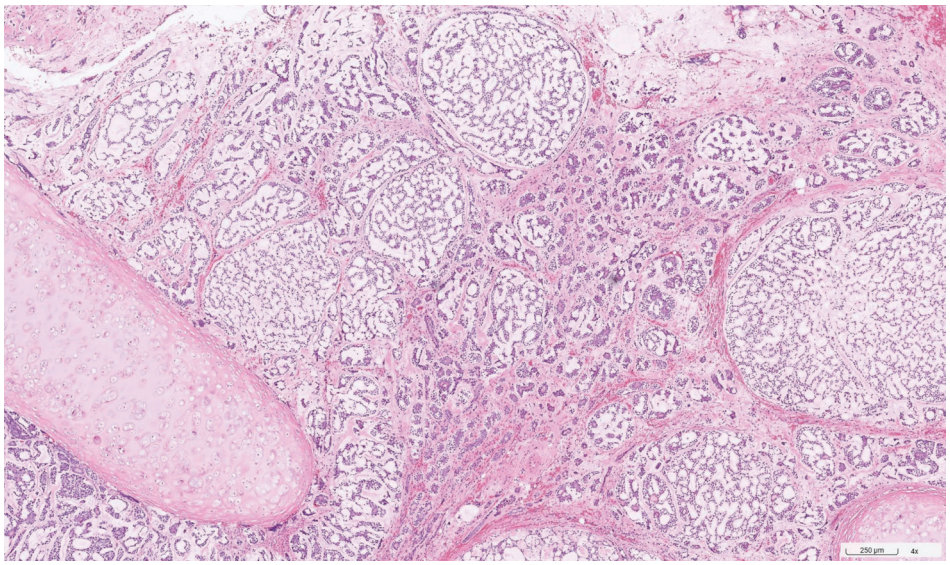

Fig. 3. Pathological examination of the adenoid cystic carcinoma showed the presence of mixed cribriform and tubular patterns.

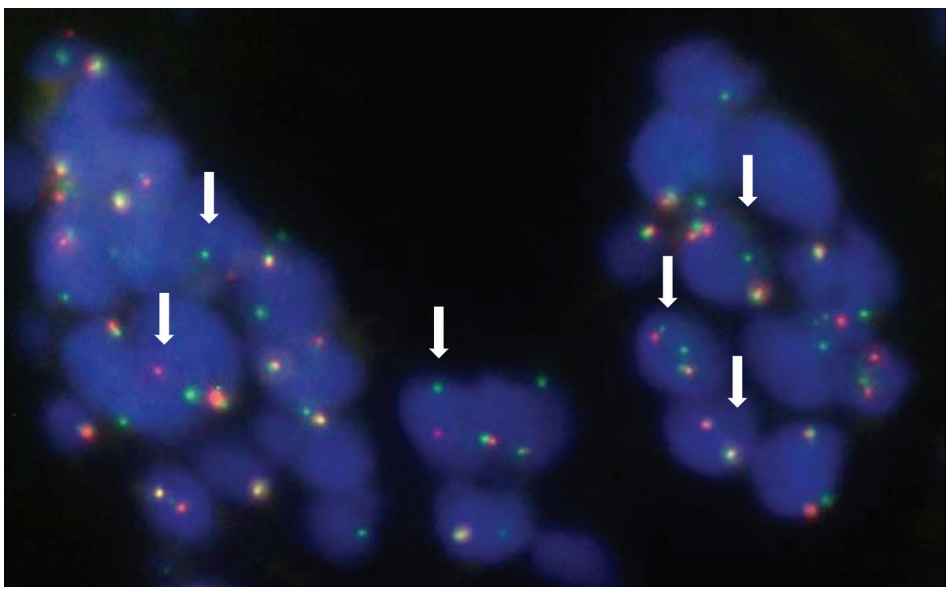

Fig. 4. MYB rearrangement was confirmed by break-apart fluorescence in situ hybridization.

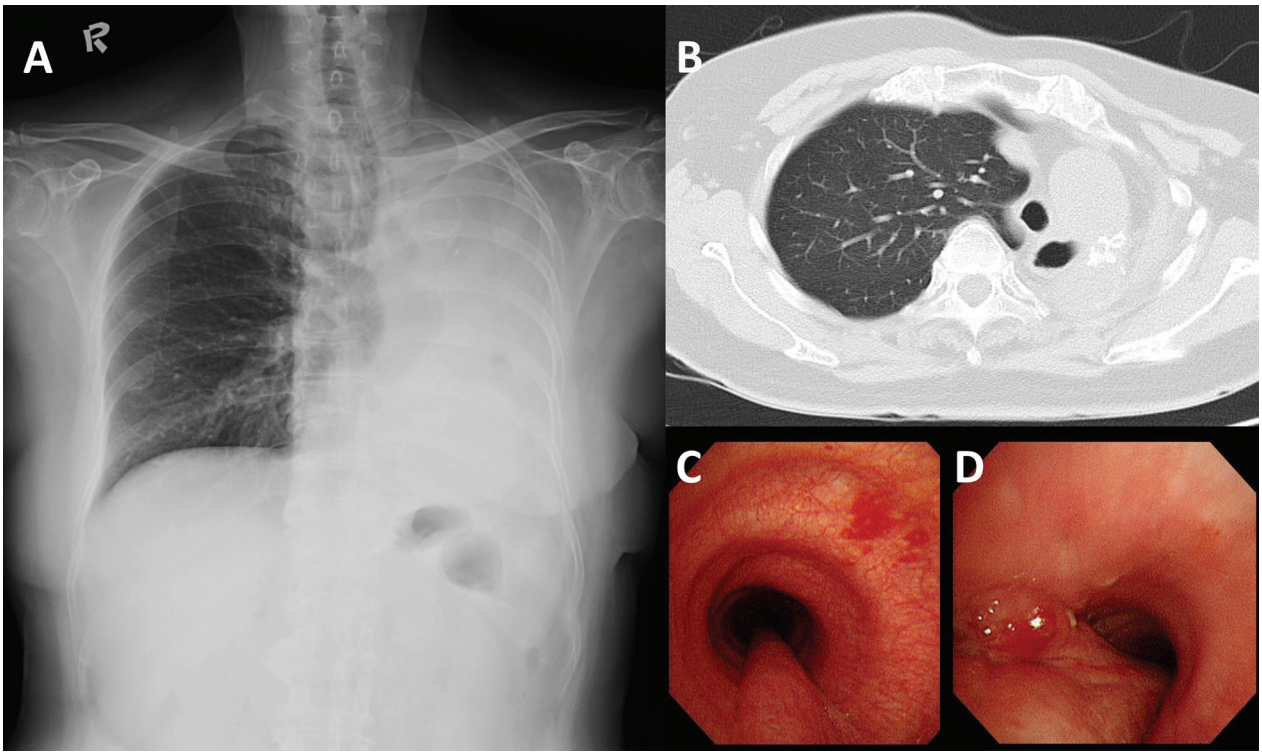

Fig. 5. (A) Chest X-ray showed left pneumonectomy, with opacity at the left-side hemothorax. (B) CT scan showed no local recurrence after left pneumonectomy. (C) Bronchoscopy revealed a patent trachea (D). Bronchoscopy revealed a patent right main bronchus, with granulation tissue formation at the resection margin.

Discussion

ACC occurs more frequently in middle-aged women [8]. Similar to its salivary gland counterpart, primary pulmonary ACC is a low-grade carcinoma that is slow-growing and locally invasive, with a risk of local recurrence and late metastasis. The reported 5-year and 10-year survival rates are approximately 52-79% and 29-56%, respectively. Tracheal ACC most frequently occurs in the distal third of the trachea [9]. In the present case, the patient was asymptomatic until the left main bronchus was completely obstructed by the ACC. Despite the challenging location of the tumor, we were able to achieve an R0 resection through a difficult surgical approach.

Pulmonary ACC is a malignant biphasic salivary gland-type tumor with epithelial and myoepithelial cells. Tubular, cribriform, and solid tumors are the 3 major histological patterns of ACC. A solid pattern is associated with a poor prognosis. Clinically, ACC arises from large airways and presents as an endotracheal or endobronchial tumor [5, 8]. As in salivary gland ACCs, MYB and MYBL1 rearrangements are characteristic genetic changes in tracheopulmonary ACCs, and 40% of pulmonary ACCs harbor MYB rearrangements, which can be detected via FISH [10-11].

Reports indicate that the postoperative 5-year survival rate for patients with ACC ranges from 52–100%, which is higher than that observed in patients with SqCC (5-year survival rates of 3–53%) [3, 12-14]. Tumors involving the airway margins are more commonly ob-

served in patients with ACC than in those with SqCC. Moreover, SqCC has poorer survival outcomes than ACC when the resection margins are involved [14]. In our case, adjuvant therapy was not administered due to the patient's tumor-free resection margins [15]. However, another study found that extraluminal invasion of ACC, even after R0 resection, was associated with poorer disease-free survival rates (66.66%) [6]. Given the presence of extraluminal extension and perineural invasion in this case, there was a relatively high risk of recurrence; therefore, close monitoring and follow-up should still be performed.

Though rare, ACC can be aggressive and difficult to treat if not detected early. Complete resection remains the mainstay of treatment for ACC. Although complete resection (R0 resection) remains the preferred treatment approach for ACC, patients at high risk of surgical complications may still benefit from R1 resection followed by postoperative radiation therapy, which can yield a favorable prognosis [4, 6-7].

Conclusion

Favorable outcomes for patients with ACC can be achieved through complete resection.

Competing interests

All authors declare to have no conflict of interest.

Funding

No funding was obtained for this manuscript. The Acknowledgement below indicates there was funding (grants) from NTUH.

Authors' contributions

CWL prepared the first draft of the manuscript. HHH provided the study materials. MSH and HHH carefully reviewed and drafted the manuscript until its final version. All the authors have read and approved the final version of the manuscript.

Acknowledgements

This study was supported by grants from National Taiwan University Hospital (MS441) to HHH.

References

1. Maziak DE, Todd TR, Keshavjee SH, *et al*. Adenoid cystic carcinoma of the airway- thirty-two-year experience. J Thorac Cardiovasc Surg 1996; 112: 1522-32.
2. Bhattacharyya N. Contemporary staging and prognosis for primary tracheal malignancies: a population-based analysis. Otolaryngol Head Neck Surg 2004; 131(5): 639-42.
3. Zhao Y, He G, Zhai Y, *et al*. Adenoid cystic carcinoma of lobar bronchial origin: 20-year experience at a single institution. Ann Surg Oncol 2022; 29: 4408-16.
4. Zhao L, Zhao Y, Guo JD, *et al*. Effective radiotherapy in tracheobronchial adenoid cystic carcinoma with positive surgical margin. Ann Thorac Surg 2021; 112(5): 1585-92.
5. Coca-Pelaz A, Rodrigo JP, Bradley PJ, *et al*. Adenoid cystic carcinoma of the head and neck--An update. Oral Oncol 2015; 51(7): 652-61.
6. Ning Y, He W, Bian D, *et al*. Tracheo-bronchial adenoid cystic carcinoma: A retrospective study. Asia Pac J Clin Oncol 2019; 15(4): 244-9.
7. Yusuf M, Gaskins J, Trawick E, *et al*. Effects of adjuvant radiation therapy on survival for patients with resected primary tracheal carcinoma: an analysis of the National Cancer Database. Jpn J Clin Oncol 2019; 49(7): 628-38.
8. Dewenter I, Otto S, Kakoschke TK, *et al*. Recent advances, systemic therapy, and molecular targets in

adenoid cystic carcinoma of the head and neck. J Clin Med 2023; 12(4): 1463-74.
9. Maziak DE. Biology of adenoid cystic carcinoma of the tracheobronchial tree and principles of management. Thorac Surg Clin 2018; 28(2): 145-8.
10. Pei J, Flieder DB, Patchefsky A, *et al*. Detecting MYB and MYBL1 fusion genes in tracheobronchial adenoid cystic carcinoma by targeted RNA-sequencing. Mod Pathol 2019; 32(10): 1416-20.
11. Roden AC, Greipp PT, Knutson DL, *et al*. Histopathologic and cytogenetic features of pulmonary adenoid cystic carcinoma. J Thorac Oncol 2015; 10(11): 1570-5.
12. Liu Y, Zheng K, Lu Q, *et al*. Surgical treatment of primary tracheobronchial tumors: 16-year experience in a single center. J Thorac Dis 2022; 14(2): 343-54.
13. Yang H, Yao F, Tantai J, *et al*. Resected tracheal adenoid cystic carcinoma: improvements in outcome at a single institution. Ann Thorac Surg 2016; 101(1): 294-300.
14. Gaissert HA, Grillo HC, Shadmehr MB, *et al*. Long-term survival after resection of primary adenoid cystic and squamous cell carcinoma of the trachea and carina. Ann Thorac Surg 2004; 78(6): 1889-97.
15. Honings J, Gaissert HA, Weinberg AC, *et al*. Prognostic value of pathologic characteristics and resection margins in tracheal adenoid cystic carcinoma. Eur J Cardiothorac Surg 2010; 37(6):1438-44.

Rupture of a Right-side Intrapulmonary Sequestration: A Case Report

Osbert Qi Yao Leow[1], Yi-Cheng Wu[1], Chien-Hung Chiu[1]

Pulmonary sequestration is a rare congenital malformation uncommonly diagnosed in adults. It has variable presentations, either asymptomatic or with severe symptoms such as hemoptysis and recurrent pneumonia. Diagnosis can be confirmed by computed tomography or angiography. Treatment with either surgery or embolization has been reported. We reported the case of a 40-year-old male patient who presented with hemoptysis and hemothorax, and was eventually diagnosed with ruptured right-side intrapulmonary sequestration. ***(Thorac Med 2024; 39: 165-169)***

Key words: Pulmonary sequestration, intrapulmonary sequestration, congenital lung anomaly, pulmonary sequestration rupture

Introduction

Pulmonary sequestration is a rare congenital lung anomaly defined as nonfunctioning pulmonary tissue supplied from an anonymous systemic blood supply, and is rarely diagnosed in an adult. We report the case of a patient who had symptoms of refractory hemoptysis and right hemothorax who underwent transarterial embolization (TAE) of the blood supply of a ruptured sequestration, followed by surgical resection of the right lower lobe (RLL) sequestration.

Case Report

A 40-year-old male patient had a history of a paraophthalmic internal carotid artery aneurysm, and underwent stenting several years ago. He was given dual antiplatelet therapy regularly after the operation. The patient was also found to have an asymptomatic RLL lesion with emphysema and atelectasis during a low-dose computed tomography scan a few years ago, and regular follow-up was suggested (Figure 1).

This time, the patient presented to our unit with the chief complaint of hemoptysis with increased frequency for days. The patient also had progressive dyspnea for 2 days. He denied chest tightness, chest pain and fever during the period. Physical examination showed diminished

[1]Division of Thoracic Surgery, Chang Gung Memorial Hospital--Linkou, College of Medicine, Chang Gung University, Taoyuan, Taiwan
Address reprint requests to: Dr. Osbert Qi Yao Leow, Division of Thoracic Surgery, Chang Gung Memorial Hospital-Linkou, Chang Gung University, Taoyuan, Taiwan

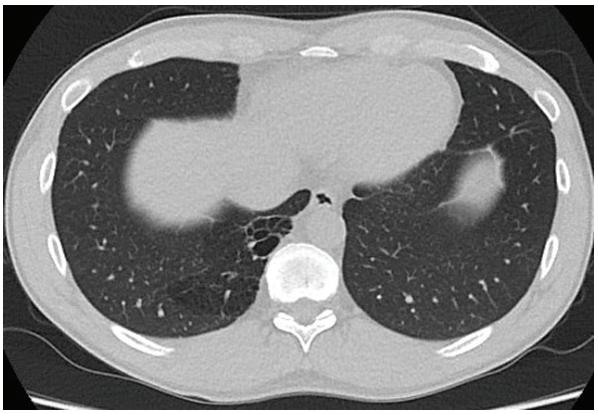

Fig. 1. Chest X-ray revealed blunting of the right chest.

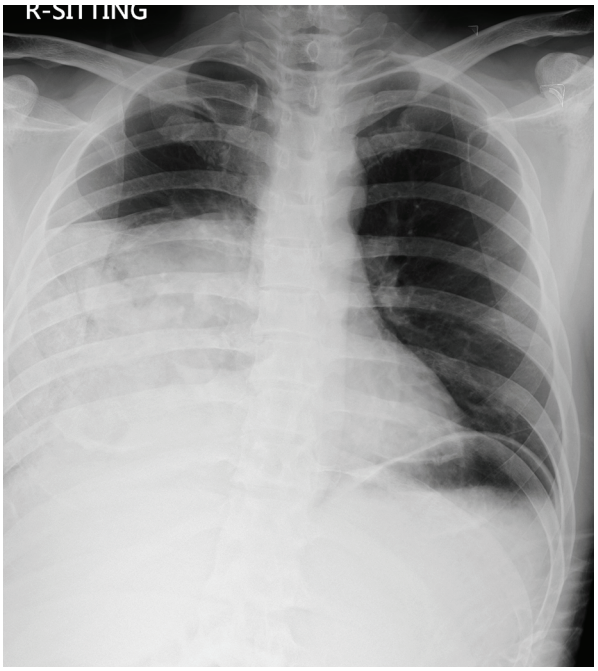

Fig. 2. Right lower lobe superior segment endobronchial mucosa appeared with persistent oozing under bronchoscopy.

respiratory sounds at the right chest wall during auscultation. Hemogram revealed anemia with Hb 9.0 g/dL. Thus, the patient was given 2 units of packed red blood cells. An initial chest X-ray at the emergency department revealed blunting of the right chest (Figure 2). Due to hemoptysis, we held the dual antiplatelet therapy and arranged a bronchoscopy examination. The RLL superior segment endobronchial (RB6) mucosa appeared to be persistently oozing with external compression under bronchoscopy (Figure 3). Computed tomography angiography was performed, which showed massive right pleural effusion, a consolidation in the RLL, and an active contrast extravasation arising from the left subphrenic artery at the celiac level (Figure 4). The patient underwent TAE with coils (Cook, Tornado Embolization Coil 0.018) from a

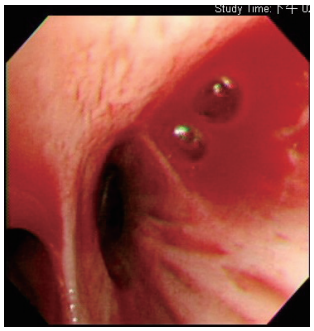

Fig. 3. Computed tomography angiography showed massive right pleural effusion and a consolidation in the right lower lobe with active contrast extravasation.

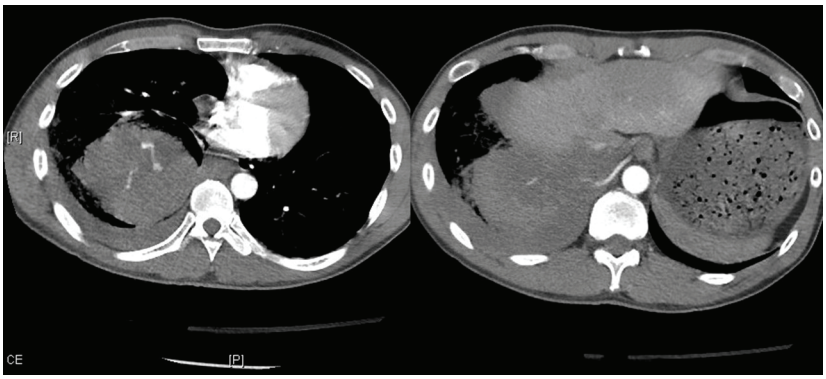

Fig. 4. Computed tomography angiography showed a feeding vessel arising from the left subphrenic artery.

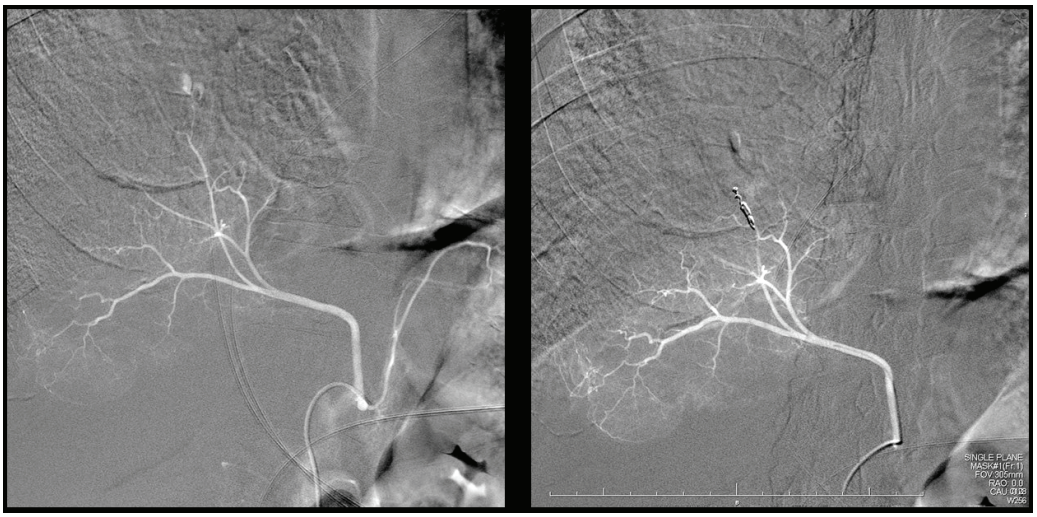

Fig. 5. (A) Angiographic image showing the transarterial embolization with coils from a branch of the left subphrenic artery before and after the procedure.

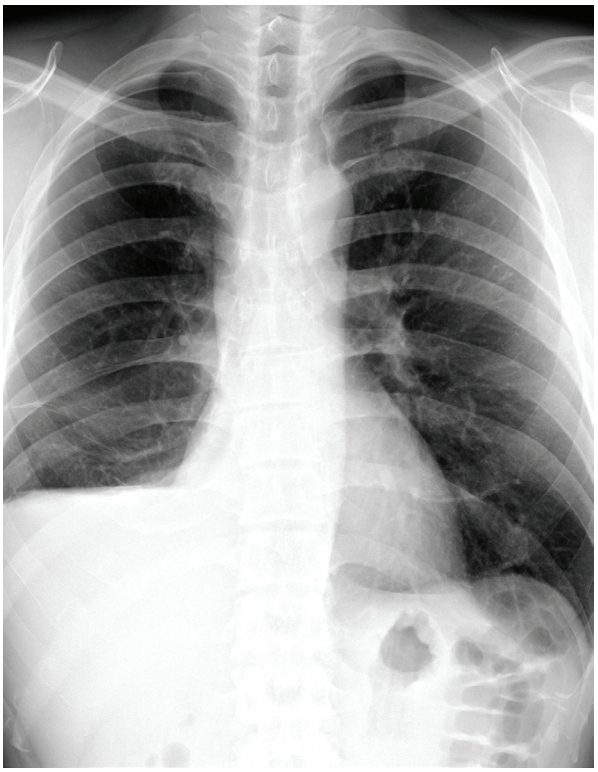

Fig. 6. Chest X-ray follow-up 3 months after the operation.

branch of the left subphrenic artery. There was no contrast extravasation in the post-TAE angiography (Figure 5).

Exploratory thoracotomy with posterolateral incision was performed 3 days after the dual antiplatelet therapy ceased. During the operation, we evacuated blood and blood clots of around 500 ml in volume first. RLL congestion and rupture with persistent oozing was noted. After division of the aberrant artery and intrapulmonary veins, RLL lobectomy was performed smoothly. No more hemoptysis was noted 1 week after surgery. The patient followed up chest X-ray regularly after the surgery (Figure 6).

Discussion

Pulmonary sequestration is a congenital anomaly characterized by abnormal nonfunctioning pulmonary tissue development with blood supplied by an anonymous systemic blood supply [1]. Pulmonary sequestration is primarily considered a childhood disease, and

comprises up to 6.4% of congenital lung malformations [2]. Two main types of pulmonary sequestration have been identified based on the localization of the malformation: intrapulmonary sequestration, in which the dysplastic tissue is located inside the normal lung, and extrapulmonary sequestration, in which the dysplastic tissue is located in an extra lobe of the lung [3, 4]. In most patients, the malformation is located in the left inferior lobe of the lung, primarily in the posterior basal segment. The ectopic variant, with intra- or subdiaphragmatic localization, has also been reported [4, 6]. The abnormal blood supply of the sequestration commonly arises from the descending aorta, or its branches. The venous system could drain into the pulmonary veins, azygos vein, hemiazygos vein, inferior vena cava, or right atrium [4, 7].

The clinical presentations of pulmonary sequestration can vary widely. Some patients may present with no symptoms, and the condition could be incidentally discovered by imaging studies. In other cases, symptoms such as recurrent pneumonia, chest pain and hemoptysis may occur [4, 8].

CT and angiography are commonly used diagnostic methods for pulmonary sequestration. CT images can help visualize the abnormal lung tissue and its blood supply. Angiography can provide detailed information about the feeding vessel of the sequestration [9]. In Figures 4 and 5, we present valuable CT and angiography images of a pulmonary sequestration feeding vessel arising from the left subphrenic artery.

In the case we described, the patient presented with hemoptysis and hemothorax, which likely resulted from the rupture of the intrapulmonary sequestration. Rupture of a sequestrated lung is a rare but lethal complication of pulmonary sequestration that could lead to both significant bleeding and respiratory distress [10, 11]. The cause of the sequestration rupture might be the higher pressure and relative fragility of the abnormal systemic blood supply. The abnormal vessels supplying the sequestration often are affected by conditions such as atherosclerosis, occlusive endarteritis, or venosclerosis, which further contributes to their vulnerability [7, 10].

Surgery is generally the preferred treatment for pulmonary sequestration, even in asymptomatic patients, to prevent further complications such as infection or inflammation. However, there is still no clear evidence on whether surgical intervention is more beneficial than a conservative approach in an asymptomatic patient [12]. In recent years, an alternative treatment option using endovascular embolization to block the aberrant vessels supplying the sequestration has been introduced [13]. In our case, a combination of both techniques was employed for the treatment. TAE was performed initially to achieve hemostasis by blocking the actively bleeding aberrant vessel, followed by surgical treatment after 3 days. The patient tolerated the treatment well. This approach offers an alternative treatment choice, particularly for patients who are taking antiplatelet medication and wish to reduce the tendency for intraoperative bleeding.

Conclusion

This case highlights the rare occurrence of pulmonary sequestration presenting in adulthood, and the importance of the use of imaging to identify an anomalous arterial supply to the sequestered segment in the RLL of the lung. The combination of TAE and subsequent surgical intervention, as performed in this case, pro-

vides a comprehensive and effective approach to managing a ruptured sequestration.

References

1. Landing BH, Dixon LG. Congenital malformations and genetic disorders of the respiratory tract (larynx, trachea, bronchi, and lungs). Am Rev Respir Dis 1979; 120(1): 151-85.
2. Van Raemdonck D, De Boeck K, Devlieger H, *et al*. Pulmonary sequestration: a comparison between pediatric and adult patients. Eur J Cardiothorac Surg 2001; 19(4): 388-95.
3. Abbey P, Das CJ, Pangtey GS, *et al*. Imaging in bronchopulmonary sequestration. J Med Imaging Radiat Oncol 2009; 53(1): 22-31.
4. Wei Y, Li F. Pulmonary sequestration: a retrospective analysis of 2625 cases in China. Eur J Cardiothorac Surg 2011; 40(1): e39-42.
5. Laje P, Martinez-Ferro M, Grisoni E, *et al*. Intraabdominal pulmonary sequestration. A case series and review of the literature. J Pediatr Surg 2006; 41(7): 1309-12.
6. Schulz MD, Gill RR, Colson YL. Ipsilateral intralobar and subphrenic pulmonary sequestration. Ann Thorac Surg 2010; 89(6): 2017-9.
7. Savic B, Birtel FJ, Tholen W, *et al*. Lung sequestration: report of seven cases and review of 540 published cases. Thorax 1979; 34(1): 96-101.
8. Gezer S, Taştepe I, Sirmali M, *et al*. Pulmonary sequestration: a single-institutional series composed of 27 cases. J Thorac Cardiovasc Surg 2007; 133(4): 955-9.
9. Gabelloni M, Faggioni L, Accogli S, *et al*. Pulmonary sequestration: what the radiologist should know. Clin Imaging 2021; 73: 61-72.
10. Chen T, Yu J, Zhang N, *et al*. Intralobar pulmonary sequestration presenting as hemothorax secondary to spontaneous pneumothorax: case report and literature review. Front Pediatr 2022; 10: 937563.
11. Erkul GSA, Erkul S, Parlar AI, *et al*. An uncommon cause of massive haemothorax and treatment under cardiopulmonary bypass. Interact Cardiovasc Thorac Surg 2021; 32(6): 996-7.
12. Sun X, Xiao Y. Pulmonary sequestration in adult patients: a retrospective study. Eur J Cardiothorac Surg 2015; 48(2): 279-82.
13. Zener R, Bottoni D, Zaleski A, *et al*. Transarterial embolization of intralobar pulmonary sequestration in a young adult with hemoptysis. J Thorac Dis 2017; 9(3): E188-e93.

Case report: Lung Transplant for Pulmonary Chronic Graft-Versus-host Disease After Fully Matched sibling Peripheral Blood Stem Cell Transplantation

Chih-Hsiang Chang[1], Ming-Shu Hsieh[2], Xu-Heng Chiang[1,3], Hsao-Hsun Hsu[1]

Pulmonary graft-versus-host disease (GvHD) with bronchiolitis obliterans is a lethal complication of allogeneic hematopoietic stem cell transplantation. Early detection and treatment initiation may slow disease progression; however, medical therapy does not always achieve the desired effect. Thus, lung transplantation is an effective treatment option. Here, we report the complicated case of a patient who underwent autologous peripheral blood stem cell transplantation and developed pulmonary GvHD. After approximately 6 months on a ventilator and developing extracorporeal membrane oxygenation dependence, the patient underwent right lung transplantation and was discharged approximately 8 months after the procedure. ***(Thorac Med 2024; 39: 170-173)***

Key words: Lung transplant, graft-versus-host disease (GvHD), stem cell transplantation

Introduction

Hematopoietic stem cell transplantation (HSCT) is a definitive treatment for hematologic malignancies, such as lymphoma. However, complications may occur. Pulmonary graft-versus-host disease (GvHD) is a complication that may lead to mortality after HSCT. Pulmonary changes in chronic pulmonary GvHD include bronchiolitis obliterans (BO), pulmonary fibrosis, and/or organizing pneumonia. Although early detection using pulmonary function tests can help slow disease progression [1], pulmonary GvHD often progresses rapidly and unstoppably. During disease progression, many complications may occur, such as pneumonia caused by prolonged intubation, recurrent pneumothorax caused by ventilator dependence [2], and coagulopathy caused by extracorporeal membrane oxygenation (ECMO) support. In the face of these complications, lung transplantation may be the last treatment option and can yield improved survival.

[1]Department of Surgery, National Taiwan University Hospital, Taipei, Taiwan. [2]Department of Pathology, National Taiwan University Hospital, Taipei, Taiwan. [3]Department of Medical Education, National Taiwan University Hospital, Taipei, Taiwan
Address reprint requests to: Dr. Xu-Heng Chiang, National Taiwan University Hospital, Taipei, Taiwan, No.7, Chung Shan S. Rd., Zhongzheng Dist., Taipei City 100225, Taiwan (R.O.C.)

Case Report

A 33-year-old female patient was diagnosed with anaplastic large cell lymphoma in 2018. Her initial symptoms included a mass on the right upper back. Computed tomography (CT) revealed lymphadenopathies at the bilateral neck, axilla, and mediastinum, and mass lesions in the C-spine, sternum, ribs, sacrum, right iliac spine, and femur. Fully matched sibling peripheral blood stem cell transplantation was performed in 2020 due to disease recurrence after multiple cycles of chemotherapy and autologous peripheral blood stem cell transplantation. There was no hyperacute or acute GvHD, and the patient was stable for a few months. A pulmonary function test (PFT) revealed normal standard spirometry and normal diffusion capacity (forced expiratory volume in the first second (FEV_1): 98% of predicted normal, forced vital capacity (FVC): 102% of predicted normal) in mid-2019, before stem cell transplantation.

She had several episodes of dyspnea and fever in mid-2020, and her pulmonary function deteriorated rapidly. By the end of 2020, she was almost entirely dependent in her daily activities. Follow-up PFT revealed significantly decreased lung function (FEV_1: 19.3% of predicted normal, FVC: 37% of predicted normal) (Table 1). High airway pressure while using a mechanical ventilator, and bilateral multicentric ground-glass opacities on chest CT were compatible with BO (Figure 1). As chronic pulmonary GvHD was suspected, the patient was treated with protein kinase inhibitors (i.e., ruxolitinib and ibrutinib).

Due to rapidly deteriorating pulmonary function, venous-venous ECMO (V-V ECMO) was started in late 2021. Recurrent bilateral pneumothorax occurred due to the patient's fragile lungs and mechanical ventilation. The patient underwent lung transplantation with V-V ECMO support at the end of 2021. During surgery, massive intraoperative blood loss (~ 4600 mL) occurred due to severe adhesions, which might have been secondary to previous recurrent pneumothorax and pleurodesis treatment. After right lung transplantation, the surgical team decided to stop the transplant procedure to control the severe bleeding. The patient was successfully weaned off V-V ECMO on postoperative day 16. The time to recovery was long, due to tracheomalacia resulting from a long ventilator-dependent period, poor performance status, and prolonged ECMO-dependence before the transplant; the patient was transferred to the general ward on postoperative day 111, and was finally discharged on postoperative day 218.

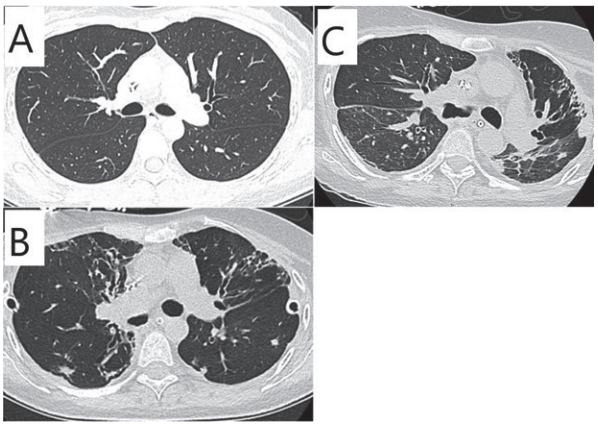

Fig. 1. Computed tomography (CT) before (A) and after (B) pulmonary GvHD diagnosis. Multiple ground-glass opacities in bilateral lung fields were found on CT after the patient received peripheral blood stem cell transplantation. The CT after unilateral right lung transplantation (C) showed some infectious and inflammatory processes in both lungs, but no bronchiectasis was found in the right lung.

During pathological examination, the recipient's right lung was 318.0 g (average adult weight: 360–570 g) and was 12.5 x 12.0 x 5.0

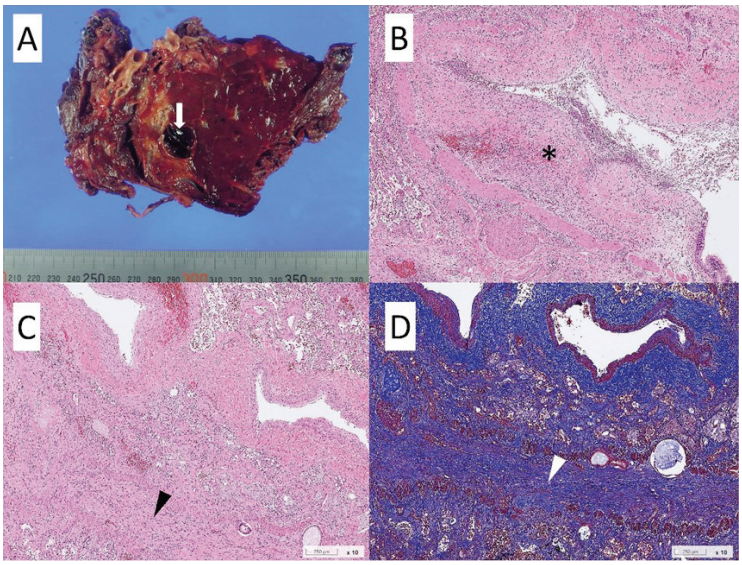

Fig. 2. (A) The transplant recipient's right lung showing fibrous adhesion, a shaggy lusterless pleural surface, and intrapulmonary hemorrhage with hematoma formation (arrow). (B) Airway showing bronchiolitis obliterans with submucosal fibrosis (asterixis), chronic inflammation, and denuded respiratory epithelium. (C) Total obstruction of some small airways (arrowhead), highlighted by (D) Masson trichrome staining (arrowhead).

cm in size. The pleural surface was shaggy and lusterless, and fibrous adhesion to the adjacent fibroadipose tissue was noted, which was consistent with the operative findings (Figure 2A). Microscopic examination showed BO involving multiple small airways, characterized by subepithelial fibrosis, variable lymphocytic inflammation, luminal stenosis, and total obstruction in some airways (Figure 2B-D).

Discussion

Patients with early pulmonary GvHD are often asymptomatic or present with nonspecific symptoms, such as mild exertional dyspnea, most of which occur between 3 months and 2 years following HSCT, and affect up to 20% of HSCT patients [3]. Due to patients' initial lack of awareness of the disease, diagnosis is often delayed until significant changes in airflow patterns and lung structure occur, or until the patient experiences marked respiratory distress. PFT is a useful tool for early detection of disease progression [1-2]. For example, in our patient, the rate of deterioration was very fast and could be detected in the subsequent PFT. In addition, high-resolution chest CT can be used as an auxiliary diagnostic tool. On high-resolution CT, BO shows diffuse mosaic attenuation patterns, which present a heterogeneous appearance caused by the coexistence of trapped air and normal parenchyma, as well as other patterns including ground-glass opacities, bronchial wall thickening, and bronchiectasis [4].

Pulmonary infection and complications may be strongly associated with GvHD with lung involvement due to oxygen dependence, immobility, poor secretion expectoration, and long-term ventilator dependence. Lung transplantation is 1 of the few therapies available for these patients. In a previous study, the survival rates at 1 and 5 years were approximately 89% and 37%, respectively [5]. Most deaths were attributed to long-term complications of allogeneic lung transplantation, including infection and BO syndrome.

BO is a type of bronchiolitis characterized by submucosal fibrosis of small bronchioles, leading to lumen stenosis and occlusion. Except for the bronchioles, the lung parenchyma shows no diffuse inflammation in pulmonary GvHD. The pathophysiology of chronic GvHD is still not well understood. It has a classic pathological manifestation of dense eosinophilic scarring of the bronchioles, resulting in some degree of luminal narrowing; during progression, the submucosal layer is replaced by fibrous tissue, and the lumen is obliterated [6]. We found lymphocytic inflammation and subepithelial fibrosis at the bronchi and bronchioles in the removed lung specimens, consistent with the pathological features of BO.

Although we only performed unilateral lung transplantation because of the difficulties encountered intraoperatively, the patient recovered well and was able to return to normal life.

Our patient was a complicated case and suffered from prolonged ventilator- and ECMO-dependent periods with an almost bedridden status before lung transplantation. However, performing only a single lung transplant was appropriate, as it avoided uncontrolled bleeding and postoperative massive blood transfusion and its complications. For lung transplant patients with a poor performance status and non-infectious end-stage lung disease, single lung transplantation can provide better perioperative outcomes [7]. Patients in a poor condition may not overcome the complications caused by a more invasive double lung transplantation.

Pulmonary GvHD with BO is a lethal complication of allogeneic HSCT. Early detection and treatment initiation may slow disease progression; however, medical therapy does not always achieve the desired effect. Thus, lung transplantation is an effective treatment option, even when only unilateral lung grafts are used, as reported in this article.

Conflict of interest

Nothing to declare.

Ethics Statement

The authors declare that appropriate written informed consent was obtained for the publication of this manuscript and accompanying images.

References

1. Yang L, Cheng J, Li F, *et al*. The predictive value of pulmonary function test before transplantation for chronic pulmonary graft-versus-host-disease after allogeneic hematopoietic stem cell transplantation. BMC Pulm Med 2022; 22(1): 473.
2. Hildebrandt GC, Fazekas T, Lawitschka A, *et al*. Diagnosis and treatment of pulmonary chronic GVHD: report from the consensus conference on clinical practice in chronic GVHD. Bone Marrow Transplant 2011 Oct; 46(10): 1283-95.
3. Bergeron A. Late-onset noninfectious pulmonary complications after allogeneic hematopoietic stem cell transplantation. Clin Chest Med 2017 Jun; 38(2): 249-262.
4. Williams KM. How I treat bronchiolitis obliterans syndrome after hematopoietic stem cell transplantation. Blood 2017 Jan 26; 129(4): 448-455.
5. Cheng GS, Edelman JD, Madtes DK, *et al*. Outcomes of lung transplantation after allogeneic hematopoietic stem cell transplantation. Biol Blood Marrow Transplant 2014 Aug; 20(8): 1169-75.
6. Xu L, Drachenberg C, Tavora F, *et al*. Histologic findings in lung biopsies in patients with suspected graft-versus-host disease. Hum Pathol 2013 Jul; 44(7): 1233-40.
7. Puri V, Patterson GA, Meyers BF. Single versus bilateral lung transplantation: do guidelines exist? Thorac Surg Clin 2015; 25(1): 47-54.

Hereditary Multiple Exostosis Presenting as a Pulmonary Nodule: A Case Report

Ying-Che Ting[1], Yi-Chen Yeh[2], Han-Shui Hsu[1,3]

Hereditary multiple exostoses (HME) involving the ribs are relatively uncommon and very rarely appear like pulmonary nodules. Computed tomography or magnetic resonance imaging could help in the diagnosis. Other important imaging differential diagnoses include enchondroma, osteoblastoma, chondroblastoma, and chondrosarcoma. We reported the case of a 16-year-old female with a solitary pulmonary nodule on a chest radiograph on presentation. Video-assisted thoracoscopic surgery with exostoses excision was performed due to a suspicious malignant transformation after 10 months of follow-up. The hospital course went smoothly, and the patient was discharged on postoperative day 4. ***(Thorac Med 2024; 39: 174-178)***

Key words: osteochondroma, rib, pulmonary nodule

Introduction

Hereditary multiple exostoses (HME) is a disease entity that is characterized by multiple osteochondromas. The prevalence of HME is estimated to be 0.9 to 2 per 100,000 in the Caucasian population [1]. The presentation of HME is usually asymptomatic, leading to possible underestimation of its prevalence. The knees and proximal humerus are the areas mostly affected [2]. Rib exostoses are less common. The precise prevalence of HME with rib involvement is unknown, but about 3% of all osteochondromas are estimated to occur in the vertebrae and ribs, and 70% of these are accompanied by HME [3]. Here, we present the case of a 16-year-old girl with HME, with the main lesion arising from the left 6th rib. The general concepts, imaging considerations, and surgical indications are also reviewed.

Case Report

A 16-year-old girl without systemic disease presented to our outpatient clinic due to a 3-cm triangular pulmonary opacity with multifocal

[1]Division of Thoracic Surgery, Department of Surgery, Taipei Veterans General Hospital. [2]Department of Pathology and Laboratory Medicine, Taipei Veterans General Hospital. [3]Institute of Emergency and Critical Care Medicine, National Yang-Ming University
Address reprint requests to: Dr. Han-Shui Hsu, 11217 No. 201, Sec. 2, Shipai Rd., Beitou Dist., Taipei City 112, Taiwan (R.O.C.)

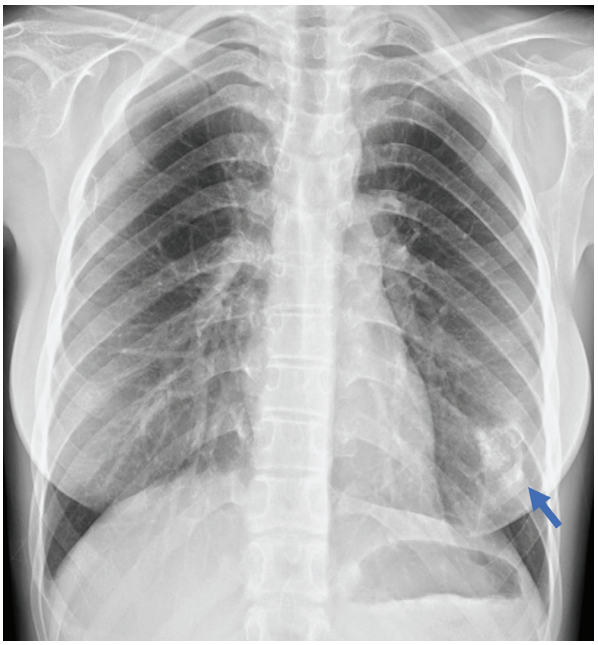

Fig. 1. Preoperative chest radiography revealed a 3-cm triangular pulmonary opacity with multifocal tiny calcifications at the lower lobe of the left lung.

tiny calcifications that was incidentally found at the lower lobe of the left lung on radiography (Fig. 1). There were no accompanying symptoms such as shortness of breath, chest pain, or chest tightness. On physical examination, clear breathing sounds were noted in both lung fields. Computed tomography (CT) of the chest revealed a 2.8-cm lobulated and pedunculated mass in the lower lobe of the left lung, with a calcified rim and protruding stalk from the left 6th rib (Fig. 2 A~D). In addition, multiple radiolucent blurs were noted at the clavicles, scapula, proximal humerus, and multiple ribs on both sides. A provisional diagnosis of HME was made, although the patient denied a positive family history.

Follow-up CT of the chest revealed an enlargement of the mass with a 0.2-cm prominent soft tissue component. Thus, the patient underwent surgery through single-port video-assisted thoracoscopy. A tree-like pedunculated bony exostosis was noticed in the left pleural space, arising from the left 6th rib at the anterior portion. Removal of the pedunculated lesion was performed without difficulty. Pathological examination revealed a 3.7-cm tumor with mature bony trabeculae and a cap of mature hyaline cartilage (Fig. 3 A~C). These findings con-

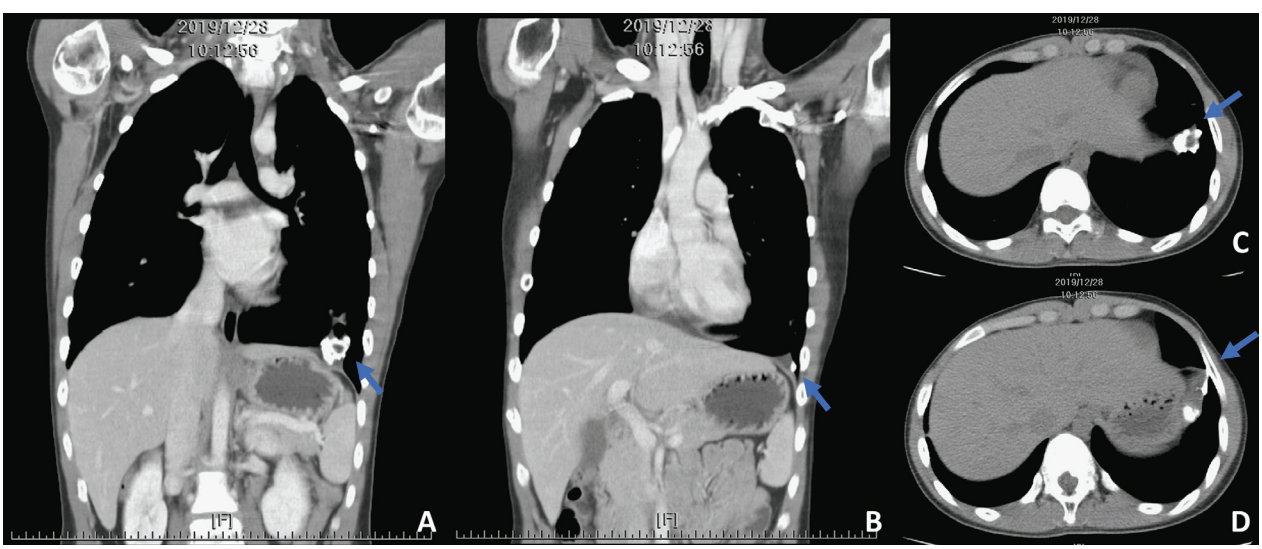

Fig. 2. Chest computed tomography images. Coronal (A, B) and axial (C, D) views showing a 2.8-cm lobulated and pedunculated mass in the lower lobe of the left lung, with a calcified rim and protruding stalk from the left 6th rib.

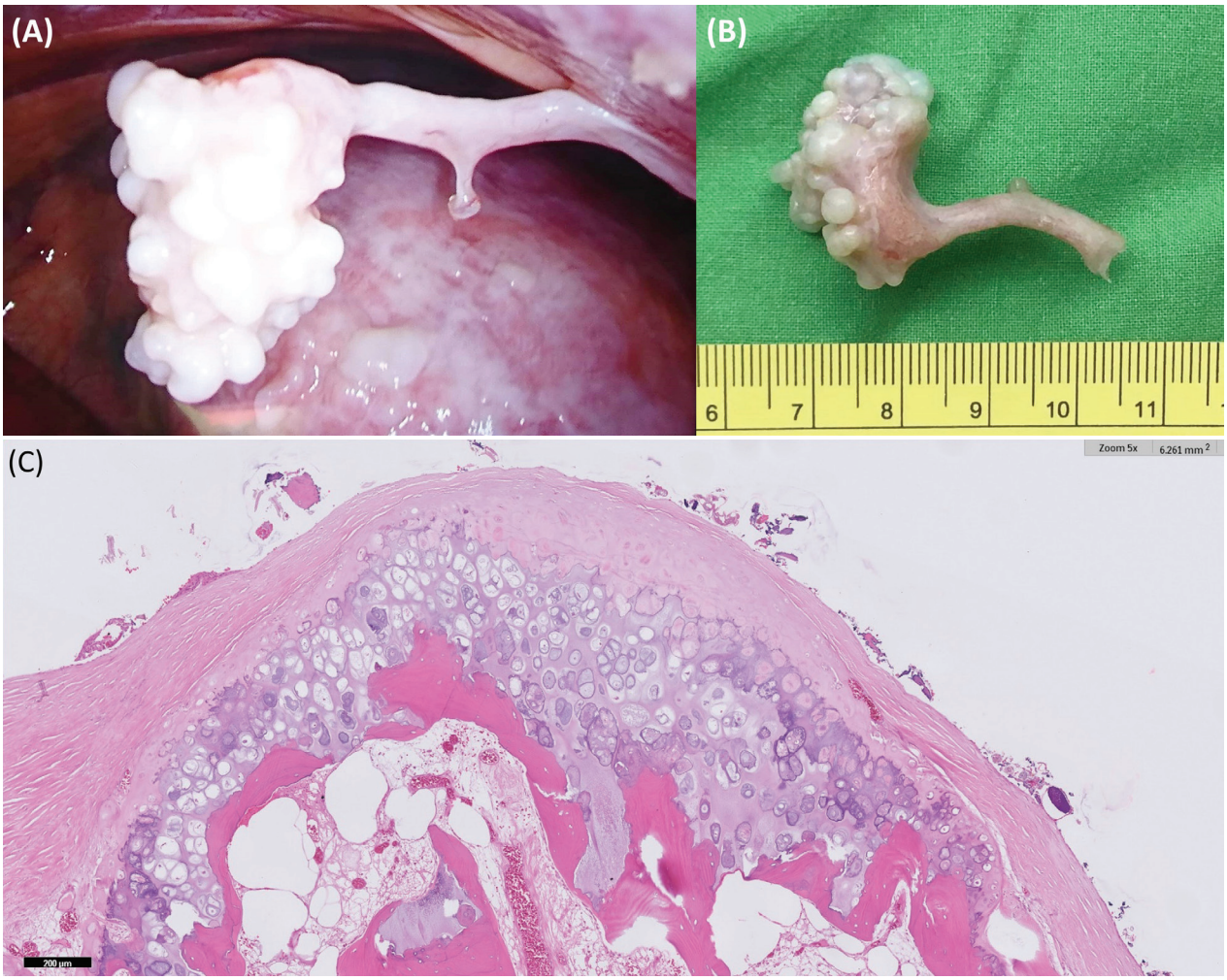

Fig. 3. (A) Thoracoscopic view, and (B) macroscopic view: A pedunculated lesion arising from the left 6th rib with inflammatory change of adjacent lung tissue. (C) The pathological picture (5x) revealed mature bony trabeculae and a cap of mature hyaline cartilage.

firmed the diagnosis of osteochondroma. The postoperative period was uneventful; the drainage was removed on postoperative day 1, and the patient was discharged on postoperative day 4.

Discussion

The pathogenesis of HME was found to be associated with heterozygous loss of function mutations in EXT1 (the enzyme) or EXT2 (the chaperone-like and non-enzymatically active partner of EXT1), genes that encode Golgi-resident glycosyltransferases responsible for the synthesis and assembly of heparan sulfate (HS) chains onto the core protein of syndecans, glypicans and other HS-rich proteoglycans [4]. Heterozygous mutations in either gene in HME patients lead to a systemic HS deficiency, which is associated with cell misbehavior and tumorigenesis [5]. Diagnosis of a HME can be made radiologically with the presentation of more than 2 osteochondromas. In addition to a positive family history, which is an important clue

for HME, genetic tests for EX1 and EX2 mutation could provide a more definite diagnosis.

A diagnosis of HME can be made radiologically with the presentation of more than 2 osteochondromas. However, it is uncommon that an osteochondroma would present as a pulmonary nodule. To our knowledge, ours is the first case of this atypical presentation.

CT or magnetic resonance imaging is usually required to visualize the continuity between the cortex of the lesion and the cortex and medulla of the underlying bone. Magnetic resonance imaging is the most accurate examination for demonstrating a cartilage cap that has a high signal intensity on T2-weighted imaging [6].

The differential diagnoses on imaging include enchondroma, osteoblastoma, chondroblastoma, and chondrosarcoma. Enchondroma usually arises from cartilaginous tissue at the costochondral junction. CT reveals a slow-growing, lobulated, well-demarcated osteolytic lesion with or without bulging of the cortical bone [6]. Osteoblastoma mostly involves the vertebral column and long bone, followed by the feet, skull, clavicle, and ribs. It usually presents as an osteolytic and expansile lesion on CT [7]. Chondroblastoma usually involves the epiphyseal and epimetaphyseal regions of the long bones. Other locations include the acetabulum, ilium, talus, calcaneus, patella, temporal bone, and ribs. Chondroblastoma is usually a well-circumscribed, round, or oval lesion on radiography. CT can show matrix mineralization, cortical erosion, and soft tissue extension [8]. Chondrosarcoma often arises in the pelvis or long bones; it is relatively rare for it to arise in the rib. CT is optimal for detecting matrix mineralization, particularly when it is subtle or when the lesion is anatomically complex [9].

Malignant transformation is one of the most concerning manifestations of HME. Nearly 2% of patients will have their exostoses progress to malignancy and become peripheral chondrosarcomas [10]. If the thickness of a cartilage cap exceeds 2 cm in adults or 3 cm in children, malignant transformation should be suspected [6]. The clinical appearance of suspicious malignant changes is characterized by a sudden increase in size, sudden onset of pain at the site, areas of radiolucency, calcification in the overlying soft tissue mass, and destruction of the base or adjacent bone.

Exostoses generally stop growing when the physes close, and they remain static throughout adulthood. Most exostoses require no treatment. Surgical intervention is indicated when local irritation or deformity develops, when the control or prevention of thoracic complications is needed, when the etiology of a chest wall tumor is not clear, or when prevention or excision for suspicious malignant transformation is required. Currently, there are no pharmacological treatments for HME other than palliative care for pain.

References

1. Pierz KA, Stieber JR, Kusumi K, *et al*. Hereditary multiple exostoses: one center's experience and review of etiology. Clin Orthop Relat Res 2002; (401): 49-59.
2. Clement ND, Porter DE. Hereditary multiple exostoses: anatomical distribution and burden of exostoses is dependent upon genotype and gender. Scott Med J 2014; 59: 35-44.
3. Masoum SH, Moradi A, Ebrahimzadeh MH. Multiple rib exostoses in a boy: a rare case resulting in surgery secondary to cosmetic concerns. Arch Bone Jt Surg 2014; 2: 243-5.
4. Nam SJ, Kim S, Lim BJ, *et al*. Imaging of primary chest wall tumors with radiologic-pathologic correlation. Radiographics 2011; 31: 749-770.

5. Pacifici M. The pathogenic roles of heparan sulfate deficiency in hereditary multiple exostoses. Matrix Biol 2018; 71-72: 28-39.
6. Nam SJ, Kim S, Lim BJ, *et al*. Imaging of primary chest wall tumors with radiologic-pathologic correlation. Radiographics 2011; 31: 749-770.
7. Ye J, Liu L, Wu J, *et al*. Osteoblastoma of the rib with CT and MR imaging: a case report and literature review. World J Surg Oncol 2012; 10: 49.
8. Brandolini J, Bertolaccini L, Pardolesi A, *et al*. Chondroblastoma of the rib in a 47-year-old man: a case report with a systematic review of literature. J Thorac Dis 2017; 9 : E907-E911.
9. Sangma MMB, Dasiah S. Chondrosarcoma of a rib. Int J Surg Case Rep 2015; 10: 126-8.
10. Jones KB, Pacifici M, Hilton MJ. Multiple hereditary exostoses (MHE): elucidating the pathogenesis of a rare skeletal disorder through interdisciplinary research. Connect Tissue Res 2014; 55: 80-88.

Case Report: A 78-Year-Old man Dies After Choking on a Piece of Meat

Che-Hao Yang[1], Chia-Hen Lin[1]

Foreign body aspiration is a cause of sudden collapse, and is a basic training subject of basic life support (BLS) instruction. In this article, we presented a case of foreign body aspiration, in which several BLS attempts failed to remove the foreign body. It was finally removed by bronchoscopy. ***(Thorac Med 2024; 39: 179-182)***

Key words: Foreign body aspiration, bronchoscopy

Introduction

Management of foreign body aspiration is a subject of basic life support (BLS) training. Thanks to the promotion of BLS in the general population, mortality due to foreign body aspiration has been so rare that it was not recorded as a leading cause of death in Taiwan [6]. However, foreign body aspiration remains potentially fatal due to suffocation. Physicians must always confirm the patency of the airway and pay attention to whether a foreign body remains inside the airway.

Case Presentation

This 78-year-old man had a past history of Parkinsonism, and had a deep brain stimulator. He presented to our emergency department on 19 December 2021, at 12:46, with a cardiac arrest status. According to the ambulance record (appendix 1) and his family, he collapsed when eating lunch at a restaurant. The family members said they saw that he kept coughing and drinking water, and soon lost consciousness. The staff at the restaurant found he was pulseless and started CPR. The emergency medical technicians (EMT) arrived at 12:20, on 19 December 2021, when resuscitation had already been underway for 5 minutes. The EMT provided a supraglottic airway (iGEL, size 4) and applied a LUCAS device for continuous chest compression. Since spontaneous circulation had not yet returned, the man continued receiving chest compression during transportation.

The attempts at resuscitation continued on his arrival at our emergency department, for he still remained pulseless. We maintained manual chest compression and intubated a 7.5 French endotracheal tube (ETT). It was recorded that

[1]Division of Thoracic Medicine, Shin Kong Wu Ho-Su Memorial Hospital
Address reprint requests to: Dr. Che-Hao Yang, No. 15-2, Aly. 45, Ln. 232, Sec. 3, Muxin Rd., Wenshan Dist., Taipei City 116018, Taiwan (R.O.C.)

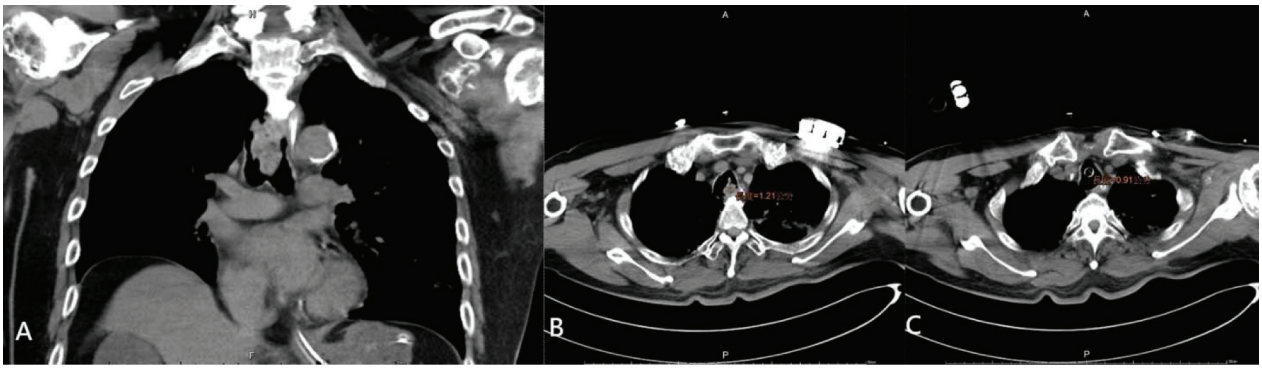

Fig. 1. (A) shows the whole chunk of the foreign body on the sagittal view. Figures 1(B) and 1(C) revealed that the size of the foreign body's tip (1.21 cm) was larger than the ETT's tip (0.9 cm).

some of the foreign body was removed during intubation. The patient finally regained his vital signs at 13:06 on the same day, with extremely low blood pressure that required 3 kinds of maximal dose vasopressors (norepinephrine, dopamine, and vasopressin) to maintain systolic blood pressure above 90 mmHg. Computed tomography (CT) revealed a foreign body larger than the endotracheal tube, lasting for several cuts of the CT, and a large area of pneumonia at the left lower lung (Figure 1).

The patient then was transported to our intensive care unit (ICU). On presentation, the ventilator was found to have a fluctuating tidal volume. A foreign body causing a ball valve effect was highly suspected. Therefore, we performed a bronchoscopy, aiming to remove the foreign body.

We encountered the foreign body upon entering (Figure 2). We then sought to remove it by foreign body forceps together with the ETT, but it tore at the trachea because it was too big. Fortunately, the foreign body could be extracted at a depth that could be approached by a Magill forceps. We then removed the whole chunk of the foreign body using the Magill forceps, intubated a new ETT, and removed the residual debris by bronchoscopy. We assumed the foreign body to be a piece of meat, based on its appearance. The patient rapidly recovered from his shock status after removing the foreign body. However, due to prolonged hypoxia, he died of hypoxic encephalopathy in the end.

Discussion

A previous article reported that the longer it took to remove a foreign body, the worse the neurological outcome. If more than 25 minutes were needed to remove the foreign body, the likelihood of a neurological outcome with a cerebral performance category (CPC) of more than 3 would be as much as 86% [1].

The success rate of the abdominal thrust was 86.5%, according to a previous review [2]. There is no recorded success rate for the chest thrust or chest compression, but it was believed to be more effective than the abdominal thrust for generating greater airway pressure [3, 4].

It was unfortunate that the foreign body in our case failed to be removed after 51 minutes of CPR. Several issues could be discussed here, including whether we should have used a laryngeal mask with the patient before the foreign body was removed [5], and conducting an airway evaluation during resuscitation. However,

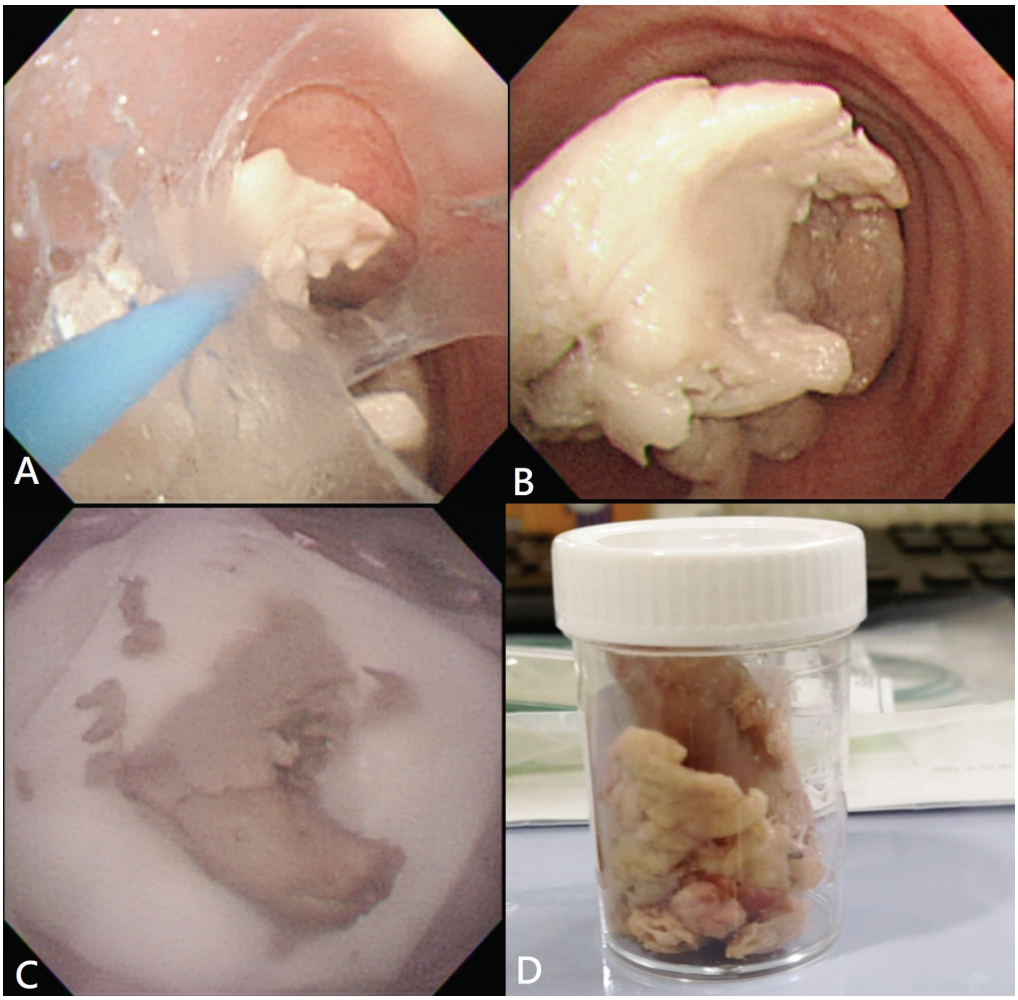

Fig. 2. (A) The foreign body was just below the ETT. (B) The foreign body tore when removing it with the ETT, but it was extracted at a depth that was visible to the bare eyes and available to the Magill forceps. (C) Collecting all of the pieces together, it looked like a piece of meat. (D) We placed the foreign body into a jar.

it was surprising that the ventilation was effective during resuscitation, based on the large size of the foreign body.

References

1. Igarashi Y, Norii T, Sung-Ho K, *et al*. Airway obstruction time and outcomes in patients with foreign body airway obstruction: multicenter observational choking investigation. Acute Med Surg 2022 Jan-Dec; 9(1): e741.
2. Soroudi A, Shipp HE, Stepanski BM, *et al*. Adult foreign body airway obstruction in the prehospital setting. Prehosp Emerg Care 2007 Jan-Mar; 11(1): 25-9.
3. Langhelle A, Sunde K, Wik L, *et al*. Airway pressure with chest compressions versus Heimlich manoeuvre in recently dead adults with complete airway obstruction. Resuscitation 2000 Apr; 44(2): 105-8.
4. Couper K, Hassan AA, Ohri V, *et al*. Removal of foreign body airway obstruction: a systematic review of interventions. Resuscitation 2020 Nov; 156: 174-81.
5. Simon LV, Torp KD. Laryngeal mask airway. NCBI, 2022 July 25.
6. Statistical Results of Causes of Death in Taiwan, 2022. Press release from Taiwan's Ministry of Health and Welfare: https://www.mohw.gov.tw/cp-16-70314-1.html.

Appendix 1. The Ambulance Record of the Case

臺北市政府消防局救護紀錄表 編號：2112191220518

派遣資料

日期	出勤單位	受案單位				
110-12-19	劍潭92	■救災救護指揮中心 □分隊自行受理				
受理時間	**出勤時間**	**到達現場時間**	**離開現場時間**	**送達醫院時間**	**離開醫院時間**	**返隊待命時間**
12:20	12:25	12:30	12:40	12:46	13:34	13:46

發生地點	台北市中山北路4段1號 地點描述:1F聯誼會西餐廳(中山區)	協同處理單位	圓山11
送往醫院或地點	新光 ■就近適當 □指揮中心 □傷病患或家屬要求	未送醫原因	□未發現 □誤報 □中途取消 □拒送 □警察處理 □現場死亡 □火警 □支援勤務 □其他

傷病患資料

傷病患姓名		性別	■男 □女 □經評估後判斷	傷病患財物明細：■未經手 □有 保管人：(簽章)
身分證字號		年齡	77 □經評估後判斷	
傷病患地址				

現場狀況

■非創傷
- □呼吸問題(喘/呼吸急促)
- □呼吸道問題(異物哽塞)
- □昏迷(意識不清)
- □胸痛/悶
- □腹痛
- □一般疾病
  - □頭痛/頭暈/昏倒/昏厥
  - □發燒
  - □噁心/嘔吐/腹瀉
  - □肢體無力
- □疑似毒藥物中毒
- □疑似一氧化碳中毒
- □癲癇/抽搐
- □路倒
- □行為急症/精神異常
- □孕婦急產
- ■到院前心肺功能停止
- ■其他不明原因

□創傷
- □一般外傷
  - □頭部外傷
  - □胸部外傷
  - □腹部外傷
  - □背部外傷
  - □肢體外傷
- 受傷機轉
  - □因交通事故
  - □非交通事故
- 事故類別(以傷病患為主)
  - □汽車□機車 □腳踏車
  - □行人□其他
- □溺水
- □摔跌傷
- □墜落傷：約___
- □穿刺傷
- □燒燙傷___度___%
- □電擊傷
- □生物咬螫傷
- □到院前心肺功能停止
- □其他:___

□男性年齡＞＝20歲
□女性年齡＞＝50歲
□有胸痛或胸悶
或下列情形之任2項：
□喘□噁心(或嘔吐)
□冒冷汗□有心臟病史

心肺功能停止登錄
□派遣時即通知
目擊者：□無 ■民眾 □EMT
旁觀者CPR：□有 ■無
使用PAD：■有 □無
ROSC： □有 時間:■無

OHCA事故地點型態
□住宅 □工廠/工作地點 □運動中心
□街道/公路 □公共建築 □療養院
□教育/學校 □捷運站/車站/機場
□診所/護理之家 ■其他 □不清楚

傷病患主訴
主訴：■家屬或友人代訴
1.感覺哪裡不舒服?OHCA
2.感覺怎麼的不舒服?OHCA
3.大約不舒服有多久了?約五分鐘
4.還有其他地方不舒服嗎?沒有
5.評估顎椎是否損傷?(創傷患者)

過去病史
□心臟疾病 □中風 ■高血壓
□肝臟疾病 □癲癇 ■糖尿病
□腎臟疾病 □氣喘 □不清楚
□精神疾病 □癌症 ■其他帕金森氏症
□慢性阻塞性肺病 □無

過敏史
□藥物___
□食物___
□其他___
□不清楚
■無

腦中風指標異常□是□否
最後正常時間
抽搐□是□否 血糖≧60□是□否
□微笑測試異常□左側/□右側舉臂測試異常
□言語測試異常□動眼測試異常

處置項目（此欄可複選）

基本呼吸道/呼吸處置
- □口咽呼吸道
- □鼻咽呼吸道
- □抽吸
- □哈姆立克法
- ■聲門上呼吸道(SGA)I-GEL 4號
- □鼻管___L/Min
- □面罩___L/Min
- □非再呼吸型面罩
- □BVM(正壓輔助呼吸)
- □霧化吸入型面罩
- □其他___

創傷處置
- □頸圈
- □清洗傷口
- □止血、包紮
- □骨折固定
- □長背板固定
- □KED固定
- □抽吸式護木
- □三角巾固定
- □髖骨固定
- □止血帶止血
- □其他___

特定後送姿勢
- ■平躺
- □半坐臥
- □左/□右側躺
- □下肢抬高

心肺復甦術
- ■使用AED
  - □電擊去顫___次
  - ■不連續電擊
- ■CPR13分鐘
  - □人工CPR
- ■使用自動心肺復甦機
  - ■Lucas
  - □Auto Pulse

藥物處置
- □靜脈輸液，部位___
  - □0.9%N/S___ml
  - □L/R___ml
  - □___%葡萄糖液___ml
- □給予口服葡萄糖液／粉
- □協助使用Aspirin
- □協助使用NTG含片___片
- □協助使用支氣管擴張劑___次

其他處置
- □保暖
- □心理支持
- □急產接生
- □約束帶
- □灌洗眼睛
- □其他___

搬運
- □自行上車
- ■以適當方式搬運

給藥

時間	藥名	途徑/劑量

ALS處置
□氣管內管:___號
(固定深度)fix:___cm
□手動電擊:___次:___Joule

□醫療/線上指導醫師核簽

請在圖上標示說明受傷部位及其尺寸

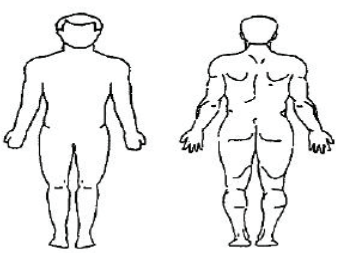

補述：1.標準防護x2 2.到達現場時，患者已無脈搏無心跳，現場有執行DACPR。3.現場使用圓山大飯店AED。。

生命徵象

時間	意識狀態	呼吸	脈搏	血壓	GCS	SpO2	體溫	血糖值
12:31	□清 □聲 □痛 ■否	0次/分	0次/分	無//)mmHg	E1V1M1	/%	/℃	/mg/dl
12:41	□清 □聲 □痛 ■否	0次/分	0次/分	//mmHg	E1V1M1	/%		
到院後檢傷站	□清 □聲 □痛 ■否	0次/分	0次/分	//mmHg	E1V1M1	/%	/℃	

簽名欄

救護人員簽名	醫護人員簽名	拒絕送醫簽名	送醫後傷病患/家屬/關係人簽名
到院前檢傷分級：□一級□二級□三級□四級□五級 案件屬性：■危急個案□非危急個案 1、 4、 2、 5、 3、6、	檢傷分級：■一級□二級□三級□四級□五級	□拒絕醫療聲明：本人聲明：救護人員已解釋傷病情與送醫之需要，但我□拒絕任何救護 □拒絕送醫 簽名：	與病人關係： 聯絡電話：

Colchicine Overdose Causing Respiratory and Multi-organ Failure

Tim Yu-Ting Lee[1], Jen-Wei Wu[2], Chao-Yu Chen[3], Ching-Tzu Huang[4,5], Han-Chung Hu[1,5], Kuo-Chin Kao[1,5]

Colchicine is usually a safe drug if taken according to therapeutic recommendations (maximum dose of 1.8 mg/hour for acute gout). However, ingesting colchicine in quantities that exceed the recommended maximum can cause serious systemic side effects and may even be life-threatening. Here, we report a rare case of colchicine overdose caused by inappropriate self-medication. Gastrointestinal symptoms and acute kidney injury developed, and hemodialysis was initiated. Acute respiratory failure, profound shock with acute heart failure, hepatitis, and pancytopenia were observed. Various treatments were implemented, and the patient gradually recovered from multi-organ dysfunction and was eventually discharged. The pharmacology of colchicine, the clinical features associated with overdose, and treatment options are discussed. ***(Thorac Med 2024; 39: 183-188)***

Key words: colchicine overdose, respiratory failure, multi-organ failure

Introduction

Colchicine is an alkaloid extracted from Colchicum autumnale and is used to treat acute gouty arthritis, familial Mediterranean fever, and pericarditis [1]. It is usually considered safe if taken according to therapeutic recommendations (maximum dose of 1.8 mg/hour for acute gout) [2]. However, although the reported lethal dose of colchicine is 0.8 mg/kg [3], patient fatalities have been reported at considerably lower doses. Moreover, mortality has been reported at a wide range of doses (7~25 mg), suggesting that the safe dose of colchicine differs between individuals. In this case report, the patient presented with symptoms and pathological processes typical of colchicine toxicity after self-medicating inappropriately.

Case Presentation

The patient was a 38-year-old man with a history of gout. He deliberately took over 20 colchicine pills (>10 mg), and approximately

[1]Department of Thoracic Medicine, Chang Gung Memorial Hospital, Taipei, Taiwan, [2]Department of Internal Medicine, Chang Gung Memorial Hospital, Taipei, Taiwan, [3]Department of Nephrology, Chang Gung Memorial Hospital, Taipei, Taiwan, [4]Department of Respiratory Therapy, Chang Gung Memorial Hospital, Taoyuan, Taiwan, [5]Department of Respiratory Therapy, Chang Gung University, Taoyuan, Taiwan
Address reprint requests to: Dr. Kuo-Chin Kao, Department of Thoracic Medicine, Chang Gung Memorial Hospital, 5 Fu-Hsing Street, Kweishan, Taoyuan 333, Taiwan

12 hours after ingestion, he experienced acute abdominal symptoms, including abdominal pain, severe and frequent watery diarrhea, and vomiting. On arrival at the emergency department of our hospital, he developed mild chest tightness and shortness of breath. His laboratory data indicated a white blood cell count (WBC) of 10,200/μL, and a platelet count of 255,000/μL. Oliguria and a creatinine level of 3.46 mg/dL were observed, indicating acute kidney injury. Total bilirubin and liver enzyme levels were within normal ranges (total bilirubin: 0.3 mg/dL, alanine aminotransferase (ALT): 32 U/L). The patient was therefore admitted to the nephrology ward in preparation for possible hemodialysis. However, his condition deteriorated rapidly. Profound shock with the need of inotropic agents for blood pressure support, progression of metabolic acidosis, progressive drowsiness, and impending respiratory failure were observed within 24 hours of admission. Because of his rapidly deteriorating condition, the patient was intubated and transferred to the medical intensive care unit (MICU).

In the MICU, the patient's hemogram revealed leukopenia and thrombocytopenia. Further laboratory data also indicated rapidly progressing acute kidney injury (creatinine: 9.75 mg/dL), acute hepatitis (total bilirubin: 0.4 mg/dL, aspartate aminotransferase: 11,540 U/L, alanine transaminase: 4,320 U/L), lactic acidosis (lactate: 61.8 mg/dL), and elevated C-reactive protein (CRP) levels (CRP: 245.94 mg/L).

Because of the patient's profound shock with severe renal dysfunction, continuous renal replacement therapy was implemented. High-dose inotropic agents and broad-spectrum antibiotics were also administered. Elevated troponin-I and brain natriuretic peptide levels were also observed, suggesting the possibility of acute heart failure with cardiogenic shock. Echocardiography revealed a left ventricular ejection fraction of 48% with global hypokinesia, which further indicated the presence of acute heart failure. Dopamine was therefore administered as the primary inotropic agent, along with norepinephrine, frozen plasma, muscle relaxant, and proton-pump inhibitors. Nevertheless, the patient developed complete hematopoietic inhibition (WBC: 900/μL, hemoglobin: 8.9 g/dL, platelets: 12000/μL), with an international normalized ratio of 2.7 and gastrointestinal bleeding. In addition, successive chest X-rays revealed rapid progression of bilateral infiltration and pleural effusion. A Pulse index Continuous Cardiac Output system was emplaced for hemodynamic monitoring, and revealed a low cardiac index (2.2 L/min/m2), relatively low systemic vascular resistance under a high concentration of inotropic agents (SVRI: 1920 dyn*s*cm-5*m2), and low extravascular lung water (EVLW: 6 ml/kg).

A whole-body computed tomography scan was performed to identify any focus of infection, but none could be identified. The aforementioned therapies were administered over 2 weeks, and the patient slowly recovered. Laboratory data on day 14 of hospitalization revealed a WBC of 10,300/μL and a platelet count of 60,000/μL. Renal function also recovered and hemodialysis was terminated after 2 weeks (creatinine: 0.75 mg/dL). Hepatic function also improved, although his jaundice remained (total bilirubin: 5.2 mg/dL, alanine transaminase: 140U/L). During treatment, the patient experienced an episode of nosocomial pneumonia with a multi-drug-resistant strain of Acinetobacter baumannii, which was successfully treated with Colistin. The patient was extubated after 22 days (Figure 1).

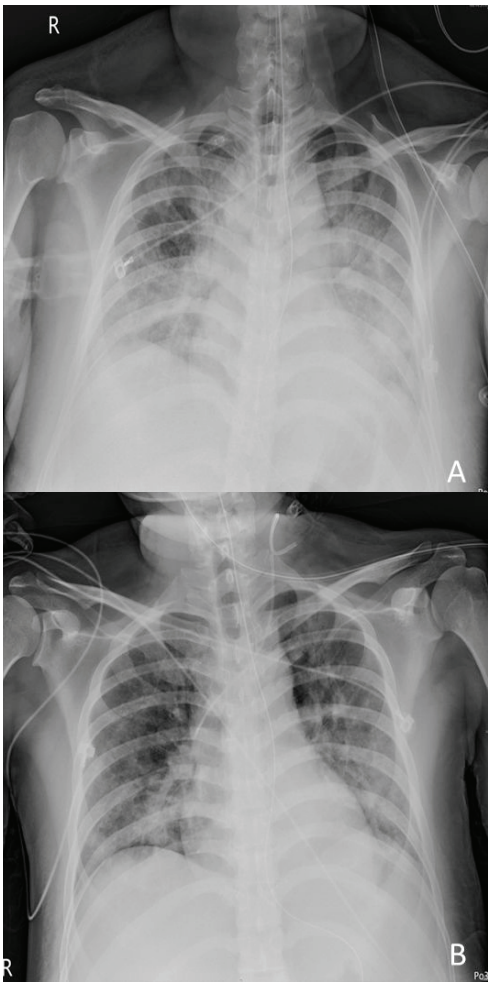

Fig. 1. Successive chest X-rays of the patient during hospitalization. (A) Chest X-ray on Day 5 of hospitalization, (B) Chest X-ray on Day 22 after extubation.

The patient was transferred to the nephrology ward for further management. He was fully ambulatory with clear consciousness and stable vital signs after 28 days, and was discharged. At follow-up after 2 months, the patient experienced no side effect from this injury; he had even recovered from the severe transient alopecia that occurred during treatment (Figure 2).

Discussion

Colchicine, an alkaloid extract, is readily absorbed from the gastrointestinal tract. In therapeutic dosing, peak serum level occurs 30-120 minutes after ingestion. Subsequently, colchicine undergoes extensive first-pass hepatic metabolism, primarily involving deacetylation [4]. It has a plasma half-life of 20 minutes, and therefore undergoes rapid initial distribution and swift uptake by tissue. Up to 40% of ingested colchicine is excreted in the urine. The majority of the drug undergoes enterohepatic recirculation and is excreted in bile and feces, with an average elimination half-life of approximately 20 hours [5].

Fig. 2. Photo of the patient with transient alopecia (anagen effluvium) during hospitalization (left), and with hair regrowth 2 months after discharge (right).

Colchicine has potent anti-mitotic activity. This is mainly caused by binding with tubulin, which disrupts the function of the mitotic spindles in cells that are dividing and migrating [6]. Colchicine downregulates multiple inflammatory pathways and modulates innate immunity when taken in therapeutic doses [7]. Although colchicine is absorbed by all types of cells, those with the highest cell turnover are considered most affected (e.g., gastrointestinal mucosa, bone marrow).

The clinical symptoms of colchicine overdose can be divided into 3 phases. The first phase, usually 10-24 hours after ingestion, involves early gastrointestinal symptoms, volume depletion, hypotension resulting from severe vomiting and diarrhea, and peripheral leukocytosis. The second phase, usually 2-7 days after ingestion, involves symptoms such as changes in mental status, oliguric renal failure, rhabdomyolysis, hematopoietic inhibition, electrolyte and acid-base imbalances, and respiratory and cardiovascular collapse. The electrolyte and acid-base disturbances often include metabolic acidosis, hyponatremia, hypocalcemia, hypokalemia, hypophosphatemia, and hypomagnesemia. The third phase, which occurs 7 days after colchicine ingestion, involves rebound leukocytosis and transient alopecia (anagen effluvium) [8, 9]. Acute lung injury usually occurs during the middle or late stages of colchicine poisoning. Respiratory distress and hypoxemia with bilateral pulmonary infiltrates are usually treated with mechanical ventilation support and negative fluid balance application.

Some of the most pronounced and rapidly apparent symptoms are the various gastrointestinal symptoms associated with the drug. One cause of their rapid onset is the extended exposure of gastrointestinal mucosal cells to colchicine. Electrolyte imbalances caused by colchicine toxicity and mitotic inhibition also result in the edema of the gastrointestinal mucosa. Extensive edema of mucosal cells in the digestive tract causes abdominal pain, diarrhea, nausea, and vomiting. As the toxicity progresses, the balance of intestinal bacterial flora changes, causing systemic infections that may lead to sepsis and shock.

The cardiovascular system is also vulnerable to the toxic effects of colchicine. Usually, cardiovascular irregularities can be identified using serum myocardial zymogram (troponin I, creatine kinase isoenzyme, brain natriuretic peptide) levels, which could indicate heart failure. Various mechanisms have been proposed to explain the effect of colchicine on the heart and skeletal muscles, such as a direct toxic effect on myocardial cells that cause cardiac conduction, or indirect effects caused by profound metabolic acidosis and electrolyte disturbances [10]. Some reports have shown that cardiac toxicity can cause arrythmia, although this was not observed in our patient. Cardiogenic dysrhythmia and shock can also cause acute renal failure, which may further exacerbate the risk of colchicine myotoxicity.

Colchicine-induced acute renal failure has been noted in many studies [11]. Oligo/anuria renal failure is the most common form of renal failure, with proteinuria also reported some studies [12]. No evidence exists of a direct toxic effect of colchicine on the kidney. Thus, some reports have attributed renal damage to hypoxia, hypotension, or myoglobinuria caused by colchicine intoxication [13]. In patients with colchicine poisoning, microscopic findings indicate diffuse renal tissue swelling without glomerular or tubular damage [14]. One report revealed that the epithelium of the collecting

tubule, distal and proximal convoluted tubules, and loops of Henle exhibit no significant change, and that glucosuria was found to be absent in a urinary analysis [15].

Hematopoietic disturbance is a harmful consequence of colchicine toxicity. In addition to the myelosuppression caused by colchicine, the severe shock, infection, and liver damage in the case of hematopoietic disturbance can cause abnormal coagulation function [11]. An increase in D-dimer levels indicates disturbance in the circulatory system, and can aggravate organ dysfunction. Disseminated intravascular coagulation is also caused by both septic shock and multi-organ failure [12].

No concrete evidence of a specific cure for colchicine toxicity exists. Early diagnosis appears to be the most effective manner of reducing colchicine-related mortality. However, some reports have indicated that because of the systemic distribution of colchicine and the characteristics of its metabolism, early diagnosis of colchicine poisoning does not always reduce mortality [13]. Moreover, no effective antagonistic drug available for clinical use exists. At present, approaches to reducing mortality comprise some combination of early diagnosis, antibiotics treatments, and supportive treatment to prevent organ failure. One study found that in porcine models, colchicine-specific antigen-binding fragments (Fabs) were highly effective if administered in high doses at an early stage [14]. Fabs are considered to bind to colchicine with high affinity, enabling the drug to remain within the intravascular compartment and away from peripheral sites. Various case studies have reported that administering active charcoal early in the course of toxicity may reduce the gastrointestinal absorption of colchicine, thereby reducing its toxicity [15].

Conclusion

Clinicians must understand the potential dangers of colchicine overdose, and must educate patients regarding colchicine's effects and the warning signs indicating the need to stop taking it. Careful monitoring of prescriptions is necessary to prevent unintentional overdose. In patients with colchicine overdose, early recognition, general supportive measures, and meticulous fluid balance monitoring are required.

References

1. Finkelstein Y, Aks SE, Hutson JR, *et al*. Colchicine poisoning: the dark side of an ancient drug. Clin Toxicol (Phila) 2010; 48(5): 407-14.
2. Dasgeb B, Kornreich D, McGuinn K, *et al*. Colchicine: an ancient drug with novel applications. Br J Dermatol 2018; 178(2): 350-56.
3. Hirayama, I., Hiruma, T., Ueda, Y. *et al*. A critically ill patient after a colchicine overdose below the lethal dose: a case report. J Med Case Reports 2018; 12: 191.
4. Angelidis C, Kotsialou Z, Kossyvakis C, *et al*. Colchicine pharmacokinetics and mechanism of action. Curr Pharm Des 2018; 24(6): 659-63.
5. Chappey O, Scherrmann JM. La colchicine: données récentes sur sa pharmacocinétique et sa pharmacologie clinique [Colchicine: recent data on pharmacokinetics and clinical pharmacology]. Rev Med Interne 1995; 16(10): 782-789.
6. Bhattacharyya B, Panda D, Gupta S, *et al*. Anti-mitotic activity of colchicine and the structural basis for its interaction with tubulin. Med Res Rev 2008; 28(1): 155-83.
7. Ben-Chetrit E. Colchicine. Textbook of Autoinflammation 2018 Jul 31: 729–49.
8. Milne ST, Meek PD. Fatal colchicine overdose: report of a case and review of the literature. Am J Emerg Med 1998; 16(6): 603-8.
9. Maxwell MJ, Muthu P, Pritty PE. Accidental colchicine overdose. A case report and literature review. Emerg Med J 2002; 19: 265-7.

10. Fu, M, Zhao J, Li ZT, *et al*. Clinical outcomes after colchicine overdose. Medicine 2019; 98(30): pe16580.
11. Naidus RM, Rodvien R, Mielke CH, Jr. Colchicine toxicity: a multisystem disease. Arch Intern Med 1977; 137(3):394-6.
12. Murray SS, Kramlinger KG, McMichan JC. Acute toxicity after excessive ingestion of colchicine. Mayo Clin Proc 1983; 58(8): 528-32.
13. Folpini A, Furfori P. Colchicine toxicity—clinical features and treatment. Massive overdose case report. J Toxicol Clin Toxicol 1995; 33(1): 71-7.
14. Macleod JG, Phillips L. Hypersensitivity to colchicine. Ann Rheum Dis 1947; 6: 224-9.
15. Stemmermann GN, Hayashi T. Colchicine intoxication. A reappraisal of its pathology based on a study of three fatal cases. Hum Pathol 1971; 2(2): 321-32.
16. Van Heyningen C, Watson ID. Troponin for prediction of cardiovascular collapse in acute colchicine overdose. Emerg Med J 2005; 22: 599-600.
17. McEwan T, Robinson PC. A systematic review of the infectious complications of colchicine and the use of colchicine to treat infections. Semin Arthritis Rheum 2021; 51(1): 101-112.
18. Rahimi M, Alizadeh R, Hassanian-Moghaddam H, *et al*. Clinical manifestations and outcomes of colchicine poisoning cases; a cross sectional study. Arch Acad Emerg Med 2020; 8(1): e53.
19. Stoupel E, Prigogine T, Kahn RJ. Intoxication à la colchicine et détresse respiratoire de l'adulte [Colchicine poisoning and respiratory distress in adults]. Acta Clin Belg 1978; 33(3): 189-194.
20. Eddleston M, Fabresse N, Thompson A, *et al*. Anti-colchicine Fab fragments prevent lethal colchicine toxicity in a porcine model: a pharmacokinetic and clinical study. Clin Toxicol (Phila) 2018; 56(8): 773-781.
21. Iosfina I, Lan J, Chin C, *et al*. Massive colchicine overdose with recovery. Case Rep Nephrol Urol 2012; 2(1): 20-24.

Diagnosis of Pulmonary Synovial Sarcoma in an Asymptomatic Patient

Yung-Chia Huang[1*], Shuoh-Yau Lee[1*], Yei-San Hseh[3], Kuo-Sheng Liao[2], Yu-Cheng Chen[1]

Synovial sarcoma is an aggressive tumor caused by the fusion of SYT and SSX genes that seldom affect the lung. We reported a 49-year-old man who presented to our outpatient department seeking consultation for an incidental finding of a left lower lung mass on the chest X-ray during a routine health exam. He complained about occasional dry cough and denied other discomforts. Initial chest radiography revealed a round mass at the left lower lung field. Under the tentative pathological diagnosis of left lung blastoma, the patient underwent video-assisted left lower lung lobectomy and mediastinal lymph node dissection. The revised pathological study after resection revealed SYT-SSX gene fusion, which is diagnostic of primary lung synovial sarcoma. The patient refused to undergo subsequent chemotherapy. No recurrence was found in the computed tomography follow-up 6 months later. ***(Thorac Med 2024; 39: 189-192)***

Key words: Synovial sarcoma, Asian, positron emission tomography, SYT-SSX mutation, video-assisted thoracic surgery

Introduction

Synovial sarcoma is a rare, aggressive soft tissue sarcoma unrelated to smoking, and is usually diagnosed in early adulthood. The tumor is classified as monophasic, biphasic, or poorly differentiated based on the histologic subtype. Synovial sarcoma accounts for around 10% of soft tissue sarcomas. It is most frequently found in the lower extremities, followed by the upper extremities. The lungs and other body parts are rarely affected [1]. Most cases of synovial sarcoma show a fusion of SYT and SSX genes. Three subtypes, SYT-SSX1, SYT-SSX2, and SYT-SSX4, have been identified. Female predominance has also been noted [2]. Previous studies have suggested that patients with the SYT-SSX2 type have a better metastasis-free

[1]Department of Internal Medicine, Taoyuan General Hospital, Ministry of Health and Welfare, [2]Department of Pathology, Taoyuan General Hospital, Ministry of Health and Welfare, [3]Department of Surgery, Taoyuan General Hospital, Ministry of Health and Welfare.
[*]These authors contributed equally to this work.
Address reprint requests to: Dr. Yu-Cheng Chen, Department of Internal Medicine, Taoyuan General Hospital, Ministry of Health and Welfare

survival rate than those with the SYT-SSX1 variant [3].

Primary lung synovial sarcoma is rarely reported in the Asian population. Here, we report a case of primary lung synovial sarcoma in an asymptomatic man who remained progression-free 6 months after tumor resection.

Case Report

A 49-year-old gentleman presented at Taoyuan General Hospital's outpatient department with a mass lesion in the left lower lobe of the lung found during a chest X-ray (Figure 1a), as part of a routine health examination. The patient denied any medical history, but had been smoking 1 pack of cigarettes daily for 10 years. No family members were affected by malignancy. The patient complained of frequent night coughs, but denied chest pain or shortness of breath.

General physical examination was unremarkable. A Contrast-enhanced computed tomography (CT) scan of the chest showed a 3.2 cm mass lesion with eccentric calcification in the left lower lung. The positron emission tomography scan (Figure 1c) showed fludeoxyglucose (FDG) hypermetabolism in the left lower lobe lung mass. There was no abnormal FDG uptake in the other organs. A CT-guided lung biopsy was performed. The initial pathology exam of the specimen was specious for pulmonary blastoma or sarcoma.

The patient then underwent left lower lung lobectomy and mediastinal lymph node dissection by video-assisted thoracic surgery. The pathological study revealed a well-circumscribed, unencapsulated, solitary mass with marked necrosis and hemorrhage within the lung parenchyma. The tumor size was 3.5 × 3.0 × 2.5 cm. The microscopic examination showed the tumor was composed of hyperchromatic

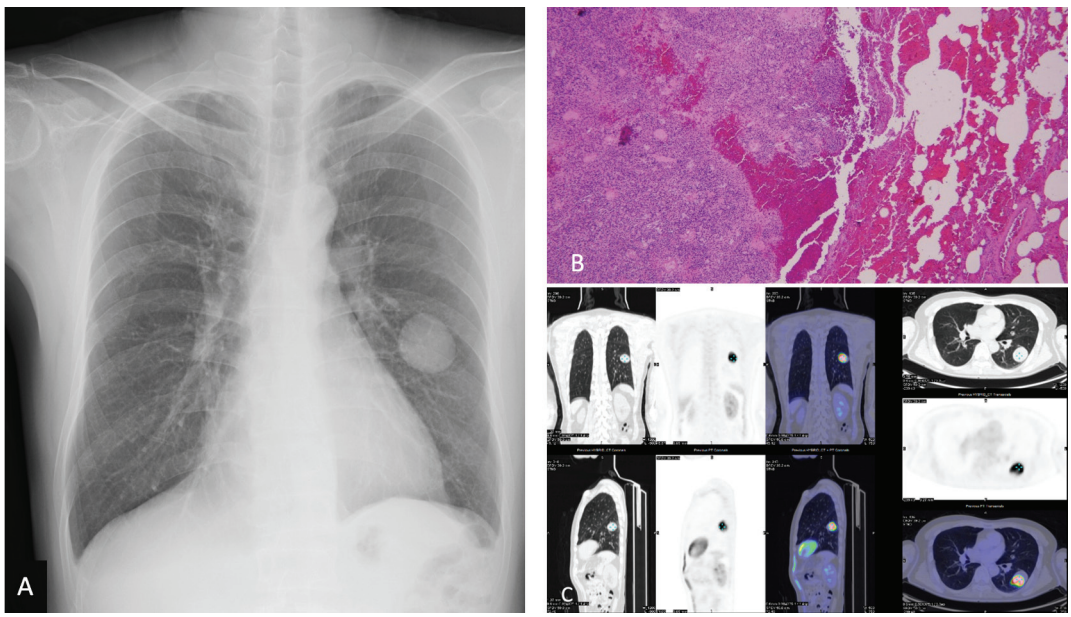

Fig. 1. (A) Plain chest posterior-anterior view X-ray showing a well-defined round lesion in the left lower lung lobe. (B) H&E stain showing compact fascicles of hyperchromatic monophasic spindle cells with hemangiopericytoma-like areas, small arteries, and irregularly distributed capillaries. The tumor is marked with necrosis and hemorrhage. (C) Positron emission tomography scan showing increased fluorine-18 uptake in the left lower lung, consistent with the finding in the chest X-ray.

monophasic spindle cells arranged into compact fascicles with hemangiopericytoma-like areas, small arteries, and irregularly distributed capillaries (Figure 1b). Immunohistochemically, the tumor cells showed strong positive and diffused reactions for Bcl-2, CD99, and vimentin. Focal cytoplasmic positivity was recorded for cytokeratin, EMA, and TLE-1. Tests for CD34, SMA, S-100, synaptophysin, and desmin were negative. About 55% of neoplastic cells within the sample were positive for Ki-67. Fluorescence in situ hybridization was used to detect fusion protein of translocation in formalin-fixed, paraffin-embedded tissues. The result showed positive for SYT-SSX gene fusion, which led to the final diagnosis of primary pulmonary synovial sarcoma, monophasic spindle cell type, T1N0M0 grade 3 stage II, according to AJCC staging for soft tissue sarcoma.

Due to the aggressive nature of this type of sarcoma, adjuvant chemotherapy was suggested. The patient refused to receive chemotherapy or radiotherapy during the subsequent outpatient department visit. A follow-up chest CT scan was done 6 months later, with no sign of recurrence; the patient was then lost to follow-up. However, a telephone follow-up was done 3 years later. The patient's family reported that the patient had expired due to COVID-19 2 years after the surgery.

Discussion

Primary pulmonary synovial sarcoma symptoms include cough and fever, due to obstructive pneumonitis and lung atelectasis [4]. An initial chest radiograph may show a mass-like lesion with a well-defined border and pleural effusion. Our patient's chest radiography revealed a rounded, smooth-border tumor without pleural effusion. The radiological finding was consistent with primary lung synovial sarcoma. The patient had a favorable prognosis, with a tumor mass of less than 5 cm [5].

The grading of the sarcoma is based on its mitotic index and the extent of necrosis. However, exceptions are synovial sarcoma and embryo sarcoma. Due to its aggressive nature, significant points are added to the grading of the tumor. Thus, the tumor is never considered a low-grade tumor [6]. A high risk of tumor metastasis and recurrence is expected.

Treatment of synovial sarcoma includes radical surgical excision, chemotherapy, and radiotherapy. Tumor removal with a safety margin may lead to complete remission in 20%-70% of patients with a noninvasive tumor [4]. Chemotherapy with doxorubicin and ifosfamide may help remove microscopic metastasis; however, the benefit to overall survival is controversial [1]. A new tyrosine kinase inhibitor, catequentinib or anlotinib, targets VEGFR1-3, FGFR1-3, PDGFR-β, and cKIT, and is being explored as second-line therapy for synovial sarcoma. The initial report of the phase III clinical trial (APROMISS) compares catequentinib against dacarbazine in patients with synovial sarcoma who failed first-line chemotherapy treatment. The clinical trial result showed better progression-free survival and less mortality at 12 months for anlotinib. The study result was expected to be complete in April 2023 [7]. Another treatment under investigation is the EZH2 inhibitor, but a phase II study showed only a limited anti-tumor effect [8]. A SSYT-SSX breakpoint peptide vaccine was also studied and passed the phase I trial. However, further studies showed limited treatment response. Of the 21 enrolled patients, only 13 had received a full dose of the vaccine. Disease progression was

noted in 6 patients, and only 4 were still alive at the end of 5 years of follow-up [9].

A search of current literature on Pubmed, Google Scholar, and Ovid showed scant case reports concerning synovial sarcoma in the chest. Most of the reported cases had already metastasized before the diagnosis was established [10-11]. Lin, *et al*., reported the case of a patient with mediastinal synovial sarcoma who developed metastasis 3 days after tumor debulking [10]. Another case presented by Sokucu, *et al*., described a patient who received chemotherapy before tumor removal. The patient later developed regional recurrence and metastasis, which required tumor removal every year for 3 years [11].

The sharp contrast of the clinical course may be due to the early detection of the tumor by routine health exam, as hinted by the small tumor size and by the lack of pleural effusion frequently mentioned in other reports. The patient also received prompt radical tumor resection before the diagnosis of synovial sarcoma was made. Even without subsequent adjuvant chemotherapy or radiotherapy, no early metastasis was found. Early referral for surgical resection and consultation with pulmonologists and oncologists may be the best treatment option.

Acknowledgments

We would like to thank the National Taiwan University Pathology Department for their work on genetic testing.

References

1. Thway K, Fisher C. Synovial sarcoma: defining features and diagnostic evolution. Ann Diagn Pathol 2014; 18: 369-80.
2. Ladanyi M, Antonescu CR, Leung DH, *et al*. Impact of SYT-SSX fusion type on the clinical behavior of synovial sarcoma: a multi-institutional retrospective study of 243 patients. Cancer Res 2002; 62: 135-40.
3. Kawai A, Woodruff J, Healey JH, *et al*. SYT–SSX gene fusion as a determinant of morphology and prognosis in synovial sarcoma. N Engl J Med 1998; 338: 153-160.
4. Brennan B. Synovial sarcoma: current perspectives. Clin Oncol Adolesc Young Adults 2016; 6: 21-6.
5. Deshmukh R, Mankin HJ, Singer S. Synovial sarcoma: the importance of size and location for survival. Clin Orthop Relat Res 2004; 204: 155-61.
6. American Joint Committee on Cancer. Soft tissue sarcoma of the trunk and extremities. In: AJCC Cancer Staging Manual. 8th ed.; 2017: 507.
7. Van Tine BA, Chawla SP, Trent JC, *et al*. A phase III study (APROMISS) of AL3818 (catequentinib, anlotinib) hydrochloride monotherapy in subjects with metastatic or advanced synovial sarcoma. J Clin Oncol 2021; 39(15_suppl): 11505-11505.
8. Schoffski P, Agulnik M, Stacchiotti S, *et al*. Phase 2 multicenter study of the EZH2 inhibitor tazemetostat in adults with synovial sarcoma (NCT02601950). J Clin Oncol 2017; 35(15_suppl): 11057-11057.
9. Kawaguchi S, Tsukahara T, Ida K, *et al*. SYT-SSX breakpoint peptide vaccines in patients with synovial sarcoma: a study from the Japanese Musculoskeletal Oncology Group. Cancer Sci 2012; 103(9): 1625-30.
10. Lin YS, H WH. Primary synovial sarcoma of the mediastinum: a case report. Thorac Med 2008; 23: 381-385. Dr., please check this reference – I can't find it online.
11. Seyhan EC., Sokucu SN., Gunluoglu G. Primary pulmonary synovial sarcoma: a very rare presentation. Case Rep Pulmonol 2014; 2014: 537618.

Lung Adenocarcinoma Coexisting with Human Pulmonary Dirofilariasis-A Case Report

Kuo-Lun Wu[1,2], Yen-Hsiang Tang[2,3], Wei-Chin Chang[2,4], Hsin-Pei Chung[1,2]

Dirofilariasis, a common parasitic infection found in stray dogs and cats, can become an accidental infection in humans under rare circumstances. Human pulmonary dirofilariasis (HPD) typically presents as a well-circumscribed, peripheral, solitary nodule on radiography, mimicking lung neoplasm. In this report, we present the rare case of a 71-year-old Taiwanese female with lung cancer that was incidentally diagnosed with HPD. HPD is a rare differential diagnosis for pulmonary nodules, and surgical intervention can achieve a definitive diagnosis. ***(Thorac Med 2024; 39: 193-197)***

Key words: adenocarcinoma; dirofilaria; heartworm disease; human pulmonary dirofilariasis; lung cancer

Introduction

Dirofilariasis is usually caused by D. immitis or D. repens infections in stray dogs or cats. Adult worms reside in the pulmonary artery and right heart [1], causing right ventricular outflow obstruction and heart failure in dogs. Under very rare circumstances, dirofilariasis in dogs or cats can lead to accidental infection in humans via an intermediate host, the mosquito [2].

The presentation of human dirofilariasis generally includes pulmonary manifestations, subcutaneous dirofilariasis, ocular dirofilariasis, and extremely rare microfilaremia. In cases of human pulmonary dirofilariasis (HPD), a larva reaches the right heart via venous return and dies in the right ventricle, then embolizes into the distal pulmonary artery, and becomes a necrotic or fibrotic nodule in the peripheral lung. The typical presentation is a well-circumscribed, peripheral, solitary nodule on radiography, mimicking lung neoplasm [1].

Since the first human dirofilariasis case was described in 1887, approximately 1,782 cases of human dirofilariasis have been reported, mostly in areas with the highest canine dirofilariasis prevalence rate; a total of 372 pulmonary manifestations and 1,410 extrapulmonary cases

[1]Division of Pulmonary and Critical Care Medicine, MacKay Memorial Hospital, Taipei, Taiwan. [2]Department of Medicine, MacKay Medical College, New Taipei City, Taiwan, [3]Department of Critical Care Medicine, MacKay Memorial Hospital, Taipei, Taiwan, [4]Department of Pathology, MacKay Memorial Hospital, Taipei, Taiwan.
Address reprint requests to: Dr. Hsin-Pei Chung, MacKay Memorial Hospital, Tamsui Branch. No. 45, Minsheng Rd., Tamshui District, New Taipei City 25160, Taiwan.

have been detected up to July 2012 [2]. Several articles have reported single or multiple HPD nodules mimicking lung cancer [4-6]. Only 2 cases of HPD coexisting with lung cancer have been reported [7-8], and 1 case coexisting with extrapulmonary neurilemmoma was recently described [9]. Here, we report a case of lung adenocarcinoma coexisting with an HPD.

Case Report

A 71-year-old female with a medical history of hyperthyroidism under oral methimazole treatment presented with the chief complaint of cough with scanty whitish sputum for 2 weeks. She denied cigarette smoking or a family history of malignancy. The patient had raised a dog for 13 years that died from heart disease 1 year previously. A chest computed tomography (CT) scan was performed for cancer screening in 2015.A pulmonary nodule about 1.6 cm in length with a well-demarcated border was detected in the right lower lobe (Fig. 1A). Due to a suspicion of malignancy, tissue sampling was suggested, but the patient refused surgical excision. Therefore, annual repeat CT screenings were performed instead. Consecutive serial CT chest scans over 3 years showed a stationary lung nodule in the right lower lobe. In 2019, in addition to the stationary nodule in the right lower lung, a newly developed, spiculated pulmonary nodule, 1 cm in length in the right middle lobe, was seen on a CT image (Fig. 1B). Detailed blood sampling for hemogram and biochemistry tests showed normal findings, with an absolute eosinophil count of 130/uL. Due to the increasing possibility of malignancy, tissue sampling was recommended, but the patient hesitated to undergo invasive intervention, including bronchoscopy. Instead, clinicoradiological follow-up was performed.

The 2 pulmonary nodules remained stable during the interval up to 2021. Subsequently, the right middle lung nodule grew from 1 cm to 1.5 cm in diameter (Fig. 1C), and a newly developed nodule, 0.4 cm in diameter, was detected in the right lower lobe, abutting the major fissure (Fig. 1D). Due to a suspicion of synchronous pulmonary tumors, the patient underwent video-assisted thoracic surgery for histological confirmation. A right middle lobectomy with complete mediastinal lymph node removal and right lower tumor wedge resection was performed. The postoperative histopathological diagnosis of the right middle lobe nod-

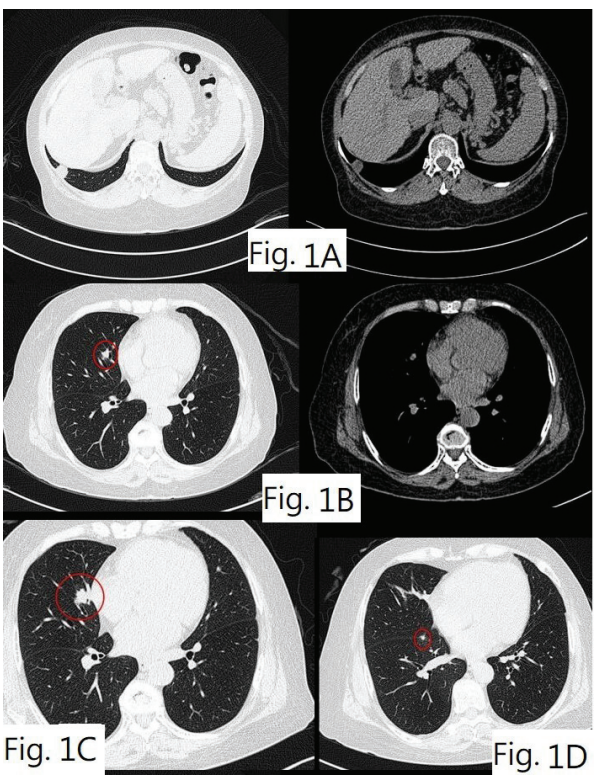

Fig. 1. A series of transverse non-enhanced CT images of a 71-year-old woman. Nodular lesion in the right lower lobe (1A, measured 1.6cm). Growing pulmonary nodule in the right middle lobe measuring 1 cm in 2019 (1B) and 1.5 cm in 2021 (1C). Newly developed nodule measuring 0.4 cm in the right lower lobe (1D).

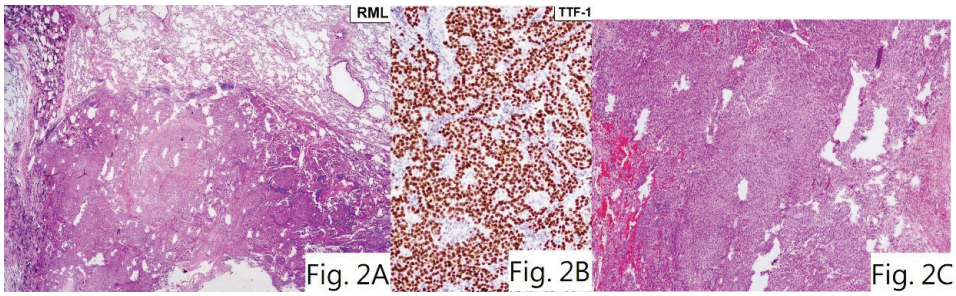

Fig. 2. Postoperative histological images of a slowly growing pulmonary nodule in the right middle lobe (2A). Nodule is consistent with non-small-cell lung cancer, with TTF-1 positive (2B) and a solid pattern predominant (2C).

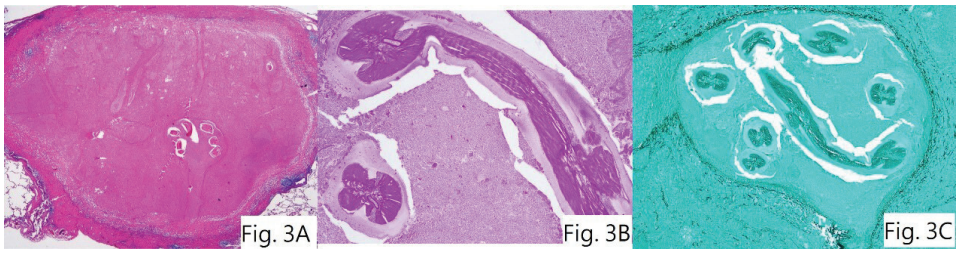

Fig. 3. Postoperative histological sections of the stationary pulmonary nodule in the right lower lobe showing a partial portion of larvae of nematode (3A), specific findings under PAS stain (3B), and GMS stain (3C).

ule was consistent with that of non-small-cell lung cancer (Fig. 2A) with thyroid transcription factor-1 (TTF-1) positivity (Fig. 2B) and a solid pattern predominance (Fig. 2C), compatible with invasive adenocarcinoma. A pathological specimen of the right lower lobe wedge resection revealed a partial portion of nematode larvae (Fig. 3A). Within the larvae, the general body cavity, cuticle, subcuticle muscular layer, and intestinal component were highlighted by periodic acid-Schiff (PAS) staining of the lung parenchyma (Fig. 3B). Under Modified Gomori Methenamine-Silver Nitrate (GMS) staining, the larvae were surrounded by blood vessels, causing intravascular thrombosis, pulmonary infarction, and necrosis (Fig. 3C). These findings indicated a diagnosis of pulmonary dirofilariasis. The patient was finally diagnosed with right middle-lung invasive adenocarcinoma pT1cN0M0 Stage IA3 and a right lower lobe HPD. After surgery, the patient recovered successfully and postoperative surveillance revealed no evidence of recurrence.

Discussion

Dirofilariasis, a zoonotic disease found throughout the world, usually affects canines as a definitive host, and is rarely transmitted to humans or felines as an incidental host via an infected vector, the mosquito [2]. According to the latest data, dirofilariasis in Western Asia, including Taiwan, has mostly been reported as D. immitis. The overall prevalence rate of dirofilariasis in Taiwanese pet dogs has been reported as 22.8% [10]. The prevalence was higher among outdoor dogs and in the southern and eastern geographical areas of Taiwan. A history

of raising pets and living in an area endemic for canine dirofilariasis may be risk factors for HPD [11,12].

Human dirofilariasis usually presents with various clinical features in accordance with the different species of Dirofilaria. D. immitis infection usually presents as pulmonary dirofilariasis in humans. D. repens infections mostly present as subcutaneous or ocular dirofilariasis [2]. Other clinical features include peritoneal infection, and male genital tract, liver, buccal mucosa, or central nervous system infection caused by other less common Dirofilaria species infections.

Most patients with HPD are asymptomatic, and an incidental pulmonary nodule is the initial presentation [12,13]. Some patients present with non-specific symptoms such as productive cough with purulent sputum, hemoptysis, dyspnea, fever, general malaise, and myalgia. Eosinophilia was present in only 10–17% of American [11,13] and Japanese [12] patients. The serological detection of human antibodies to dirofilariasis may not be reliable because antibody levels decay after the initial infection, and low accessibility exists in hospitals for humans.

HPD can have radiographic findings similar to those of malignancy, and an accurate diagnosis is difficult before surgical excision. The typical radiological features of HPD include a well-circumscribed, peripheral, solitary pulmonary nodule. HPD nodules, usually 1–3 cm in diameter, are caused by trapped worm embolization [4-6]. HPD has been located more frequently in the right hemi-lung, with a random lobe distribution [11], as was the case with the patient presented here. Some previous studies described the HPD nodule as an angiocentric lesion, and identified the connection to a branch of the pulmonary artery with a central low-attenuation area, indicated as central necrosis caused by infarction [2,7,14]. These findings may provide some clues to differentiate HPD from a pulmonary malignancy. In a previous report, ovoid or spherical HPD nodules mostly remained stationary without radiological modification during follow-ups, the longest lasting for 13 years [2], usually indicating a benign profile. In rare cases, HPD can present as a growing nodule [6]. Positron emission tomography (PET) scanning may be useful to differentiate HPD from malignancy, but inflammation in HPD can lead to hypermetabolic activity on a PET scan [15,16]. In some cases, multiple nodules in the same lobe or bilateral lung fields imitate metastatic pulmonary tumors [2,3]. Needle or transbronchial lung biopsy is not diagnostic, and almost all cases require surgical excision to establish a definitive diagnosis. Therefore, limited thoracoscopic resections are required for the ultimate etiology, without excessive complications in HPD diagnosis [17].

Systemic treatment for HPD is unnecessary and not recommended. Antiparasitic agents are unnecessary because humans are dead-end hosts and the parasite is already dead at the time of diagnosis. For these patients, no systemic treatment is required for early-stage lung cancer, and wedge resection of nodules is usually considered.

Conclusion

HPD is a rare diagnosis of solitary pulmonary nodules that can coexist with pulmonary malignancies. HPD may mimic pulmonary malignancy on radiographic examination. Limited thoracoscopic resections are required for the ultimate diagnosis.

Institutional Review Board Statement

The study was conducted in accordance with the Declaration of Helsinki and approved by the Institutional Review Board of Mackay Memorial Hospital in Taipei, Taiwan (protocol code: 22MMHIS338e; date of approval: 15 September 2022). Informed consent was obtained from all subjects involved in the study.

Conflicts of interest

The authors declare that there is no conflict of interest.

Acknowledgements

The authors thank Pei-Ran Chen and Jian Su for their expert advice and encouragement throughout the study.

References

1. Morchon R, Carreton E, Gonzalez-Miguel J, *et al*. Heartworm disease (Dirofilaria immitis) and their vectors in Europe - new distribution trends. Front Physiol 2012; 3: 196.
2. Simon F, Siles-Lucas M, Morchon R, *et al*. Human and animal dirofilariasis: the emergence of a zoonotic mosaic. Clin Microbiol Rev 2012; 25: 507-44.
3. Saha BK, Bonnier A, Chong WH, *et al*. Human pulmonary dirofilariasis: a review for the clinicians. Am J Med Sci 2022; 363: 11-7.
4. Biswas A, Reilly P, Perez A, *et al*. Human pulmonary dirofilariasis presenting as a solitary pulmonary nodule: A case report and a brief review of literature. Respir Med Case Rep 2013; 10: 40-2.
5. Ferrari PA, Grisolia A, Reale S, *et al*. A rare case of human pulmonary dirofilariasis with nodules mimicking malignancy: approach to diagnosis and treatment. J Cardiothorac Surg 2018; 13: 65.
6. Haro A, Tamiya S, Nagashima A. A rare case of human pulmonary dirofilariasis with a growing pulmonary nodule after migrating infiltration shadows, mimicking primary lung carcinoma. Int J Surg Case Rep 2016; 22: 8-11.
7. Mulanovich EA, Mulanovich VE, Rolston KV. A case of Dirofilaria pulmonary infection coexisting with lung cancer. J Infect 2008; 56: 241-3.
8. Hsiao YH, Feng JY, Wu YC, *et al*. Human pulmonary dirofilariasis coexisting with lung cancer. Thorac Med 2014; 29: 85-91.
9. Li CY, Chang YL, Lee YC. Human pulmonary dirofilariasis coexisting with intercostal neurilemmoma: a case report and literature review. J Formos Med Assoc 2013; 112: 644-7.
10. Lu TL, Wong JY, Tan TL, *et al*. Prevalence and epidemiology of canine and feline heartworm infection in Taiwan. Parasit Vectors 2017; 10: 484.
11. Asimacopoulos PJ, Katras A, Christie B. Pulmonary dirofilariasis: the largest single-hospital experience. Chest 1992; 102: 851-5.
12. Miyoshi T, Tsubouchi H, Iwasaki A, *et al*. Human pulmonary dirofilariasis: a case report and review of the recent Japanese literature. Respirology 2006; 11: 343-7.
13. Robinson NB, Chavez CM, Conn JH. Pulmonary dirofilariasis in man: A case report and review of the literature. J Thorac Cardiovasc Surg 1977; 74: 403-8.
14. Wand A, Kasirajan LP, Sridhar S. Solitary pulmonary nodule due to dirofilariasis. J Thorac Imaging 2000; 15: 198-200.
15. Silva MJ, Costa AR, Calvinho P. Human pulmonary dirofilariasis: a pitfall in solitary pulmonary nodule. Pulmonology 2022 Sep-Oct; 28(5): 413-414.
16. Moore W, Franceschi D. PET findings in pulmonary dirofilariasis. J Thorac Imaging 2005; 20: 305-6.
17. Schweigert M, Dubecz A, Beron M, *et al*. Pulmonary infections imitating lung cancer: clinical presentation and therapeutical approach. Ir J Med Sci 2013; 182: 73-80.